



UNIVERSITATEA DIN BUCUREŞTI
Facultatea de Fizică



DANA AVRAMESCU

HYBRID SIMULATIONS OF RELATIVISTIC HEAVY-ION COLLISIONS

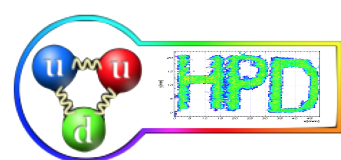
MASTER THESIS

Scientific Advisers

Prof. Dr. MIHAI PETROVICI
Prof. Dr. VIRGIL BĂRAN



HORIA HULUBEI NATIONAL INSTITUTE FOR
PHYSICS AND NUCLEAR ENGINEERING
Hadron Physics Department



CONTENTS

1 Introduction	1
INITIAL STAGE	
2 High Energy QCD	5
2.1 QCD	5
2.2 Light-cone QCD	8
2.3 Small-x landscape	11
3 Classical Chromodynamics	15
3.1 The McLerran-Venugopalan model	15
3.2 The classic color field	19
3.3 Gluon saturation from the MV model	23
4 Simulating the Glasma	33
4.1 Boost-invariant Glasma	33
4.2 Lattice gauge theory	44
4.3 Numerical simulation	48
HYDRODYNAMIC EVOLUTION	
5 Couple to Hydrodynamics	59
5.1 Landau matching	59
5.2 Centrality selection	64
5.3 Relativistic viscous hydrodynamics	66
6 Conclusions	75
APPENDIX	
A Light-Cone Quantization	79
A.1 Light-front form	79
A.2 Poincaré on the light-cone	82
A.3 Light-cone QCD	85
Bibliography	99

1

INTRODUCTION

“Solving a mystery is not the same as deducing from first principles. Nor does it amount simply to collecting a number of particular data from which to infer a general law. It means, rather, facing one or two or three particular data apparently with nothing in common, and trying to imagine whether they could represent so many instances of a general law you don’t yet know, and which perhaps has never been pronounced.”

Umberto Eco, *The Name of the Rose*

Relativistic heavy-ion collisions provide the means to study a multitude of phenomena.¹ From a theoretical point of view, these collisions may be described within effective theories. Nevertheless, trying to grasp a unitary physical picture from a mosaic of disjoint theories is extremely difficult.

1: Such as collective flow [1], jet quenching [2] and many others.

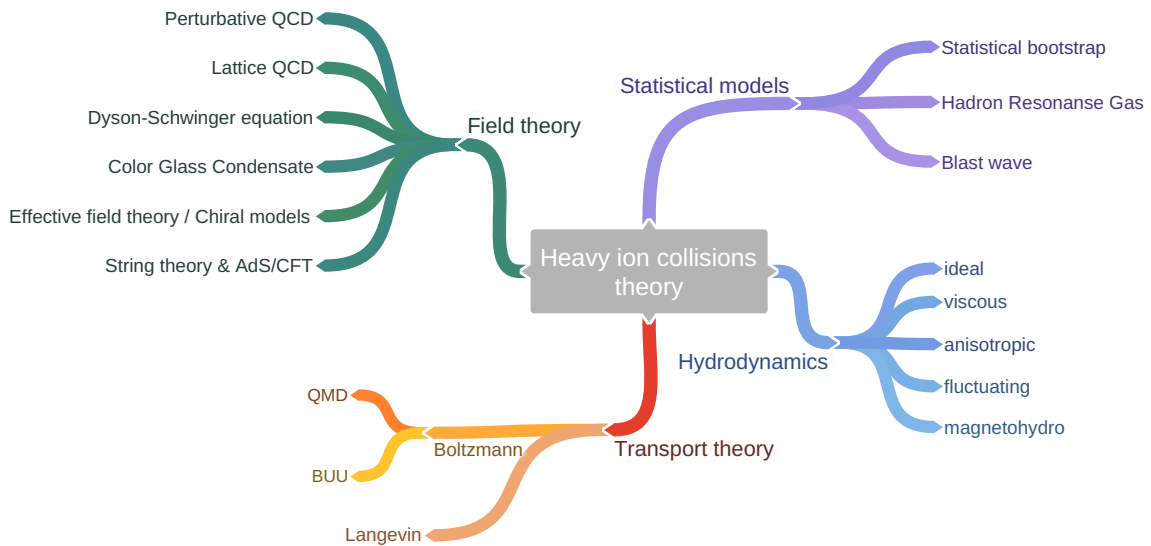


Figure 1.1: Various theoretical models which aim to describe different aspect of heavy-ion collisions. Diagram taken from [3].

The ultimate test is the comparison to experimentally measured data, which may not be done using a single effective theory. For this reason, **hybrid** approaches² are more suitable. They consist in coupling various theoretical descriptions,

2: See for example [4–6].

each within its appropriate range of applicability, and reconstruct heavy-ion collisions stage by stage.

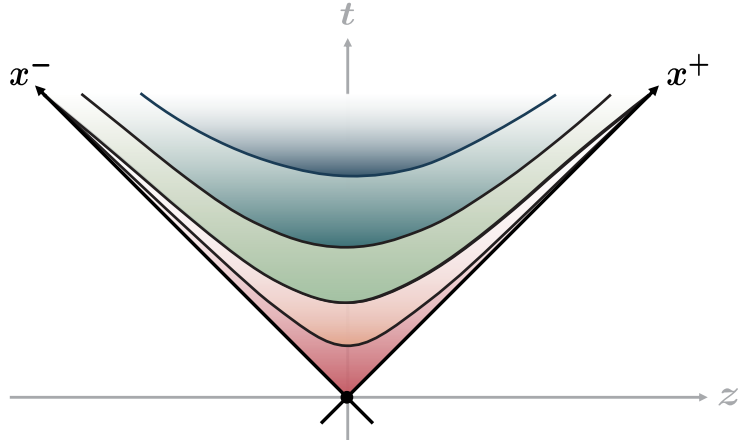


Figure 1.2: Light-cone diagram revealing different stages of heavy-ion collisions. The idea for such a representation is borrowed from [7].

Before collision

$$\tau < \tau_{\text{col}}$$

Before the collision, the nuclei propagate along the light-cone. They may be described using the CGC model, constructed as a high-energy limit of QCD.

Initial stage

$$\tau_{\text{col}} < \tau < \tau_{\text{sat}}$$

Immediately after the collision, a state of matter referred to as the Glasma, which consists of strong classical color fields, is produced in the forward light-cone.

Thermalization

$$\tau_{\text{sat}} < \tau < \tau_{\text{eq}}$$

The pre-equilibrium matter resulting from the initial stage undergoes a process of fast thermalization, described within an effective kinetic theory approach.

QGP transport

$$\tau_{\text{eq}} < \tau < \tau_{\text{fo}}$$

The QGP expands due to pressure gradients. This evolution may successfully be modeled with ideal or viscous relativistic hydrodynamics.

Hadronization

$$\tau_{\text{fo}} < \tau < \tau_{\text{dec}}$$

Once the critical QCD phase transition temperature is reached, the deconfined quarks and gluons recombine into hadrons.

Free streaming

$$\tau < \tau_{\text{det}}$$

When all interactions among hadrons cease, kinetic freeze-out is reached. After the decoupling takes place, produced particles free stream towards the detectors.

3: Simulated with Curraun.

4: Implemented in MUSIC.

5: For Au-Au collision with $\sqrt{s_{\text{NN}}} = 200$ GeV from RHIC.

In this thesis, a modest hybrid simulation approach is presented: initial conditions obtained from the MV model and implemented using real-time lattice gauge theory³ are coupled to relativistic viscous hydrodynamics⁴ and afterwards compared to experimental data⁵.

INITIAL STAGE

HIGH ENERGY QCD 2

PREVIEW

Some basic concepts of QCD shall briefly be presented, with focus on gauge transformations and Yang-Mills equations. The formulation and quantization of chromodynamics using light-cone coordinates will schematically be provided, with detailed proofs in Appendix A. Afterwards, an overview of high-energy QCD and the small- x physics which arise from DIS will be given.

2.1 QCD	5
2.2 Light-cone QCD	8
2.3 Small- x landscape	11

2.1 QCD

Quantum chromodynamics is the theory of strong interactions.¹ It aims to describe the interactions between elementary constituents, namely the quarks,² mediated by the carriers of the color force, the gluons.

The existence of color charge was proposed as an additional quantum number which would solve the violation of Pauli's exclusion principle for some particular baryons.³ Since the quarks were never experimentally evidenced, it was proposed that the strong interaction constrains the free particles to only exist in color neutral states. This particularity of QCD is known as color confinement. Nevertheless, in the partonic picture,⁴ deep inelastic scattering⁵ experiments between an electron and a proton confirmed the already predicted Bjorken scaling⁶ of the electrons' differential cross-section.

In essence, QCD is an extension of the original $SU(2)$ gauge theory of Yang and Mills [12] to local non-Abelian $SU(3)$ gauge transformations.

Field content

Following textbook expositions [13–15], the QCD Lagrangian \mathcal{L} is constructed from symmetry principles, namely $SO(1, 3)$ Lorentz invariance and local gauge invariance under $SU(3)$.

1: A brief historical review about the development of QCD may be found at [8].

2: The quarks were firstly predicted in Gell-Mann's Eightfold Way [9].

3: For example, Δ^{++} , which consists of three up quarks.

4: Feynman proposed that high energy nuclei are made of elementary constituents, generically called partons [10].

5: DIS is a process during which the structure of a hadron may be probed via interaction with, in general, a lepton.

6: Bjorken deduced an expression for the cross-section of the electron by imagining that it interacts electromagnetically with each parton from the proton [11].

The fields should transform according to irreducible representations of these groups. The quark content of the Lagrangian is described by the quark and anti-quark fields $\psi_{\alpha,i,f}(x)$ and $\bar{\psi}_{\alpha,i,f}(x)$. They are Dirac spinors (spinorial index α), transform according to the fundamental representation of $SU(3)$ (color index $i = 1, 2, 3$ or red, green, blue) and come in different flavours (flavour index $f = \overline{1, N_f}$ or up, down, strange, charm, bottom, up). The gluon fields $A_a^\mu(x)$ are Lorentz vectors and each correspond to a generator t^a ($a = \overline{1, 8}$) which, in the fundamental representation, is given by the Gell-Mann matrices $t^a = \lambda^a/2$.

Gauge transformations

The quark and anti-quark fields must be invariant under local $SU(3)$ gauge transformations⁷

$$\psi(x) \mapsto U(x)\psi(x), \quad \bar{\psi} \mapsto \bar{\psi}(x)U^\dagger(x),$$

with the group transformation expressible, via exponentiation, from the Lie algebra generators, with space-time dependent group parameters $\varepsilon^a(x)$, as

$$U(x) = \exp \left\{ i \sum_a \varepsilon^a(x) t^a \right\}. \quad (2.1)$$

The gauge fields⁸ $A_\mu(x) = \sum_a A_\mu^a(x)t^a$ must transform according to

$$A_\mu(x) \mapsto U(x)A_\mu(x)U^\dagger(x) + \frac{i}{g}U(x)[\partial_\mu U^\dagger(x)], \quad (2.2)$$

where g denotes the coupling constant. It is important to notice that one may generate gluon fields out of a null one, that is $A_\mu = 0$ by applying a local gauge transformation. Such field configurations take the form

$$A_\mu^{\text{pure}} = \frac{i}{g}U(\partial_\mu U^\dagger) \quad (2.3)$$

and are called pure gauge fields [16, 17]. The corresponding field strength tensor is null $F_{\mu\nu}^{\text{pure}} = 0$.

Let us now introduce the covariant derivative⁹

$$D_\mu = \partial_\mu - igA_\mu.$$

7: For simplicity, all the field indices will be dropped in the following computations.

8: For each algebra element t^a , one may introduce a gauge field A_a^μ . These may be then used to construct a Lie-algebra valued gauge potential A^μ . This potential depends on the chosen representation.

9: The covariant derivative has an elegant geometrical interpretation [18]: it represents the rate of change when fields from different space-time points are parallel transported along a given path. During this procedure, they are being aligned such that they may be properly compared. The corresponding connection is actually the gauge field.

Further, one may define the field strength tensor as the commutator between covariant derivatives¹⁰

$$F_{\mu\nu} = \frac{i}{g} [D_\mu, D_\nu],$$

which yields an expression in terms of gauge fields

$$F_{\mu\nu} = \partial_\mu A_\nu - \partial_\nu A_\mu - ig[A_\mu, A_\nu], \quad (2.4)$$

or equivalently, by color components $F_{\mu\nu} = F_{\mu\nu}^a t^a$, as

$$F_{\mu\nu}^a = \partial_\mu A_\nu^a - \partial_\nu A_\mu^a + gf^{abc} A_\mu^b A_\nu^c,$$

where f^{abc} are the structure constants of the Lie algebra $\mathfrak{su}(3)$. The last term from the above equation, when plugged in the Lagrangian, will give rise to gluonic self-interactions, a particular feature of QCD. The field strength tensor gauge transforms in the usual manner as

$$F_{\mu\nu}(x) \mapsto U(x) F_{\mu\nu}(x) U^\dagger(x).$$

QCD Lagrangian

We may now proceed to constructing the Lagrangian. The quark content is that of a free fermionic Lagrangian,¹¹ but built with covariant derivatives, in order to satisfy gauge invariance

$$\mathcal{L}_{\text{quarks}} = \bar{\psi}(x) (i\cancel{D} - M) \psi(x), \quad (2.5)$$

where $M = \text{Diag}\{m_1, \dots, m_{N_f}\}$ is the diagonal quark mass matrix in flavour space.¹²

The dynamics of the gluon fields is described by the following construction¹³

$$\mathcal{L}_{\text{gluons}} = -\frac{1}{2} \text{Tr} \{ F_{\mu\nu} F^{\mu\nu} \}, \quad (2.6)$$

where the color tracing over the contraction of field strength tensors assured gauge invariance. Equivalently, one may rewrite the above expression in terms of color components as

$$\mathcal{L}_{\text{gluons}} = -\frac{1}{4} F_{\mu\nu}^a F^{a,\mu\nu}, \quad (2.7)$$

10: Since it arises as a commutator between covariant derivatives, which describe the parallel transport, the field strength tensor may be interpreted as a measure of the path dependence of parallel transport. For this reason, it is also referred to as the curvature [18].

11: After replacing the partial derivative with the covariant derivative, the Lagrangian will also contain an interaction term

$$\mathcal{L}_{\text{int}} = g \bar{\psi} \gamma^\mu A_\mu^a t^a \psi.$$

12: In the Standard Model, the quark mass matrix is no longer diagonal. After spontaneous symmetry breaking, the mixing between different flavoured quark masses is given by the CKM matrix [19].

13: It is important to notice that such a construction contains not only standard kinetic terms but also interaction vertices with three gluons, which are proportional to g and four gluons, proportional to g^2 .

valid in the fundamental representation, where $\text{Tr} \{t^a t^b\} = \delta^{ab}/2$. Therefore, the QCD Lagrangian takes the form

$$\mathcal{L}_{\text{QCD}} = \bar{\psi}(x)(i\cancel{D} - \mathbf{M})\psi(x) - \frac{1}{4}F_{\mu\nu}^a F^{a,\mu\nu}. \quad (2.8)$$

14: There is an additional equation, called the Bianchi identity, which follows from the definition and properties of $F_{\mu\nu}$. It may be expressed as [20]

$$D_\mu {}^* F^{\mu\nu} = 0, \quad (2.10)$$

where we introduced the dual field strength tensor as

$${}^* F^{\mu\nu} = \frac{1}{2}\epsilon^{\mu\nu\rho\sigma} F_{\rho\sigma}.$$

15: As opposed to the standard quantization, done in the framework of path integrals [21]. We shall see that this approach brings considerable simplifications and there will be no need for Faddeev-Popov ghosts [22].

16: Detailed computations may be found in Appendix A.

17: We are going to use the Kogut-Soper convention [22]. There also exists the Lepage-Brodsky choice for defining these coordinates as $x^\pm \triangleq x^0 \pm x^3$. Even though quantities such as the Dirac matrices, projection operators, Dirac spinors, polarization vectors and others differ in these conventions, the final results remain the same.

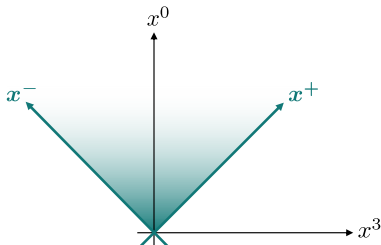


Diagram of light-cone and cartesian coordinates.

18: Defined in Equations (A.3) and (A.4).

Field equations

The variational derivatives with respect to the color spinor fields give the colored Dirac equations

$$(i\cancel{D} - \mathbf{M})\psi = 0, \quad (2.9)$$

and similarly for the anti-quark fields

$$\bar{\psi}(i\overset{\leftarrow}{\cancel{D}} - \mathbf{M}) = 0.$$

The Euler-Lagrange equations corresponding to the gluon fields yield the Yang-Mills equations, or equivalently, colored Maxwell equations¹⁴

$$D_\nu F^{\nu\mu} = gJ^\mu, \quad (2.11)$$

in which $J^\mu = \sum_a J^{a,\mu} t^a$ with $J^{a,\mu} = \bar{\psi} \gamma^\mu t^a \psi$ being the color current. The color current is covariantly conserved $D_\mu J^\mu = 0$.

2.2 Light-cone QCD

Further, the light-cone quantization of chromodynamics¹⁵ shall briefly be presented.¹⁶ For this purpose, we are going to work in one of the forms of relativistic dynamics proposed by Dirac [23], namely the **light-front form**, by using **light-cone coordinates** defined as¹⁷

$$x^\pm \triangleq \frac{1}{\sqrt{2}}(x^0 \pm x^3). \quad (2.12)$$

The Poincaré group in light-cone coordinates possesses a sub-group isomorphic to the two-dimensional Galilean group. For this reason, one may attribute the following physical interpretations [24] to the generators:¹⁸ $P^+ \leftrightarrow$ mass, $P^- \leftrightarrow$ time translation, $\vec{P}_\perp^i \leftrightarrow$ spatial translations, $\vec{B}_\perp^i \leftrightarrow$ boosts,

$J^3 \leftrightarrow$ rotation.

Due to this isomorphism, any theory formulated on the light-cone has an intrinsic non-relativistic structure: the dispersion relation simplifies to $P^- = (\vec{P}_\perp^2 + M^2)/(2P^+)$ ¹⁹. Another important consequence is that the light-cone vacuum has a simple structure and most often is trivial.

The light-cone Dirac matrices and projection operators²⁰ are defined in the KS convention as

$$\gamma^\pm \triangleq \frac{\gamma^0 \pm \gamma^3}{\sqrt{2}}, \quad \Lambda_\pm \triangleq \frac{1}{2} \gamma^\mp \gamma^\pm.$$

After fixing the gauge to the light-cone gauge $A^+ = A_- = 0$, the Lagrangian from Equation (2.8) becomes²¹

$$\begin{aligned} \tilde{\mathcal{L}} = & -\frac{1}{4} F_a^{ij} F_{a,ij} + \frac{1}{2} (F_a^{+-})^2 + F_a^{+i} F_a^{-i} + i\sqrt{2} (\psi_+^\dagger D^- \psi_+ + \psi_-^\dagger \partial^+ \psi_-) - \\ & - \frac{1}{\sqrt{2}} [\psi_+^\dagger \gamma^- (m + i\vec{\gamma}_\perp \vec{D}_\perp) \psi_- + \psi_-^\dagger \gamma^+ (m + i\vec{\gamma}_\perp \vec{D}_\perp) \psi_+]. \end{aligned}$$

The colored Maxwell equations expressed in light-cone coordinates are²²

$$D_a^- (\partial^+ A_a^i) + \partial^+ F_a^{-i} + (D_j F^{ji})_a = g J_a^i, \quad (2.13a)$$

$$(\partial^+)^2 A_a^- + (D_i \partial^+ A^i)_a = g J_a^+, \quad (2.13b)$$

whereas the colored Dirac equations become²³

$$\partial^+ \psi_- = -\frac{i}{2} (-i\vec{\gamma}_\perp \vec{D}_\perp + m) \gamma^+ \psi_+, \quad (2.14a)$$

$$D^- \psi_+ = -\frac{i}{2} (-i\vec{\gamma}_\perp \vec{D}_\perp + m) \gamma^- \psi_-. \quad (2.14b)$$

Straight-forward computations lead to the expression for the conjugate momenta of the fields²⁴ A_a^i and ψ_+ as

$$\Pi_{A_a^i} = \partial^+ A_a^i, \quad \Pi_{\psi_+} = i\sqrt{2} \psi_+^\dagger.$$

On the other hand, the conjugate momenta associated to the fields A_a^- and ψ_- are null

$$\Pi_{A_a^-} = 0, \quad \Pi_{\psi_-} = 0.$$

Equations (2.13b) and (2.14b) may be seen as constraints for these fields and formally inverted to obtain²⁵

19: Proven in Equation (A.7).

20: They obey the usual properties $\Lambda_\pm \Lambda_\mp = 0$, $\Lambda_+ + \Lambda_- = 1$ and $(\Lambda_\pm)^2 = \Lambda_\pm$, as proven in Equations (A.13a), (A.13b) and (A.15). The projected quark fields will thus be given by $\Lambda_\pm \psi = \psi_\pm$.

21: By using the results from Equations (A.18) and (A.20).

22: As proven in Equations (A.23a) and (A.23b).

23: From Equations (A.22a) and (A.22b).

24: Derivation done in Equations (A.24a) and (A.24c).

25: At this point, the importance of choosing the light-cone gauge $A^+ = 0$ becomes visible. Due to this gauge fixing, one doesn't obtain terms containing A^+ in the denominator, which will further complicate the structure of the resulting Hamiltonian and consequently its quantization.

$$\begin{aligned}\psi_- &= -\frac{i}{2\partial^+} \left(m - i\vec{\gamma}_\perp \vec{D}_\perp \right) \gamma^+ \psi_+, \\ A_a^- &= \frac{1}{(\partial^+)^2} \left\{ g J_a^+ - [\mathcal{D}_i (\partial^+ A^i)]_a \right\}.\end{aligned}$$

Following Dirac's quantization procedure [25] for a system with constraints, the above expressions must be inserted back in the light-cone Lagrangian. This leads to the expression for the Lagrangian²⁶ and the light-cone Hamiltonian as

$$\begin{aligned}\tilde{\mathcal{H}} = &\frac{1}{2} \left\{ g J_a^+ - [\mathcal{D}_i (\partial^+ A^i)]_a \right\} \frac{1}{(\partial^+)^2} \left\{ g J_a^+ - [\mathcal{D}_i (\partial^+ A^i)]_a \right\} + \\ &+ \frac{i}{\sqrt{2}} \psi_+^\dagger \left(m - i\vec{\gamma}_\perp \vec{D}_\perp \right) \frac{1}{\partial^+} \left(m + i\vec{\gamma}_\perp \vec{D}_\perp \right) \psi_+ - \frac{1}{4} F_a^{ij} F_{ij}^a.\end{aligned}$$

One may now proceed to quantize the dynamical gluonic fields as

$$A_a^\mu(x^+, \vec{x}) = \int_{k^+ > 0} \frac{dk^+ d^2 k_\perp}{\sqrt{(2\pi)^3 2k^+}} \sum_\lambda \left[a_a^\lambda(x^+, \vec{k}) \epsilon_\lambda^\mu(\vec{k}) e^{-i\vec{k} \cdot \vec{x}} + a_a^{\lambda\dagger}(x^+, \vec{k}) \epsilon_\lambda^{\mu\dagger}(\vec{k}) e^{i\vec{k} \cdot \vec{x}} \right].$$

These fields and the corresponding conjugate momenta obey canonical equal light-cone commutation relations

$$\begin{aligned}[A_a^i(x), A_b^j(y)]_{x^+ = y^+} &= 0, \quad [\Pi_{A_a^i}(x), \Pi_{A_b^j}(y)]_{x^+ = y^+} = 0, \\ [A_a^i(x), \Pi_{A_b^j}(y)]_{x^+ = y^+} &= i\delta_{ab}\delta^{ij}\delta(x^- - y^-)\delta(\vec{x}_\perp - \vec{y}_\perp),\end{aligned}$$

which follow from the fundamental commutation relations satisfied by the bosonic creation and annihilation operators²⁷

$$\begin{aligned}[a_a^\lambda(x^+, \vec{k}), a_b^{\lambda'}(x^+, \vec{k}')] &= 0, \quad [a_a^{\lambda\dagger}(x^+, \vec{k}), a_b^{\lambda'\dagger}(x^+, \vec{k}')] = 0, \\ [a_a^\lambda(x^+, \vec{k}), a_b^{\lambda'\dagger}(x^+, \vec{k}')] &= \delta_{ab}\delta^{\lambda\lambda'}\delta(k^+ - k'^+)\delta(\vec{k}_\perp - \vec{k}'_\perp).\end{aligned}$$

Similarly, one may quantize the fermionic field²⁸ ψ_+ .

These quantized fields shall be used in a later section to compute an important observable for the saturation phenomena, namely the gluon occupation number of a high energy nucleus. But first, let us briefly introduce some basic concepts about saturation physics.

26: After collecting the results from Equations (A.26) and (A.29).

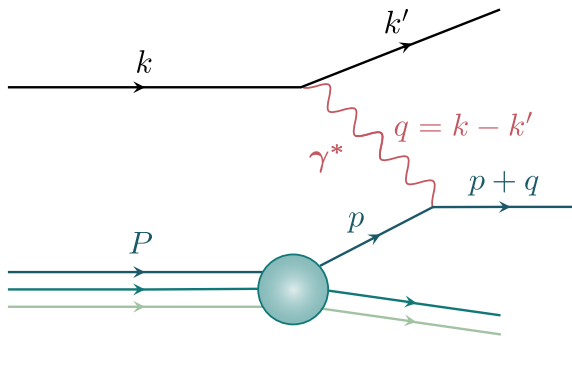
27: The index $\lambda = \pm 1$ labels the polarization vectors

$$\epsilon_\lambda^\mu = \left(0, \frac{\epsilon_\lambda \cdot k}{k^+}, \epsilon_\lambda \right).$$

28: See Equation (A.33), with elementary fermionic creation and annihilation obeying the anti-commutation relations from Equation (A.34).

2.3 Small- x landscape

Deep inelastic scattering or simply DIS offers insight about the structure of highly energetic protons and provide key features towards understanding the behaviour of QCD at high energies. We shall briefly²⁹ consider the DIS of an electron off a proton.



Let $Q^2 \stackrel{\Delta}{=} -q^2$ denote the virtuality of the photon.³⁰ One may construct another kinematic invariant, called the **Bjorken-x** variable, as³¹

$$x \stackrel{\Delta}{=} \frac{Q^2}{2P \cdot q} = \frac{Q^2}{s + Q^2 - M^2} \simeq \frac{Q^2}{s + Q^2}.$$

From this relation, one may immediately conclude that the high energy limit $s \gg Q^2$ is equivalent to having small- x values $x \ll 1$.

Further, let us work in a certain IMF for the proton³² where its longitudinal momentum is chosen to be null. In such a frame, called the Breit frame, the photon is actually mostly transverse,³³ that is $Q^2 \simeq q_\perp^2$. The virtuality Q^2 , and consequently the transverse virtuality of the photon, may thus be experimentally varied.

Moreover, one may prove [26] that the photon only interacts with partons having a transverse momentum smaller than its virtuality, that is $k_\perp^2 \lesssim Q^2$. Using Heisenberg's uncertainty principle, this is equivalent to constraining partons to belong to a transverse area of $r_\perp^2 \sim 1/Q^2$.

From all these considerations, one may assign a more physical interpretation to Q^2 as being the resolution with which the constituents of the proton are being probed.

29: For a more detailed review, one may consult [14, 26].

Figure 2.1: Diagram depicting a DIS between an electron with momentum k and a proton P , which takes place through a highly virtual photon γ^* , which then interacts with a parton p within the proton. By measuring the final k' of the electron, one may extract information about the structure of the proton.

30: DIS occurs when $Q^2 \gg M^2$, with M being the proton mass.

31: Where $s \stackrel{\Delta}{=} (P + q)^2$ is the center of mass energy.

32: In an infinite momentum frame, most of the proton momentum is carried along the collision axis $P \rightarrow \infty$, where

$$\begin{aligned} P^\mu &= \left(\sqrt{P^2 + M^2}, \vec{P}_\perp, P \right) \\ &\simeq \left(P, \vec{0}_\perp, P \right). \end{aligned}$$

33: The Breit frame fixes the photon $q^\mu = (q^0, \vec{q}_\perp, 0)$ but

$$q_0 = \frac{P \cdot q}{P} \xrightarrow{P \rightarrow \infty} 0.$$

34: Which is parametrized as

$$\sigma_{\gamma^* p} = \frac{4\pi^2 \alpha_{\text{em}}}{Q^2} F_2(x, Q^2),$$

where $F_2(x, Q^2)$ is the proton structure function.

By measuring the virtual photon-proton cross section,³⁴ one may extract information about the proton structure function and thus obtain parton distribution functions.

This may be done after expressing

$$F_2(x, Q^2) = \sum_f e_f^2 [xq_f(x, Q^2) + x\bar{q}_f(x, Q^2)],$$

where $xq_f(x, Q^2)$ and $x\bar{q}_f(x, Q^2)$ denote the quark and anti-quark distribution functions. At moderate x values, the structure function $F_2(x, Q^2)$ remains almost constant while varying Q^2 , feature known as Bjorken scaling.³⁵

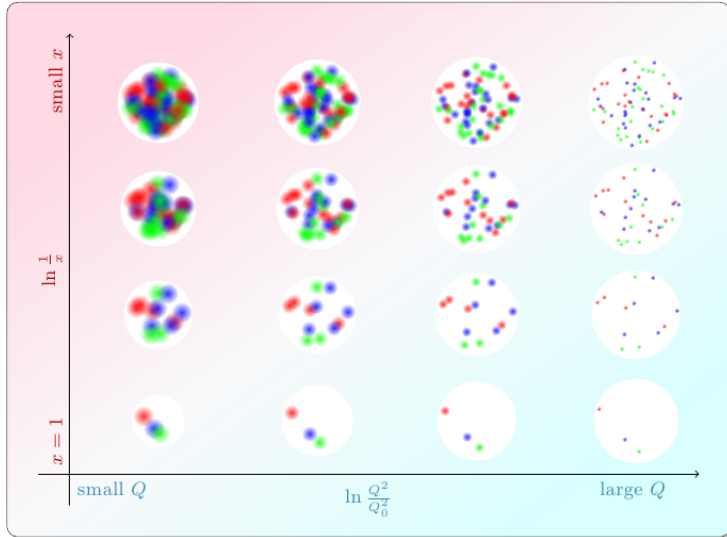
³⁵: This scaling is violated when further increasing Q^2 and radiative corrections to DIS must be taken into account.

Figure 2.2: Diagram with the phase-space available through DIS, in terms of $\ln 1/x$ and $\ln Q^2$, taken from [27]. A proton at low energies, consisting of three valence quarks, is shown in the left lower corner. As Q increases, one may probe quarks with smaller transverse resolutions. As x decreases, more gluons are produced until at very small- x values a regime of gluon saturation is reached.

³⁶: Which describes to leading-logarithmic the evolution of PDFs with increasing virtuality Q^2 .

³⁷: Describing how the gluon distribution functions change when going to smaller- x values.

³⁸: In the high-energy limit, this equation breaks the unitarity of the S matrix and the Froissart bound on total cross section.



The study on how the parton distribution functions change when varying Q^2 and x began with the DGLAP³⁶ and BFKL³⁷ evolutions, constructed using perturbative QCD. Nevertheless, the high-energy limit of QCD may not be governed by the BFKL equation since³⁸ it does not incorporate the phenomena of **gluon saturation**. As evidenced by the HERA measurements [28], the gluon distribution function grows rapidly when going to smaller- x values. Thus, the high-energy limit of QCD should also be an evolution towards higher gluon densities.

Since the QCD coupling constant is small at high energies, that is $\alpha \ll 1$, one would be tempted to assume that perturbation theory is applicable. Even though the system is weakly coupled, extremely high occupation numbers for the gluons may lead to an effective coupling of order unity at

very small- x values. On the other hand, high occupation numbers imply classical fields. This idea lead to the development [29–31] of the MV model, which along with the JIMWLK evolution [32] are the fundamental components of CGC [33, 34], an effective theory for high-energy QCD.

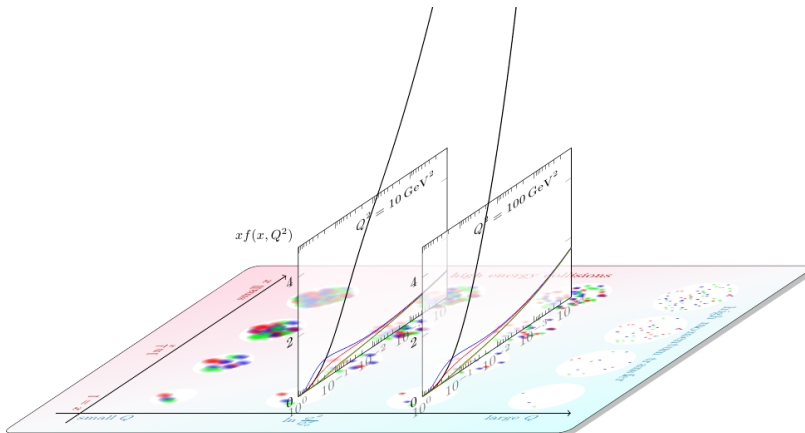


Figure 2.3: Plots with parton distribution functions superimposed over the phase-space diagram of DIS, for different values of Q^2 , taken from [27]. One may notice the dramatic growth of the gluon distribution function $xg(x, Q^2)$ when going to smaller- x values.

PREVIEW

Following the pedagogical sources [26, 33, 35–37], the MV model is introduced and then employed to obtain an analytic solution for the gluon fields generated by a single nucleus. Using the light-cone quantization of these fields, the gluon occupation factor is computed, revealing the phenomena of gluon saturation.

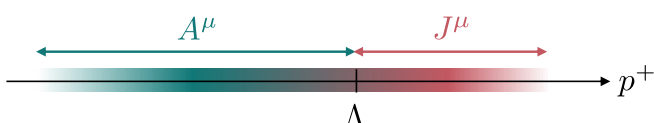
3.1 The McLerran-Venugopalan model	15
3.2 The classic color field	19
3.3 Gluon saturation from the MV model	23

3.1 The McLerran-Venugopalan model

McLerran and Venugopalan [29–31] derived a classical effective field theory which describes the gluon distribution function for a large nucleus at moderate small- x values.¹ It also provides initial conditions for the quantum evolution of the CGC towards smaller- x values.

Separation of scales

This model is formulated using light-cone coordinates² and by performing a boost to the infinite momentum frame.³ In this frame, a separation between the small- x and large- x partons exhibits itself.



A high-energy nucleus, whose radius may be parametrized as $R_A \approx R_0 A^{1/3}$, is Lorentz contracted with

$$\gamma = \frac{P_A^+}{M_A} = \frac{P^+}{M}, \quad (3.1)$$

where P_A^+ and M_A are the momentum and mass of the nucleus, whereas M is the mass of a single nucleon. Thus,

1: At higher energies, the classical approximation would break and one would need to incorporate quantum effects.

2: As defined in Equation (2.12).

3: In which the momentum of a nucleus moving along the x^+ direction is $P^+ \rightarrow \infty$.

Figure 3.1: Separation of scales between taken at an arbitrary cut-off Λ .

the nucleus is squeezed to

$$\Delta x_A^- \sim \frac{2R_A}{\gamma} \xrightarrow{(3.1)} \frac{2R_A}{MP^+}. \quad (3.2)$$

Heisenberg's uncertainty principle on the LC gives the spatial extent of a parton as⁴

$$\Delta x^- \sim \frac{1}{p^+} \xrightarrow{(3.3)} \frac{1}{xP^+}. \quad (3.4)$$

Let us compare Equations (3.2) and (3.4). For a large- x parton,⁵ that is $x \gg 1$, $\Delta x_{\text{large-}x}^- \ll \Delta x_A^-$, which means that such a parton is **well localized**. On the other hand, a small- x parton⁶ with $x \ll 1$ has $\Delta x_{\text{small-}x}^- \gg \Delta x_A^-$, which implies that it is **delocalized** along the x^+ direction.

Model for the color source

With increasing x , large- x partons radiate small- x partons. Hence, they act as color sources for the small- x degrees of freedom. Since we chose the nucleus to be moving along the light-cone direction x^+ , the generated color current will only consist of the component J^+ , hence $J^\mu \sim \delta^{\mu+}$.

We deduced⁸ that the small- x partons are delocalized, as opposed to the large- x partons. This implies that the small- x partons see the large- x partons as belonging to an **infinitely thin sheet** of color charge, that is $J^\mu \sim \delta(x^-)$.

The small- x partons see the large- x partons as **static sources** of color charge, that is $J^\mu \neq J^\mu(x^+)$.

One may also evaluate Heisenberg's uncertainty principle as

$$\Delta x^+ \sim \frac{1}{p^-} \xrightarrow{(A.7)} \frac{2p^+}{m_\perp^2} \xrightarrow{(3.3)} \frac{2xP^+}{p_\perp^2},$$

in which we used the light-cone dispersion relation for a massless particle. Hence, $\Delta x_{\text{small-}x}^+ \ll \Delta x_{\text{large-}x}^+$, implying that on the timescale of a small- x parton, the large- x partons live considerably longer and thus appear to be frozen in time. Since their momenta are significantly greater, they radiate the small- x partons without recoil.

This particular feature also shows the **glassy behaviour** of such a nucleus.⁹

One now has a model for the light-cone color current generated by the large- x partons: $J^\mu = \delta^{\mu+}\delta(x^-)\rho(\vec{x}_\perp)$, where

4: Where we use the momentum fraction defined as

$$x \triangleq \frac{p^+}{P^+}. \quad (3.3)$$

5: For example, valence quarks are large- x partons.

6: Also referred to as wee partons.

7: This also leads to a condition for how large the small- x variable must be. More precisely, after directly plugging in Equations (3.2) and (3.4), it becomes $x \ll M/2R_A$ but since $R_A \sim A^{1/3}$, this roughly translates to

$$x \ll A^{-1/3}. \quad (3.5)$$

8: From Equations (3.2) and (3.4).

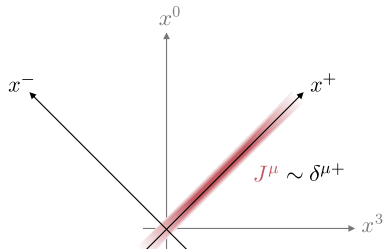


Diagram of light-cone current in the MV model.

9: It is characteristic of a glass type system to evolve slowly in time, compared to the timescales at which it is being probed.

$\rho(\vec{x}_\perp)$ is the transverse color charge associated to the distribution of these large- x partons.

Nevertheless, we are going to relax the assumption of an infinitely thin sheet and write the current as¹⁰

$$J^\mu = \delta^{\mu+} \rho(x^-, \vec{x}_\perp). \quad (3.7)$$

In the appropriate range of validity, the large- x partons may be treated as **classical random source** of color charge.

Let us consider a small- x parton interacting with the nucleus via a virtual photon. In the dipole picture of DIS, this translates to a quark-antiquark dipole probing the nucleus. If the dipole has a transverse resolution Q^2 , then it may couple to large- x partons contained in a transverse area $S_\perp = 1/Q^2$ of the nucleus.¹¹ The density of probed valence quarks per transverse area would be $n = N_c A / \pi R_A^2$, from which one may derive the total number of probed color charges as

$$\Delta N = n \Delta S_\perp = \frac{N_c A}{\pi R_A^2 Q^2} \sim \frac{\Lambda_{\text{QCD}}^2}{Q^2} N_c A^{1/3}. \quad (3.8)$$

The emerging picture is as following: there are many large- x partons¹² which act as sources of color charge and belong to different nucleons in a very large nucleus, thus being uncorrelated. Under these circumstances, one may assume that these color sources are **distributed randomly** in the transverse plane. Therefore, the average of the total color charge seen by the probe is null¹³

$$\langle \mathcal{Q}^a \rangle_A = 0. \quad (3.10)$$

The squared color charge of a single quark is $g^2 t^a t^a = g^2 C_F$ ¹⁴ multiplied with the total number of charges in the transverse plane ΔN enables us to express the two-point function of total color charges¹⁵ as

$$\langle \mathcal{Q}^a \mathcal{Q}^a \rangle_A = g^2 C_F \Delta N \xrightarrow{(3.8)} \underbrace{\frac{C_F N_c}{Q^2}}_{\triangleq \mu_A} \underbrace{\frac{g^2 A}{2\pi R_A^2}}_{\triangleq \mu_A}. \quad (3.11)$$

In the last expression we introduced μ_A , the average color charge per transverse area of the valence quarks. Because $\Delta N \gg 1$, we also have $(\mathcal{Q}^c)^2 \gg 1$. Consequently, the com-

10: Or on color components

$$J^{\mu,a} = \delta^{\mu+} \rho^a(x^-, \vec{x}_\perp), \quad (3.6)$$

where the color charge is written as $\rho(x^-, \vec{x}_\perp) = \rho^a(x^-, \vec{x}_\perp) t_a$.

11: The nucleus having a radius $R_A = R_0 A^{1/3}$ with $R_0 \sim \Lambda_{\text{QCD}}^{-1}$.

12: If the virtuality of the photon is high enough to penetrate the nucleus, that is $Q^2 \gg \Lambda_{\text{QCD}}^2$ but low enough

$$Q^2 \ll \Lambda_{\text{QCD}}^2 N_c A^{1/3}, \quad (3.9)$$

it sees a collection of many color charges $\Delta N \gg 1$.

13: On average, the nucleus must be seen as color neutral.

14: Here C_F denotes the Casimir operator in the fundamental representation of $\text{SU}(3)$, more precisely

$$C_F = \frac{N_c^2 - 1}{2N_c}.$$

15: All higher-order averages are assumed to vanish.

mutator

$$|[Q^a, Q^b]| = |if^{abc}Q^c| \ll (\mathcal{Q}^c)^2,$$

becomes negligible and we may treat the large- x as a **classical source** of color charges. These color charges enclosed in a tube of transverse size $S_\perp = 1/Q^2$ are generated by continuous a charge distribution $\rho^a(x^-, \vec{x}_\perp)$ as

$$\mathcal{Q}^a = \int_{1/Q^2} d^2\vec{x}_\perp \underbrace{\int dx^- \rho^a(x^-, \vec{x}_\perp)}_{\triangleq \rho^a(\vec{x}_\perp)}. \quad (3.12)$$

16: They may be derived by inserting Equation (3.12) in Equations (3.10) and (3.11).

$$\langle \rho^a(x^-, \vec{x}_\perp) \rangle_A = 0, \quad (3.13a)$$

$$\langle \rho^a(x^-, \vec{x}_\perp) \rho^b(y^-, \vec{y}_\perp) \rangle_A = \delta^{ab} \delta(x^- - y^-) \delta^{(2)}(\vec{x}_\perp - \vec{y}_\perp) \lambda_A(x^-), \quad (3.13b)$$

17: It is introduced through the relation $\mu_A = \int dx^- \lambda_A(x^-)$.

18: Where \mathcal{N} denotes the normalization constant.

where λ_A represents the average color charge per unit volume.¹⁷ Higher order non-vanishing correlators may be generated from a Gaussian weight functional¹⁸

$$\mathcal{W}_A[\rho] = \mathcal{N} \exp \left\{ -\frac{1}{2} \int dx^- d^2\vec{x}_\perp \frac{\rho^a(x^-, \vec{x}_\perp) \rho^a(x^-, \vec{x}_\perp)}{\lambda_A(x^-)} \right\},$$

which may be then used to compute the average of an arbitrary observable \mathcal{O} computable from the field A_μ corresponding to a configuration of the color charge ρ as

$$\langle \mathcal{O}[A_\mu] \rangle_A = \frac{\int \mathcal{D}[\rho] \mathcal{W}_A[\rho] \mathcal{O}[A_\mu]}{\int \mathcal{D}[\rho] \mathcal{W}_A[\rho]}.$$

Range of validity

19: Deduced in Equation (3.5).

20: The probability for a small- x parton, that is $x \ll 1$, to radiate a gluon is given by

$$\int_x^1 d\mathcal{P}_{\text{Bremsstrahlung}} \sim \alpha \ln \frac{1}{x}.$$

Uncertainty principle on the light-cone constraints the upper bound¹⁹ of the x value for a small- x parton to $x \ll A^{-1/3}$. On the other hand, if the small- x value is too small, the classical picture would not remain valid anymore and one would need to take into account radiative effects.²⁰ This further restricts $\ln 1/x \ll 1/\alpha$. Therefore, the MV model is

valid in the kinematic range

$$\ln A^{1/3} \ll \ln 1/x \ll 1/\alpha,$$

for a parton with a transverse resolution²¹ within

$$\Lambda_{\text{QCD}}^2 \ll Q^2 \ll \Lambda_{\text{QCD}}^2 N_c A^{1/3}.$$

3.2 The classic color field

The classical gluon fields are obtained as solutions of the colored Yang-Mills equations,²² with the current of the valence quarks expressed from the MV model.²³ This yields

$$(D_\nu F^{\nu\mu})(x^-, \vec{x}_\perp) = \delta^{\mu+} \rho(x^-, \vec{x}_\perp). \quad (3.14)$$

The fields A^+ and A^i must be independent of the light-cone time,²⁴ that is²⁵

$$\partial^- A^+ = \partial^- A^i = 0.$$

Moreover, in order for the light-cone current to be covariantly conserved,²⁶ that is $D_+ J^+ = 0$, one must also impose

$$A^- = 0. \quad (3.16)$$

This further leads to $D_j F^{ji} = 0$.

The components of the field strength tensor become

$$F^{+-} \stackrel{(3.15)}{=} \partial^+ A^- - \partial^- A^+ - ig[A^+, A^-] = 0, \quad (3.17a)$$

$$F^{i-} \stackrel{(3.15)}{=} \partial^i A^- - \partial^- A^i - ig[A^i, A^-] = 0, \quad (3.17b)$$

$$F^{i+} = \partial^i A^+ - \partial^+ A^i - ig[A^i, A^+]. \quad (3.17c)$$

Equation (3.14) for the $\mu = -$ component²⁷ is immediately satisfied

$$D_+ F^{+-} + D_i F^{i-} \stackrel{(3.17a)}{=} 0, \quad (3.17b)$$

whereas for the $\mu = i$ it yields

$$D_+ F^{+i} - D_- F^{i-} + D_j F^{ji} \stackrel{(3.17b)}{=} D_+ F^{+i} + D_j F^{ji}.$$

21: Showed in Equation (3.9).

22: As given in Equation (2.11).

23: See Equation (3.6).

24: Since the charge distribution ρ is static, it is fair to assume that this property is passed to the fields generated by this distribution.

25: Or equivalently

$$\partial^+ A^+ = \partial^+ A^i = 0. \quad (3.15)$$

26: This is not automatically assured since

$$D_+ J^+ = \partial_+ \rho - ig[A^-, \rho],$$

with $\partial_+ \rho = 0$, because the current is static, but generally $[A^-, \rho] \neq 0$.

27: For the $\mu = +$, it becomes an equation for the only non-vanishing field strength, that is

$$D_- F^{++} + D_i F^{i+} = \rho. \quad (3.18)$$

Since simple manipulations allow us to write

$$\begin{aligned} D_+ F^{+i} &\stackrel{(3.16)}{=} (\partial^- - ig A^i) F^{+i} \\ &\stackrel{(3.17c)}{=} \partial^- (\partial^i A^+ - \partial^+ A^i - ig [A^i, A^+]) \stackrel{(3.15)}{=} 0, \end{aligned}$$

which immediately leads to $D_j F^{ji} = 0$.

Therefore $F^{ij} = 0$, satisfied by a A^i which is a **pure gauge field** in the transverse plane. Such a field may be written as²⁸

28: According to Equation (2.3).

$$A^i(x^-, \vec{x}_\perp) = \frac{i}{g} W(x^-, \vec{x}_\perp) \partial^i W^\dagger(x^-, \vec{x}_\perp). \quad (3.19)$$

With these choices, the only remaining independent fields are A^+ and A^i . On top of that, one may also fix the gauge, which further reduces the number of field degrees of freedom.

Solution in the covariant gauge

29: This may be checked by simply gauge transforming the pure gauge field as

$$\begin{aligned} \tilde{A}^i &\stackrel{(2.2)}{=} U^\dagger A^i U + \frac{i}{g} U^\dagger (\partial^i U) \\ &\stackrel{(3.19)}{=} \frac{i}{g} \left[\underbrace{U^\dagger U}_{1} (\partial^i U^\dagger) U + U^\dagger (\partial^i U) \right] \\ &= \frac{i}{g} \left[\underbrace{\partial^i (U^\dagger U)}_{0} - \underbrace{U^\dagger (\partial^i U)}_{0} + \underbrace{U^\dagger (\partial^i U)}_{0} \right] = 0. \end{aligned}$$

30: A notation borrowed from the non-Abelian case.

31: The LHS of Equation (3.18) in the covariant gauge becomes

$$(\partial_i - ig \tilde{A}^i) \tilde{F}^{i+} \stackrel{(3.21)}{=} \underbrace{\partial_i \partial^i}_{-\nabla_\perp^2} \alpha,$$

where ∇_\perp^2 represents the transverse Laplace operator Δ_\perp .

32: Which is related to the color charge in the light-cone gauge through

$$\tilde{\rho} = W^\dagger \rho W. \quad (3.23)$$

From this, it follows that $\partial_i \tilde{A}^i = 0$. We previously had $\partial_+ A^+ = 0$, which also remains valid in this gauge $\partial_+ \tilde{A}^+ = 0$. Since $A^- = 0$, we will still have $\tilde{A}^- = 0$ and hence $\partial_- \tilde{A}^- = 0$. Summarizing, the fields in this particular gauge satisfy $\partial_\mu \tilde{A}^\mu = 0$, which is the condition for the **covariant gauge**.

In this gauge, the only remaining field strength tensor further simplifies to

$$\tilde{F}^{i+} \stackrel{(3.17c)}{=} \partial^i \tilde{A}^+ - \partial^+ \tilde{A}^i - ig [\tilde{A}^i, \tilde{A}^+], \quad (3.20)$$

which after introducing the notation³⁰

$$\tilde{A}^+(x^-, \vec{x}_\perp) \triangleq \alpha(x^-, \vec{x}_\perp),$$

leads to a Poisson equation in the transverse plane for the gauge field³¹

$$\Delta_\perp \alpha(x^-, \vec{x}_\perp) = -\tilde{\rho}(x^-, \vec{x}_\perp), \quad (3.22)$$

where $\tilde{\rho}$ is the color charge in the covariant gauge.³² This

equation has the following solution

$$\alpha(x^-, \vec{x}_\perp) = - \int d^2 \vec{y}_\perp \mathsf{G}_\perp(\vec{x}_\perp - \vec{y}_\perp) \rho(x^-, \vec{y}_\perp),$$

in which we introduced the Green function for the transverse Laplace operator as³³

$$\begin{aligned} \mathsf{G}_\perp(\vec{x}_\perp - \vec{y}_\perp) &\stackrel{\Delta}{=} \left\langle \vec{x}_\perp \left| \frac{1}{\nabla_\perp^2} \right| \vec{y}_\perp \right\rangle \\ &= \frac{1}{4\pi} \ln \frac{1}{(\vec{x}_\perp - \vec{y}_\perp)^2 \Lambda^2}. \end{aligned} \quad (3.24)$$

The solution of Equation (3.22) may formally be written in the Fourier space as

$$\alpha(x^-, \vec{x}_\perp) = - \int d^2 \vec{y}_\perp \int \frac{d^2 k_\perp}{(2\pi)^2} \frac{\rho(x^-, \vec{y}_\perp)}{k_\perp^2} e^{i\vec{k}_\perp(\vec{x}_\perp - \vec{y}_\perp)}.$$

Let us perform a change of variables $\vec{r}_\perp \stackrel{\Delta}{=} \vec{x}_\perp - \vec{y}_\perp$, which yields

$$\alpha(x^-, \vec{x}_\perp) = - \int d^2 \vec{r}_\perp \underbrace{\int \frac{d^2 k_\perp}{(2\pi)^2} \frac{1}{k_\perp^2} e^{i\vec{k}_\perp \vec{r}_\perp}}_{\stackrel{\Delta}{=} \mathsf{G}_\perp(\vec{r}_\perp)} \rho(x^-, \vec{x}_\perp - \vec{r}_\perp).$$

At this point, one may easily recognise the Green function for the two-dimensional Laplace equation.³⁴ The infrared divergence that appears in this expression may be artificially eliminated by considering an inferior limit to the integration, namely Λ , which then leads to³⁵

$$\mathsf{G}_\perp(\vec{r}_\perp) = \frac{1}{(2\pi)^2} \int_{\Lambda}^{\infty} \int_0^{2\pi} k_\perp dk_\perp d\theta \frac{1}{k_\perp^2} e^{ik_\perp r \cos \theta} = \frac{1}{2\pi} \int_{\Lambda}^{\infty} \frac{dk_\perp}{k_\perp} \underbrace{\frac{1}{2\pi} \int_0^{2\pi} d\theta e^{ik_\perp r \cos \theta}}_{J_0(k_\perp r)} = \frac{1}{4\pi} \ln \frac{1}{r_\perp^2 \Lambda^2}.$$

Solution in the light-cone gauge

Since we intent to use the light-cone quantization of the fields, let us perform a gauge transformation³⁶ of the gauge field from the covariant gauge $\tilde{A}^i = 0$ to the light-cone gauge

33: It is also necessary to introduce an infrared cutoff Λ .

34: Which is just the definition from Equation (3.24) written explicitly as a Fourier transform.

35: Where J_0 is the Bessel function of first kind and order zero.

36: We shall denote it as $W(x^-, \vec{x}_\perp) \in SU(N_c)$.

$A^+ = 0$ as

$$A^\mu = W^\dagger \left(\tilde{A}^\mu + \frac{i}{g} \partial^\mu \right) W.$$

37: For the $\mu = +$ component.

This gives³⁷ an equation for the gauge transformation

$$W^\dagger \left(\alpha + \frac{i}{g} \partial^+ \right) W = 0,$$

which one may recognise as the **parallel transport equation for a Wilson line** along a given path, whose solution is a path ordered exponential³⁸

$$W^\dagger(x^-, \vec{x}_\perp) = \mathcal{P} \exp \left\{ ig \int_{-\infty}^{x^-} dz^- \alpha(z^-, \vec{x}_\perp) \right\}. \quad (3.25)$$

38: Written for $\mu = i$.

40: As already guessed in Equation (3.19).

41: In the literature, it is commonly referred to as the non-Abelian Weizsäcker-Williams field [38].

42: Or equivalently in momentum space

$$F^{i+}(k) = ik^+ A^i(k). \quad (3.26)$$

43: Which is a solution of Equation (3.22).

44: As written in Equation (3.21)

45: Also for the covariant solution $\alpha(x^-, \vec{x}_\perp) = \alpha_a(x^-, \vec{x}_\perp)t^a$

The gauge transformation³⁹ provides the solution in the light-cone gauge,⁴⁰ which looks like a transverse pure gauge rotated in the color space.⁴¹ The corresponding field strength in the light-cone gauge is given by⁴²

$$F^{i+} = \partial^i A^+ - \partial^+ A^i - ig[A^i, A^+].$$

Nevertheless, it is more useful to express it in terms of the field α in the covariant gauge.⁴³ This may be achieved by performing a gauge transforming the field strength from the covariant gauge⁴⁴ as

$$F^{i+} = W^\dagger \tilde{F}^{i+} W. \quad (3.27)$$

On color components $F_a^{i+} = F_a^{i+} t^a$, this yields⁴⁵.

$$F_a^{i+}(x^-, \vec{x}_\perp) = W_{ba}(x^-, \vec{x}_\perp) \partial^i \alpha_b(x^-, \vec{x}_\perp). \quad (3.28)$$

Simple manipulations of already obtained results give

$$F_a^{i+} \xrightarrow[\substack{(3.21)}]{(3.27)} W^\dagger (\partial^i \underbrace{\alpha_b t^b}_{\alpha}) W = \underbrace{W^\dagger t^b W}_{W_{ba} t^a} \partial^i \alpha_b = \underbrace{W_{ba} \partial^i \alpha_b t^a}_{F_a^{i+}}.$$

3.3 Gluon saturation from the MV model

Computing observables

The MV model along with LC quantization provide a framework for computing the gluon distribution function, as probed in DIS experiments.

Light-cone gluon distribution

A parton which carries a momentum fraction $x = k^+ / P^+$ may probe the distribution of gluons $xG(x, Q^2)$, defined as the number of gluons contained in a transverse plane⁴⁶ of size $\Delta S_\perp \sim Q^2$

$$xG(x, Q^2) = \int_{k^+ = xP^+}^{Q^2} d^2\vec{k}_\perp k^+ \frac{dN}{dk^+ d^2\vec{k}_\perp} = \int d^3k \Theta(Q^2 - k_\perp^2) x \delta\left(x - \frac{k^+}{P^+}\right) \frac{dN}{d^3k}. \quad (3.29)$$

In the MV model, the transverse gluon fields⁴⁷ may be quantized in the light-cone gauge as⁴⁸

$$A_a^i(x^+, \vec{x}) = \int_{k^+ > 0} \frac{d^3k}{(2\pi)^3 2k^+} \left[a_a^i(x^+, \vec{k}) e^{i\vec{k} \cdot \vec{x}} + a_a^{i\dagger}(x^+, \vec{k}) e^{-i\vec{k} \cdot \vec{x}} \right],$$

with the creation and annihilation operators obeying equal light-cone time commutation relations.⁴⁹ These enables us to explicitly write the density of gluons in the Fock space as⁵⁰

$$\begin{aligned} \frac{dN}{d^3k} &= \langle a_a^{i\dagger}(x^+, \vec{k}) a_a^i(x^+, \vec{k}) \rangle \\ &= \frac{2k^+}{(2\pi)^3} \langle A_a^i(x^+, \vec{k}) A_a^i(x^+, -\vec{k}) \rangle. \end{aligned} \quad (3.30)$$

Since in the light-cone gauge the only non-vanishing field strength F^{i+} is linearly related to the A^i gauge fields,⁵¹ the gluon distribution function may further be expressed as⁵²

$$xG(x, Q^2) = \int \frac{d^2k_\perp}{4\pi^3} \Theta(Q^2 - k_\perp^2) \langle F_a^{i+}(\vec{k}) F_a^{i+}(-\vec{k}) \rangle. \quad (3.31)$$

46: Or having momenta $k_\perp < Q$. This will introduce the step function Θ .

47: See Equation (3.19).

48: Following the LC quantization, as in Equation (A.31). We introduce the notation $\vec{x}^\Delta = (x^-, \vec{x}_\perp)$.

49: See Equation (A.32).

50: The averages are taken over the hadron wavefunction.

51: As in Equation (3.26).

52: By replacing Equation (3.29) back in Equation (3.30) and making use of the fact that the fields are independent of the light-cone time. For this reason, we shall omit it in the following computations.

Gauge invariance

The above expression is not gauge invariant, which may be easily deduced by looking at the expression contained in the two-point function

$$F_a^{i+}(\vec{k})F_a^{i+}(-\vec{k}) = \int d^3x \int d^3y e^{i(\vec{x}-\vec{y})\cdot\vec{k}} \text{Tr}\{F^{i+}(\vec{x})F^{i+}(\vec{y})\}. \quad (3.32)$$

53: Written in coordinate space, it involves field strengths at different points \vec{x} and \vec{y} and thus is not gauge invariant.

54: The path γ is oriented from \vec{x} to \vec{y} .

55: With $\vec{A}^\Delta \equiv (A^+, \vec{A}_\perp)$.

Nevertheless, it may be given a gauge invariant⁵³ significance through an appropriate choice of gauge, path and boundary conditions for the gauge fields. In general, one may construct from $\text{Tr}\{F^{i+}(\vec{x})F^{i+}(\vec{y})\}$ a gauge invariant operator as⁵⁴

$$\text{Tr}\{F^{i+}(\vec{x})U_\gamma(\vec{x}, \vec{y})F^{i+}(\vec{y})U_\gamma(\vec{y}, \vec{x})\}. \quad (3.33)$$

by simply inserting Wilson lines⁵⁵

$$U_\gamma(\vec{x}, \vec{y}) = \mathcal{P} \exp \left\{ ig \int_\gamma d\vec{z} \cdot \vec{A}(z^-, \vec{z}_\perp) \right\}.$$

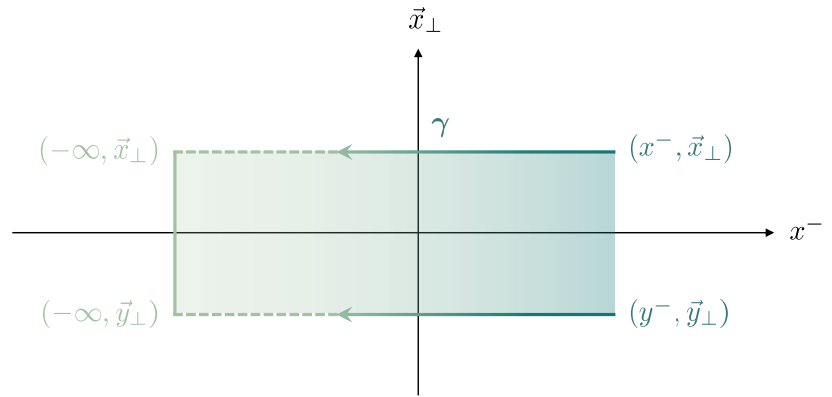


Figure 3.2: Path chosen such that the gluon distribution function will have a gauge invariant meaning.

56: With respect to x^- .

For a specific choice of the path, using the light-cone gauge $A^+ = 0$ and by imposing retarded boundary conditions⁵⁶

$$A^i(x^-, \vec{x}_\perp) \xrightarrow{x^- \rightarrow \infty} 0,$$

the term from the exponent of the Wilson line gives a null contribution

$$\int_\gamma d\vec{z} \cdot \vec{A}(z^-, \vec{z}_\perp) = \int_{y^-}^{-\infty} dz^- A^+(z^-, \vec{y}_\perp) + \int_{\vec{y}_\perp}^{\vec{x}_\perp} d^2\vec{z}_\perp \vec{A}_\perp(-\infty, \vec{z}_\perp) + \int_{-\infty}^{x^-} dz^- A^+(z^-, \vec{x}_\perp).$$

This leads to $U_\gamma(\vec{x}, \vec{y}) \rightarrow 1$ and thus the two-point function correlator which enters in the expression for the gluon distribution becomes gauge invariant.⁵⁷

Gluon occupation number

Let us define the gluon distribution in the transverse plane as⁵⁸

$$n_y(k_\perp, b_\perp) \triangleq \frac{d^5 N}{dy d^2 k_\perp d^2 b_\perp} = \frac{d^2 x G(x, k_\perp^2)}{d^2 k_\perp d^2 b_\perp}. \quad (3.34)$$

In the case of a nucleus which is homogeneous in transverse plane, the gluon density further simplifies to

$$n_y(k_\perp) \approx \frac{x G(x, Q^2)}{S_\perp} \xrightarrow{(3.31)} \frac{\langle F_a^{i+}(\vec{k}) F_a^{i+}(-\vec{k}) \rangle}{4\pi^3 S_\perp}. \quad (3.35)$$

We may construct a dimensionless quantity which encodes the gluon overlapping as⁵⁹

$$f_y(k_\perp, b_\perp) \triangleq \frac{(2\pi)^3}{2(N_c^2 - 1)} \frac{d^5 N}{dy d^2 k_\perp d^2 b_\perp} \xrightarrow{(3.34)} \frac{(2\pi)^3 n_y(k_\perp, b_\perp)}{2(N_c^2 - 1)},$$

which in the case of a transversely homogeneous nucleus reduces to

$$f_y(k_\perp) \approx \frac{(2\pi)^3 n_y(k_\perp)}{2(N_c^2 - 1)} \xrightarrow{(3.35)} \frac{\langle F_a^{i+}(\vec{k}) F_a^{i+}(-\vec{k}) \rangle}{(N_c^2 - 1)\pi S_\perp}. \quad (3.36)$$

Gluon saturation

Exact expressions for the gluon distribution⁶⁰ and gluon occupation number⁶¹ may analytically be computed in the MV model. Both involve the two-point function⁶² $\langle F_a^{i+}(\vec{x}) F_a^{i+}(\vec{y}) \rangle_A$. It is more suitable to express it as a correlator of fields in the covariant gauge⁶³

$$\langle F_a^{i+}(\vec{x}) F_a^{i+}(\vec{y}) \rangle_A = \langle (\mathcal{W}_{ab} \partial^i \alpha_b)(\vec{x}) (\mathcal{W}_{ac} \partial^i \alpha_c)(\vec{y}) \rangle_A. \quad (3.37)$$

This expectation value may be evaluated by making use of

$$\langle \alpha^a(x^-, \vec{x}_\perp) \rangle_A = 0, \quad (3.38a)$$

$$\langle \alpha^a(x^-, \vec{x}_\perp) \alpha^b(y^-, \vec{y}_\perp) \rangle_A = \delta^{ab} \delta(x^- - y^-) \lambda_A(x^-) \mathcal{L}(\vec{x}_\perp - \vec{y}_\perp), \quad (3.38b)$$

57: The gauge invariant operator from Equation (3.33) reduces to $\text{Tr}\{F^{i+}(\vec{x}) F^{i+}(\vec{y})\}$.

58: The number of gluons per unit of rapidity $y \triangleq \ln 1/x$ per unit of transverse momentum k_\perp per unit of transverse area given by the impact parameter b_\perp .

59: The number of gluons with a certain spin and color per unit rapidity and per unit of transverse phase-space.

60: From Equation (3.31)

61: As defined in Equation (3.36)

62: See Equation (3.32)

63: By using Equation (3.28)

where we introduced

$$\mathcal{L}(\vec{x}_\perp - \vec{y}_\perp) \triangleq \int \frac{d^2 \vec{k}_\perp}{(2\pi)^2} \frac{e^{i\vec{k}_\perp(\vec{x}_\perp - \vec{y}_\perp)}}{k_\perp^4}. \quad (3.39)$$

64: As given in Equations (3.13a) and (3.13b).

65: See Equation (3.24).

$$\langle \tilde{\rho}^a(x^-, \vec{x}_\perp) \rangle_A = 0, \quad (3.40a)$$

$$\langle \tilde{\rho}^a(x^-, \vec{x}_\perp) \tilde{\rho}^b(y^-, \vec{y}_\perp) \rangle_A = \delta^{ab} \delta(x^- - y^-) \delta^{(2)}(\vec{x}_\perp - \vec{y}_\perp) \lambda_A(x^-). \quad (3.40b)$$

66: From Equation (3.38a)

The vanishing expectation value of the covariant gauge field⁶⁶ is a direct consequence of

$$\begin{aligned} \langle \alpha^a(x^-, \vec{x}_\perp) \rangle_A &\stackrel{(3.22)}{=} \left\langle \frac{\tilde{\rho}^a(x^-, \vec{x}_\perp)}{-\nabla_\perp^2} \right\rangle_A \\ &\stackrel{(3.40a)}{=} - \int d^2 \vec{y}_\perp \int \frac{d^2 \vec{k}_\perp}{(2\pi)^2} \frac{\langle \tilde{\rho}(x^-, \vec{y}_\perp) \rangle_A}{k_\perp^2} e^{i\vec{k}_\perp(\vec{x}_\perp - \vec{y}_\perp)}. \end{aligned}$$

67: From Equation (3.38b)

In a similar manner, the two-point correlator⁶⁷ may be derived as

$$\begin{aligned} \langle \alpha^a(x^-, \vec{x}_\perp) \alpha^b(y^-, \vec{y}_\perp) \rangle_A &\stackrel{(3.22)}{=} \left\langle \frac{\tilde{\rho}^a(x^-, \vec{x}_\perp)}{-\nabla_\perp^2} \frac{\tilde{\rho}^b(y^-, \vec{y}_\perp)}{-\nabla_\perp^2} \right\rangle_A \\ &\stackrel{(3.40b)}{=} \int d^2 \vec{x}'_\perp \int \frac{d^2 \vec{k}_\perp}{(2\pi)^2} \frac{e^{i\vec{k}_\perp(\vec{x}_\perp - \vec{x}'_\perp)}}{k_\perp^2} \int d^2 \vec{y}'_\perp \int \frac{d^2 \vec{k}'_\perp}{(2\pi)^2} \frac{e^{i\vec{k}'_\perp(\vec{y}_\perp - \vec{y}'_\perp)}}{k'_\perp^2} \underbrace{\langle \tilde{\rho}^a(x^-, \vec{x}'_\perp), \tilde{\rho}^b(y^-, \vec{y}'_\perp) \rangle_A}_{\delta^{ab} \delta(x^- - y^-) \delta^{(2)}(\vec{x}'_\perp - \vec{y}'_\perp) \lambda_A(x^-)} \\ &= \delta^{ab} \delta(x^- - y^-) \lambda_A(x^-) \underbrace{\int d^2 \vec{x}'_\perp e^{-i\vec{x}'_\perp(\vec{k}_\perp + \vec{k}'_\perp)}}_{(2\pi)^2 \delta^{(2)}(\vec{k}_\perp + \vec{k}'_\perp)} \int \frac{d^2 \vec{k}_\perp}{(2\pi)^2} \frac{e^{i\vec{k}_\perp \vec{x}_\perp}}{\vec{k}_\perp^2} \int \frac{d^2 \vec{k}'_\perp}{(2\pi)^2} \frac{e^{i\vec{k}'_\perp \vec{y}_\perp}}{\vec{k}'_\perp^2} \\ &\stackrel{(3.39)}{=} \delta^{ab} \delta(x^- - y^-) \lambda_A(x^-) \underbrace{\int \frac{d^2 \vec{k}_\perp}{(2\pi)^2} \frac{e^{i\vec{k}_\perp(\vec{x}_\perp - \vec{y}_\perp)}}{k_\perp^4}}_{\mathcal{L}(\vec{x}_\perp - \vec{y}_\perp)}. \end{aligned}$$

68: From Equation (3.37).

Since the two-point field correlator⁶⁸ contains only terms local in x^- , it may be expressed as

$$\langle F_a^{i+}(\vec{x}) F_a^{i+}(\vec{y}) \rangle_A = \langle \partial^i \alpha_b(\vec{x}) \partial^i \alpha_c(\vec{y}) \rangle_A \langle W_{ab}(\vec{x}) W_{ac}(\vec{y}) \rangle_A. \quad (3.41)$$

The first term may further be evaluated as⁶⁹

$$\langle \partial^i \alpha_b(x^-, \vec{x}_\perp) \partial^i \alpha_c(y^-, \vec{y}_\perp) \rangle_A = \delta_{bc} \delta(x^- - y^-) \frac{\partial \mu_A(x^-)}{\partial x^-} \frac{1}{4\pi} \ln \frac{1}{r_\perp^2 \Lambda_{\text{QCD}}^2}. \quad (3.42)$$

Following the same type of computation,⁷⁰ such a term would yield

$$\begin{aligned} \langle \partial^i \alpha_b(\vec{x}) \partial^i \alpha_c(\vec{y}) \rangle_A &\stackrel{(3.39)}{=} \delta_{bc} \delta(x^- - y^-) \lambda_A(x^-) \times \\ &\times \underbrace{\int \frac{d^2 \vec{k}_\perp}{(2\pi)^2} \frac{e^{i\vec{k}_\perp(\vec{x}_\perp - \vec{y}_\perp)}}{k_\perp^2}}_{-\nabla_\perp^2 \mathcal{L}(\vec{x}_\perp - \vec{y}_\perp)}. \end{aligned}$$

Nevertheless, we recognise the already computed⁷¹ Green function for the two-dimensional Laplace operator.⁷² By rewriting the color charge density,⁷³ we obtain

$$\langle \partial^i \alpha_b(\vec{x}) \partial^i \alpha_c(\vec{y}) \rangle_A \stackrel{(3.24)}{=} \delta_{bc} \delta(x^- - y^-) \underbrace{\frac{\partial \mu_A(x^-)}{\partial x^-}}_{\lambda_A(x^-)} \frac{1}{4\pi} \ln \frac{1}{r_\perp^2 \Lambda_{\text{QCD}}^2}.$$

This further leads to⁷⁴

$$\begin{aligned} \langle F_a^{i+}(\vec{x}) F_a^{i+}(\vec{y}) \rangle_A &= \frac{\partial \mu_A(x^-)}{\partial x^-} \frac{1}{4\pi} \ln \frac{1}{r_\perp^2 \Lambda_{\text{QCD}}^2} \times \\ &\times \langle W_{ab}(x^-, \vec{x}_\perp) W_{ba}^\dagger(x^-, \vec{y}_\perp) \rangle_A. \end{aligned} \quad (3.44)$$

One may now recognise, up to a color factor, the dipole operator in the adjoint representation

$$D_A(x^-, \vec{r}_\perp) \stackrel{\Delta}{=} \frac{1}{N_c^2 - 1} \left\langle \text{Tr} \{ W(x^-, \vec{x}_\perp) W^\dagger(x^-, \vec{y}_\perp) \} \right\rangle_A. \quad (3.45)$$

In the MV model, it may approximately be computed as

$$D_A(x^-, \vec{r}_\perp) \approx \exp \left\{ -\frac{r_\perp^2}{4} Q_s^2(x^-, \vec{r}_\perp) \right\}, \quad (3.46)$$

where we introduced the saturation momentum of the gluons

$$Q_s^2(x^-, \vec{r}_\perp) \stackrel{\Delta}{=} \alpha_s N_c \mu_A(x^-) \ln \frac{1}{r_\perp^2 \Lambda_{\text{QCD}}^2}. \quad (3.47)$$

69: We introduce the notation $\vec{r}_\perp \stackrel{\Delta}{=} \vec{x}_\perp - \vec{y}_\perp$.

70: Writing the fields in terms of the color charges from Equation (3.22), working in the Fourier space and using the correlator of such charges from Equation (3.40b)

71: See Equation (3.24), from which it follows that

$$-\nabla_\perp^2 \mathcal{L}(\vec{r}) = G_\perp(\vec{r}_\perp).$$

72: With $\Lambda = \Lambda_{\text{QCD}}$.

73: The color charge density per transverse area may be obtained from the color charge density as

$$\mu_A(x^-) = \int_{-\infty}^{x^-} dz^- \lambda_A(z^-). \quad (3.43)$$

74: By inserting the result from Equation (3.42) back in Equation (3.41).

We aim to compute the following quantity

$$\frac{\partial D_A(x^-, \vec{r}_\perp)}{\partial x^-} = \lim_{\epsilon \rightarrow 0} \frac{D_A(x^- + \epsilon, \vec{r}_\perp) - D_A(x^-, \vec{r}_\perp)}{\epsilon}. \quad (3.48)$$

Let us begin by discretizing the Wilson line along the direction $x^- \stackrel{\Delta}{=} n\epsilon$, such that the Wilson line at a later $x^- + \epsilon$ is obtained by applying a gauge rotation to the Wilson line at x^- as

$$\mathcal{P} \exp \left\{ ig \int_{-\infty}^{x^- + \epsilon} dz^- \alpha(z^-, \vec{z}_\perp) \right\} = \mathcal{P} \exp \left\{ ig \int_{-\infty}^{x^-} dz^- \alpha(z^-, \vec{z}_\perp) \right\} \exp \left\{ ig \int_{x^-}^{x^- + \epsilon} dz^- \alpha(z^-, \vec{z}_\perp) \right\},$$

or equivalently, since ϵ is an infinitesimal parameter

$$W(x^- + \epsilon, \vec{z}_\perp) \approx W(x^-, \vec{z}_\perp) \left\{ 1 + ig\epsilon \alpha_a(x^-, \vec{z}_\perp) t^a + \frac{1}{2!} (ig)^2 \epsilon^2 [\alpha_a(x^-, \vec{z}_\perp) t^a]^2 \right\}. \quad (3.49)$$

With this discretization, the one and two-point correlators⁷⁵ become⁷⁶

$$\langle \alpha_a(x^-, \vec{x}_\perp) \rangle_A = 0, \quad (3.50a)$$

$$\langle \alpha_a(x^-, \vec{x}_\perp) \alpha_b(y^-, \vec{y}_\perp) \rangle_A = \delta_{ab} \frac{\delta_{nm}}{\epsilon} \lambda_A(x^-) L(\vec{x}_\perp - \vec{y}_\perp). \quad (3.50b)$$

One may now proceed to evaluating

$$\begin{aligned} D_A(x^- + \epsilon, \vec{r}_\perp) &\stackrel{(3.45)}{=} \frac{1}{N_c^2 - 1} \left\langle \text{Tr} \{ W(x^- + \epsilon, \vec{x}_\perp) W^\dagger(x^- + \epsilon, \vec{y}_\perp) \} \right\rangle_A \\ &\stackrel{(3.49)}{=} \frac{1}{N_c^2 - 1} \text{Tr} \left\langle W(x^-, \vec{x}_\perp) \left[1 + ig\epsilon \alpha_a(x^-, \vec{x}_\perp) t^a - \frac{g^2}{2} \epsilon^2 \alpha_a(x^-, \vec{x}_\perp) t^a \alpha_b(x^-, \vec{x}_\perp) t^b \right] \times \right. \\ &\quad \times \left. \left[1 - ig\epsilon \alpha_a(x^-, \vec{y}_\perp) t^a - \frac{g^2}{2} \epsilon^2 \alpha_a(x^-, \vec{y}_\perp) t^a \alpha_b(x^-, \vec{y}_\perp) t^b \right] W^\dagger(x^-, \vec{y}_\perp) \right\rangle_A \\ &\stackrel{(3.45)}{=} D_A(x^-, \vec{r}_\perp) \left\{ 1 + \frac{g^2}{2} \epsilon^2 \text{Tr} \left\langle [\alpha_a(x^-, \vec{x}_\perp) t^a]^2 + [\alpha_b(x^-, \vec{y}_\perp) t^b]^2 - 2 \alpha_a(x^-, \vec{x}_\perp) t^a \alpha_b(x^-, \vec{y}_\perp) t^b \right\rangle_A \right\} \\ &\stackrel{(3.50b)}{=} D_A(x^-, \vec{r}_\perp) \left\{ 1 + \frac{g^2}{2} \epsilon^2 \left[\underbrace{\langle \alpha_a(x^-, \vec{x}_\perp) \alpha_a(x^-, \vec{x}_\perp) \rangle_A (t^a)^2}_{\lambda_A(x^-) L(\vec{0}_\perp)/\epsilon} + \underbrace{\langle \alpha_b(x^-, \vec{y}_\perp) \alpha_b(x^-, \vec{y}_\perp) \rangle_A (t^b)^2}_{\lambda_A(x^-) L(\vec{0}_\perp)/\epsilon} - \right. \right. \\ &\quad \left. \left. - 2 \underbrace{\langle \alpha_a(x^-, \vec{x}_\perp) \alpha_b(x^-, \vec{y}_\perp) \rangle_A t^a t^b}_{\delta_{ab} \lambda_A(x^-) L(\vec{x}_\perp - \vec{y}_\perp)/\epsilon} \right] \right\} = D_A(x^-, \vec{r}_\perp) \left\{ 1 + \epsilon g^2 \underbrace{(t^a)^2}_{N_c} \lambda_A(x^-) [L(\vec{0}_\perp) - L(\vec{r}_\perp)] \right\} \end{aligned}$$

75: As written in Equations (3.38a) and (3.38b).

76: For $x^- = n\epsilon$ and $y^- = m\epsilon$, the delta function becomes

$$\delta(x^- - y^-) = \frac{\delta_{nm}}{\epsilon}.$$

This gives⁷⁷ a differential equation for the dipole operator

$$\frac{\partial D_A(x^-, \vec{r}_\perp)}{\partial x^-} = D_A(x^-, \vec{r}_\perp) \left\{ g^2 N_c \lambda_A(x^-) [L(\vec{0}_\perp) - L(\vec{r}_\perp)] \right\},$$

whose solution is given by

$$D_A(x^-, \vec{r}_\perp) \xrightarrow{(3.43)} \exp \left\{ -g^2 N_c \underbrace{\int_{-\infty}^{x^-} dz^- \lambda_A(z^-) [L(\vec{0}_\perp) - L(\vec{r}_\perp)]}_{\mu_A(x^-)} \right\}.$$

Nevertheless, in the small momenta regime, one may compute the term from the exponent as

$$\begin{aligned} L(\vec{0}_\perp) - L(\vec{r}_\perp) &\xrightarrow{(3.39)} \int \frac{d^2 \vec{k}_\perp}{(2\pi)^2} \frac{1}{k_\perp^4} \left(1 - e^{i \vec{k}_\perp \cdot \vec{r}_\perp} \right) \approx \int \frac{d^2 \vec{k}_\perp}{(2\pi)^2} \frac{1}{k_\perp^4} \cancel{k_\perp^2} r_\perp^2 \cos^2 \theta \\ &= \frac{r_\perp^2}{8\pi^2} \underbrace{\int_0^\pi d\theta \cos^2 \theta}_{\cancel{1/2}} \underbrace{\int_{\Lambda^2}^{1/r_\perp^2} dk_\perp \cancel{k_\perp^2} \frac{1}{k_\perp^4}}_{\ln 1/(r_\perp^2 \Lambda^2)} = \frac{r_\perp^2}{16\pi} \ln \frac{1}{r_\perp^2 \Lambda^2}. \end{aligned}$$

This eventually gives⁷⁸

$$D_A(x^-, \vec{r}_\perp) \approx \exp \left\{ -\frac{r_\perp^2}{4} \underbrace{\frac{\alpha_s}{4\pi} N_c \mu_A(x^-) \ln \frac{1}{r_\perp^2 \Lambda^2}}_{Q_s^2(x^-, \vec{r}_\perp)} \right\}. \quad (3.51)$$

77: By plugging the result obtained above back in Equation (3.48)

78: After using the definition of the saturation momentum from Equation (3.47).

We may finally compute the correlator

$$\langle F_a^{i+}(\vec{k}) F_a^{i+}(-\vec{k}) \rangle_A = \frac{2S_\perp C_F}{\alpha_s \pi} \int d^2 \vec{r}_\perp \frac{e^{i \vec{k}_\perp \cdot \vec{r}_\perp}}{r_\perp^2} \left(1 - \exp \left\{ -\frac{r_\perp^2}{4} Q_s^2(r_\perp) \right\} \right). \quad (3.52)$$

Let us successively collect all of the obtained results and write

$$\begin{aligned}
\langle F_a^{i+}(\vec{k}) F_a^{i+}(-\vec{k}) \rangle_A &\stackrel{(3.32)}{=} \int d^3x \int d^3y e^{i(\vec{x}-\vec{y}) \cdot \vec{k}} \langle F_a^{i+}(\vec{x}) F_a^{i+}(\vec{y}) \rangle_A \\
&\stackrel{(3.44)}{=} \int dx^- \int d^2\vec{x}_\perp \int d^2\vec{y}_\perp e^{i(\vec{x}_\perp - \vec{y}_\perp) \cdot \vec{k}_\perp} \frac{\partial \mu_A(x^-)}{\partial x^-} \frac{1}{4\pi} \ln \frac{1}{r_\perp^2 \Lambda_{\text{QCD}}^2} (N_c^2 - 1) D_A(x^-, \vec{r}_\perp) \\
&\stackrel{(3.45)}{=} \frac{N_c^2 - 1}{4\pi} \underbrace{\int d^2\vec{x}_\perp}_{S_\perp} \int d^2\vec{r}_\perp e^{i\vec{r}_\perp \cdot \vec{k}_\perp} \int dx^- \frac{\partial \mu_A(x^-)}{\partial x^-} \ln \frac{1}{r_\perp^2 \Lambda_{\text{QCD}}^2} \exp \left\{ -\frac{r_\perp^2}{4} \alpha_s N_c \mu_A(x^-) \ln \frac{1}{r_\perp^2 \Lambda_{\text{QCD}}} \right\}
\end{aligned}$$

By performing the change of variables

$$\tilde{\mu}_A(x^-) \triangleq 1 - \exp \left\{ -\frac{r_\perp^2}{4} \alpha_s N_c \mu_A(x^-) \ln \frac{1}{r_\perp^2 \Lambda_{\text{QCD}}} \right\},$$

we immediately obtain

$$\frac{\partial \tilde{\mu}_A(x^-)}{\partial x^-} = -\frac{r_\perp^2}{4} \alpha_s N_c \frac{\partial \mu_A(x^-)}{\partial x^-} \ln \frac{1}{r_\perp^2 \Lambda_{\text{QCD}}^2} \exp \left\{ -\frac{r_\perp^2}{4} \alpha_s N_c \mu_A(x^-) \ln \frac{1}{r_\perp^2 \Lambda_{\text{QCD}}} \right\}$$

which after simple manipulations leads to

$$\begin{aligned}
\langle F_a^{i+}(\vec{k}) F_a^{i+}(-\vec{k}) \rangle_A &= \frac{N_c^2 - 1}{4\pi} S_\perp \int d^2\vec{r}_\perp e^{i\vec{r}_\perp \cdot \vec{k}_\perp} \frac{4}{r_\perp^2 \alpha_s N_c} \underbrace{\int dx^- \frac{\partial \tilde{\mu}_A(x^-)}{\partial x^-}}_{\tilde{\mu}_A(x^-)} \\
&= \underbrace{\frac{2S_\perp}{\alpha_s \pi} \frac{N_c^2 - 1}{2N_c}}_{C_F} \int d^2\vec{r}_\perp \frac{e^{i\vec{k}_\perp \cdot \vec{r}_\perp}}{r_\perp^2} \left(1 - \exp \left\{ -\frac{r_\perp^2}{4} \alpha_s N_c \mu_A(x^-) \ln \frac{1}{r_\perp^2 \Lambda_{\text{QCD}}} \right\} \right)
\end{aligned}$$

79: With $r_\perp < 1/\Lambda_{\text{QCD}}$, such that the quantity $\ln 1/r_\perp^2 \Lambda_{\text{QCD}}^2$ from the exponent doesn't change the sign.

This enables us to evaluate the gluon occupation number, as obtained from the MV model⁷⁹

$$f(k_\perp) \stackrel{(3.36)}{=} \int d^2\vec{r}_\perp e^{i\vec{k}_\perp \cdot \vec{r}_\perp} \frac{1 - \exp \left\{ -\frac{r_\perp^2}{4} Q_s^2(r_\perp) \right\}}{\pi \alpha_s N_c r_\perp^2}. \quad (3.53)$$

Two regimes distinguish themselves, namely one in which the exponent is higher than unity, where saturation occurs, and one where the exponent is sub-unitary, known as the dilute regime. It will turn out useful to define

$$Q_A^2 \triangleq \alpha_s N_c \mu_A \stackrel{(3.11)}{=} \alpha_s N_c \frac{A}{2\pi R_A^2} \underbrace{4\pi \alpha_s^2}_{g^2} = \frac{2\alpha_s^2 N_c A}{R_A^2} \sim A^{1/3},$$

such that the saturation momentum⁸⁰ may be rewritten as

80: Defined in Equation (3.47).

$$Q_s^2(A, r_\perp) = Q_A^2 \ln \frac{1}{r_\perp^2 \Lambda_{\text{QCD}}}.$$

The **saturation momentum** is the scale which separates the two regimes and it is customary defined as the value at which, for

$$Q_s(A) \triangleq Q_s \left(A, r_\perp \triangleq \frac{2}{Q_s(A)} \right),$$

the exponent reaches unity, that is

$$-\frac{r_\perp^2}{4} Q_A^2 \ln \frac{1}{r_\perp^2 \Lambda_{\text{QCD}}} \Big|_{r_\perp=2/Q_s(A)} \approx 1.$$

This yields the saturation scale

$$Q_s^2(A) \approx Q_A^2 \ln \frac{Q_A^2}{\Lambda_{\text{QCD}}^2} \sim A^{1/3} \ln A^{1/3}.$$

With respect to this saturation scale, the gluon occupation factor⁸¹ behaves as

81: From Equation (3.53)

$$f(k_\perp) \approx \begin{cases} \frac{1}{\alpha N_c} \frac{Q_A^2}{k_\perp^2} \left\{ 1 + \frac{Q_A^2}{k_\perp^2} \left[\ln \frac{k_\perp^2}{\Lambda_{\text{QCD}}^2} + 2\gamma_E - 2 \right] \right\} \sim \frac{A^{1/3}}{k_\perp^2}, & \text{for } k_\perp \gg Q_s(A) \\ \frac{1}{\alpha N_c} \ln \frac{Q_s^2(A)}{k_\perp^2} \sim \ln \frac{A^{1/3}}{k_\perp^2}, & \text{for } k_\perp \ll Q_s(A) \end{cases}$$

In the dense limit, this factor grows only logarithmically and is thus said to reach a saturation regime.

4

SIMULATING THE GLASMA

PREVIEW

The Glasma fields which arise from the collision of two nuclei are described using the previously derived solution for a single nucleus. Initial conditions and equations of motion are derived in the boost-invariant approximation. These are then discretized using principles from real-time lattice gauge theory and then numerically simulated. Details about implementation, numerical parameters, observables are provided, along with results tuned for RHIC collisions of Au+Au nuclei at $\sqrt{s_{NN}} = 200$ GeV.

4.1 Boost-invariant Glasma	33
4.2 Lattice gauge theory	44
4.3 Numerical simulation	48

4.1 Boost-invariant Glasma

Generalized MV model

In the original MV model, the small- x partons see the large- x partons as being distributed on an infinitely thin color sheet. The associated color current is thus generated as¹

$$J^\mu(x) = \delta^{\mu+} \delta(x^-) \rho(\vec{x}_\perp) \quad (4.1)$$

The one-point and two-point functions of the color charge reduce to²

$$\begin{aligned} \langle \rho^a(\vec{x}_\perp) \rangle_A &= 0, \\ \langle \rho^a(\vec{x}_\perp) \rho^b(\vec{y}_\perp) \rangle_A &= \mu^2 \delta^{ab} \delta^{(2)}(\vec{x}_\perp - \vec{y}_\perp), \end{aligned}$$

where μ represents the average color charge per unit surface and is usually referred to as the MV parameter. The transverse pure gauge fields are given by³

$$A^i(x^-, \vec{x}_\perp) = \theta(x^-) \alpha^i(\vec{x}_\perp), \quad (4.2)$$

where we introduced the notation

$$\alpha^i(\vec{x}_\perp) \triangleq \frac{i}{g} V(\vec{x}_\perp) \partial^i V^\dagger(\vec{x}_\perp), \quad (4.3)$$

1: In comparison with the current from Equation (3.7).

2: As opposed to the more general correlators from Equation (3.13a) and (3.13b).

3: Similarly to Equation (3.19).

4: Since it's the more general Wilson line from Equation (3.25) in the limit $x^- \rightarrow \infty$.

5: In analogy with Equation (3.22). The color charge from the covariant gauge may be expressed in terms of the light-cone gauge one as $\tilde{\rho} = V^\dagger \rho V$, as in Equation (3.24).

6: For this reason, all the computations from Chapter 3 were performed in this framework.

7: For which the one-point and two-point correlators are given in Equations (3.13a) and (3.13b).

8: Because of $\delta(x^- - y^-)$ from the two-point correlator given in Equation (3.13b).

9: As in Equation (4.4).

10: See Equations (4.2) and (4.3).

with the asymptotic Wilson line⁴ expressed as

$$\begin{aligned} V^\dagger(\vec{x}_\perp) &\stackrel{\Delta}{=} \lim_{x^- \rightarrow \infty} W^\dagger(x^-, \vec{x}_\perp) \\ &\stackrel{(3.25)}{=} \mathcal{P} \exp \left\{ ig \int_{-\infty}^{\infty} dx^- \alpha(x^-, \vec{x}_\perp) \right\}. \end{aligned}$$

Here the light-cone gauge solution satisfies a transverse Poisson equation⁵

$$\Delta_\perp \alpha(\vec{x}_\perp) = -\tilde{\rho}(\vec{x}_\perp). \quad (4.4)$$

Nevertheless, for very small- x values, it is more appropriate to consider a color charge with finite longitudinal support⁶ $\rho(x^-, \vec{x}_\perp)$, as emphasized in [39]. In this generalized MV model⁷ the nucleus may be thought of as being composed of a multitude of uncorrelated infinitely thin sheets of color charge.⁸ One may not recover the single sheet approximation from the generalized MV model by simply taking the limit $\rho(x^-, \vec{x}_\perp) \rightarrow \delta(x^-) \rho(\vec{x}_\perp)$.

As argued in [40], one may construct a two-point charge correlator as

$$\langle \rho_n^a(\vec{x}_\perp) \rho_m^b(\vec{y}_\perp) \rangle_A = \mu^2 \frac{\delta_{nm}}{N_s} \delta^{ab} \delta^{(2)}(\vec{x}_\perp - \vec{y}_\perp), \quad (4.5)$$

where $n, m \in \overline{1, N_s}$ denote the indices of the color sheets and N_s the total number of these stacked sheets of color charge. Each color charge obeys a Poisson equation⁹

$$\Delta_\perp \alpha_n(\vec{x}_\perp) = -\tilde{\rho}_n(\vec{x}_\perp). \quad (4.6)$$

The fields generated by such a color sheet are also given by¹⁰

$$A_n^i(x^-, \vec{x}_\perp) = \frac{i}{g} \theta(x^-) V(\vec{x}_\perp) \partial^i V^\dagger(\vec{x}_\perp),$$

with the Wilson line

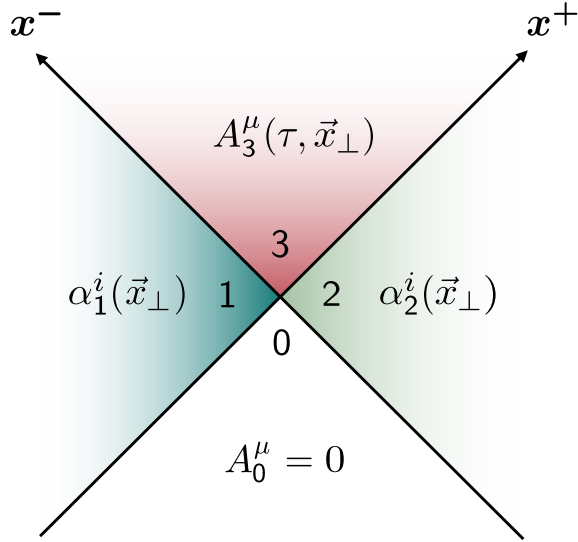
$$V^\dagger(\vec{x}_\perp) = \prod_{n=1}^{N_s} \exp \{ ig \alpha_n(\vec{x}_\perp) \}. \quad (4.7)$$

For $N_s = 1$, one obtains the original MV model, while $N_s \rightarrow \infty$ gives the proper ultrarelativistic limit of the generalized MV model. As we shall see, N_s will further appear as a

numerical parameter.¹¹

Constructing the glasma fields

The MV model provides an expression for the classical gauge fields generated by a high-energy nucleus. This analytic solution, which describes the color fields before a collision occurs, may be used to model the melting of the CGC during the collision of ultrarelativistic nuclei.



¹¹: It will influence the relation between the MV parameter μ and the saturation momentum Q_s .

Figure 4.1: Light-cone diagram of a collision in the MV model, where 4 regions distinguish themselves. The Glasma fields produced in the forward light-cone shall further be studied.

This may be schematically represented in a light-cone diagram, in which 4 regions emerge. In region 0, since it is enclosed in the past light-cone and is thus causally disconnected from the others, the gauge field may be set to be null $A_0^\mu = 0$. In regions 1 and 2, one may employ the MV solutions and express the fields as¹²

$$A_{1,2}^i(x^\mp, \vec{x}_\perp) = \frac{i}{g} W_{1,2}(x^\mp, \vec{x}_\perp) \partial^i W_{1,2}^\dagger(x^\mp, \vec{x}_\perp), \quad (4.8)$$

expressed in terms of the Wilson lines

$$W_{1,2}^\dagger(x^\mp, \vec{x}_\perp) = \mathcal{P} \exp \left\{ -ig \int_{-\infty}^{x^\mp} dz^\mp \frac{1}{\nabla_\perp^2} \tilde{\rho}_{1,2}(z^\mp, \vec{x}_\perp) \right\}.$$

Let us recall that¹³

$$A_1^i(x^-, \vec{x}_\perp) \xrightarrow{(3.19)} \frac{i}{g} W_1(x^-, \vec{x}_\perp) \partial^i W_1^\dagger(x^-, \vec{x}_\perp),$$

¹²: Notice that we write the most general solution, without employing the previously introduced generalization of the MV model.

¹³: For a nucleus, which we shall label with 1, moving along the x^+ axis, working in the light-cone gauge $A_1^+ = 0$, with only transverse color fields A_1^i generated by a color charge distribution ρ_1 .

with the Wilson line given by

$$W_1^\dagger(x^-, \vec{x}_\perp) \xrightarrow[(3.22)]{(3.25)} \mathcal{P} \exp \left\{ -ig \int_{-\infty}^{x^-} dz^- \frac{1}{\nabla_\perp^2} \tilde{\rho}_1(z^-, \vec{x}_\perp) \right\}.$$

In a similar manner, one may write the fields produced by the other nucleus¹⁴

$$A_2^i(x^+, \vec{x}_\perp) = \frac{i}{g} W_2(x^+, \vec{x}_\perp) \partial^i W_2^\dagger(x^+, \vec{x}_\perp),$$

with the Wilson line given by

$$W_2^\dagger(x^+, \vec{x}_\perp) = \mathcal{P} \exp \left\{ -ig \int_{-\infty}^{x^+} dz^+ \frac{1}{\nabla_\perp^2} \tilde{\rho}_2(z^+, \vec{x}_\perp) \right\}.$$

These fields generated from region 3 are conventionally named the **Glasma** color fields. They are generated by the total color current

$$\begin{aligned} J_3^\mu(x) &= J_1^\mu(x) + J_2^\mu(x) \\ &\stackrel{(3.7)}{=} \delta^{\mu+} \rho_1(x^-, \vec{x}_\perp) + \delta^{\mu-} \rho_2(x^+, \vec{x}_\perp). \end{aligned}$$

As we shall see, the Glasma fields may be written in terms of the single-nucleus solutions,¹⁵ with the appropriate boundary conditions and equations of motion.

We may further employ the infinitely thin sheet approximation¹⁶ and express the fields as¹⁷

$$A_{1,2}^i(x^\mp, \vec{x}_\perp) = \theta(x^\mp) \alpha_{1,2}^i(\vec{x}_\perp).$$

Before the collision, the fields from regions 0, 1 and 3 may be written in a compact manner, by stitching together the fields generated by the two nuclei, as

$$\begin{aligned} A_{0,1,2}^\pm(x) &= 0, \\ A_{0,1,2}^i(x) &= \theta(-x^+) \theta(x^-) \alpha_1^i(\vec{x}_\perp) + \theta(x^+) \theta(-x^-) \alpha_2^i(\vec{x}_\perp). \end{aligned} \tag{4.9}$$

In regions 1 and 2, one imposes the light-cone gauge fixing $A_1^+ = A_2^- = 0$. Recall that, in order for the light-cone current to be covariantly conserved,¹⁸ one must also choose¹⁹ $A_1^- = 0$, and analogously $A_2^+ = 0$. These relations should remain valid at the boundary between region 3 and regions 1 and 2. For

18: And not to experience a color rotation.

19: See Equation (3.16)

this reason, in region 3 it is appropriate to use the Fock-Schwinger gauge²⁰

$$x^+ A_3^- + x^- A_3^+ = 0.$$

After the collision, the fields from region 3 may be chosen as²¹

$$\begin{aligned} A_3^+(x) &= x^+ \alpha^\eta(x), \\ A_3^-(x) &= -x^- \alpha^\eta(x), \\ A_3^i(x) &= \alpha^i(x). \end{aligned} \quad (4.10)$$

A general solution may be constructed by patching together the proposed solutions from all the regions²²

$$A^+(x) = \theta(x^+) \theta(x^-) x^+ \alpha^\eta(x), \quad (4.11a)$$

$$A^-(x) = -\theta(x^+) \theta(x^-) x^- \alpha^\eta(x), \quad (4.11b)$$

$$A^i(x) = \theta(x^+) \theta(x^-) \alpha^i(x) + \theta(-x^+) \theta(x^-) \alpha_1^i(\vec{x}_\perp) + \theta(x^+) \theta(-x^-) \alpha_2^i(\vec{x}_\perp). \quad (4.11c)$$

20: Notice that this choice assures vanishing $A_1^- = A_2^+ = 0$ along the x^\pm axis of the light-cone current.

21: In order to satisfy the Fock-Schwinger gauge condition.

22: By using Equations (4.9) and (4.10).

Boost-invariant fields

In the original MV model for the color current generated by a nucleus is given by²³

$$J_{1,2}^\mu(x) = \delta^{\mu\pm} \delta(x^\mp) \rho_{1,2}(\vec{x}_\perp), \quad (4.12)$$

which then yields a total color current

$$J_3^\mu(x) = \delta^{\mu+} \delta(x^-) \rho_1(\vec{x}_\perp) + \delta^{\mu-} \delta(x^+) \rho_2(\vec{x}_\perp).$$

Such a current is boost invariant, symmetry which will then be passed on to the fields generated by it.

By applying a longitudinal Lorentz boost,²⁴ the light-cone coordinates transform as²⁵

$$x^\pm \mapsto x'^\pm = e^{\pm\beta} x^\pm, \quad \vec{x}_\perp \mapsto \vec{x}'_\perp = \vec{x}_\perp.$$

Hence, the only non-vanishing component of the color current²⁶ becomes

$$J^\pm(x) \mapsto J^{\pm'}(x) = e^{\pm\beta} J^\pm(x),$$

24: With velocity v .

25: Where we introduce the rapidity

$$\beta = \frac{1}{2} \ln \frac{1+v}{1-v}.$$

26: More precisely, J_1^+ for nucleus 1 and J_2^- for nucleus 2.

which for the MV model remains unchanged by this Lorentz boost

$$J_{1,2}^\pm(x) \mapsto e^{\pm\beta} \delta(x^\mp) \rho_{1,2}(\vec{x}_\perp) = \underbrace{e^{\pm\beta} \delta(e^{\pm\beta} x'^\mp)}_{\delta(x'^\mp)} \rho_{1,2}(\vec{x}'_\perp) = J_{1,2}^\pm(x').$$

27: In which the condition of boost-invariance of the fields suppresses any η dependence

$$\begin{aligned}\alpha^\eta(x) &= \alpha^\eta(\tau, \vec{x}_\perp), \\ \alpha^i(x) &= \alpha^i(\tau, \vec{x}_\perp).\end{aligned}$$

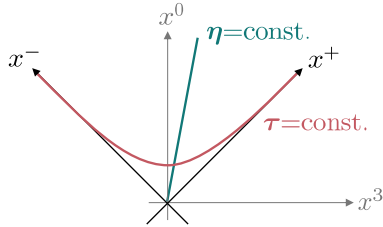


Diagram of light-cone and boost-invariant coordinates.

28: For this reason, the Fock-Schwinger gauge is also called the temporal gauge.

For this reason, in region 3 we shall use a special set of coordinates²⁷ \$(x^+, \vec{x}_\perp, x^-) \mapsto (\tau, \vec{x}_\perp, \eta)\$, where the proper time \$\tau\$ and space-time rapidity \$\eta\$ are defined as

$$\tau \triangleq \sqrt{2x^+x^-}, \quad (4.13a)$$

$$\eta \triangleq \frac{1}{2} \ln \left(\frac{x^+}{x^-} \right). \quad (4.13b)$$

The gauge fields transform accordingly, yielding a null temporal component²⁸

$$A^\tau = \frac{1}{\tau} (x^- A^+ + x^+ A^-) \overset{0}{\cancel{+}} = 0,$$

and similarly

$$\begin{aligned}A^\eta(x) &= \frac{1}{\tau^2} (x^- A^+ - x^+ A^-) \\ &\stackrel{(4.11a)}{=} \frac{1}{2x^-x^+} \theta(x^+) \theta(x^-) 2x^-x^+ \alpha^\eta(\tau, \vec{x}_\perp).\end{aligned}$$

Simple manipulations lead to the useful relations

$$\frac{\partial \tau}{\partial x^\pm} \stackrel{(4.13a)}{=} \frac{\partial}{\partial x^\pm} (\sqrt{2x^+x^-}) = \frac{x^\pm}{\sqrt{2x^+x^-}} \stackrel{(4.13a)}{=} \frac{x^\pm}{\tau} \quad (4.14)$$

and analogously

$$\frac{\partial \eta}{\partial x^\pm} \stackrel{(4.13b)}{=} \frac{\partial}{\partial x^\pm} \left[\frac{1}{2} \ln \left(\frac{x^+}{x^-} \right) \right] = \pm \frac{1}{2x^\pm} \stackrel{(4.13a)}{=} \pm \frac{x^\mp}{\tau}. \quad (4.15)$$

The gauge fields may be expressed in the coordinates \$(\tau, \eta)\$ by applying a transformation

$$A^\mu(x') = \frac{\partial x'^\mu}{\partial x^\nu} A^\nu(x),$$

which for $\mu = \tau$ yield

$$A^\tau = \frac{\partial \tau}{\partial x^+} A^+ + \frac{\partial \tau}{\partial x^-} A^- \xrightarrow{(4.14)} \frac{1}{\tau} (x^- A^+ + x^+ A^-)$$

and for $\mu = \eta$ give

$$A^\eta = \frac{\partial \eta}{\partial x^+} A^+ + \frac{\partial \eta}{\partial x^-} A^- \xrightarrow{(4.15)} \frac{1}{\tau^2} (x^- A^+ - x^+ A^-).$$

The solution is thus completely given by²⁹

29: Together with the result from Equation (4.11c).

$$\begin{aligned} A^i(x) &= \theta(x^+) \theta(x^-) \alpha^i(\tau, \vec{x}_\perp) + \theta(-x^+) \theta(x^-) \alpha_1^i(\vec{x}_\perp) + \theta(x^+) \theta(-x^-) \alpha_2^i(\vec{x}_\perp) \\ A^\eta(x) &= \theta(x^+) \theta(x^-) \alpha^\eta(\tau, \vec{x}_\perp). \end{aligned} \quad (4.16)$$

Boost-invariant equations of motion

The Yang-Mills action expressed in flat coordinates is given by³⁰

$$S = \int d^4x \left(-\frac{1}{2} \text{Tr} \{ F_{\mu\nu} F^{\mu\nu} \} \right), \quad (4.17)$$

30: See the gluon Lagrangian from Equation (2.6)

which in (τ, η) coordinates becomes

$$S = \int d\tau d^2\vec{x}_\perp d\eta \text{Tr} \left\{ \tau F_{\tau i} F_{\tau i} + \frac{1}{\tau} F_{\tau\eta} F_{\tau\eta} - \frac{\tau}{2} F_{ij} F_{ij} - \frac{1}{\tau} F_{\eta i} F_{\eta i} \right\}. \quad (4.18)$$

The metric tensor in the (τ, η) coordinates becomes³¹

31: And similarly

$$g_{\mu\nu} = \text{Diag}\{1, -1, -1, -\tau^2\}.$$

$$g^{\mu\nu} = \text{Diag}\{1, -1, -1, -1/\tau^2\}.$$

The infinitesimal volume element is given by

$$d^4x = \underbrace{\sqrt{\text{Det } g}}_{\tau} d\tau d^2\vec{x}_\perp d\eta.$$

Therefore, one may express the Yang-Mills action³² as

32: From Equation (4.17).

$$S = - \int d\tau d^2\vec{x}_\perp d\eta \frac{1}{2} \text{Tr} \left\{ 2\tau F_{\tau i} \underbrace{F^{\tau i}}_{-F_{\tau i}} + 2\tau F_{\tau\eta} \underbrace{F^{\tau\eta}}_{-\frac{F_{\tau\eta}}{\tau^2}} + 2\frac{\tau}{2} F_{ij} \underbrace{F^{ij}}_{F_{ij}} + 2\tau F_{\eta i} \underbrace{F^{\eta i}}_{\frac{F_{\eta i}}{\tau^2}} \right\}.$$

One may define canonical momenta as

$$\begin{aligned} P^\eta &\triangleq \frac{\delta S}{\delta(\partial_\tau A_\eta)} = \frac{1}{\tau} F_{\tau\eta}, \\ P^i &\triangleq \frac{\delta S}{\delta(\partial_\tau A_i)} = \tau F_{\tau i}. \end{aligned} \quad (4.19)$$

33: Given in Equation (4.18).

Varying this action³³ with respect to A_τ , before employing the Fock-Schwinger gauge condition $A_\tau = 0$, and requiring that $\delta_\tau S = 0$, yields the so-called Gauss constraint

$$\tau D_i F_{\tau i} + \frac{1}{\tau} D_\eta F_{\tau\eta} = 0. \quad (4.20)$$

34: More concisely

$$\delta_\mu S \triangleq \frac{\delta S}{\delta A_\mu}.$$

In general, varying the action³⁴ with respect to A_μ is done through

$$\begin{aligned} \delta_\mu F_{\mu\nu} &= \delta_\mu(\partial_\mu A_\nu - \partial_\nu A_\mu + ig[A_\mu, A_\nu]) \\ &= -\partial_\nu \delta A_\mu + ig[\delta A_\mu, A_\nu] = -D_\nu \delta A_\mu. \end{aligned} \quad (4.21)$$

35: For a given $\mu \neq \nu$.

36: After performing integration by parts and making use of the trace relation

$$\text{Tr}\{A[B, C]\} = \text{Tr}\{[A, B]C\}.$$

Notice that we wrote the most general form, in order to also consider the case for $\mu = \tau$, which has an extra τ from the volume element and any additional ones that may come from lowering the indices of $F^{\mu\nu}$.

The only terms from the action which bring contributions³⁵ are³⁶

$$\begin{aligned} \delta_\mu S &= \delta_\mu \left(\int d^4x \text{Tr}\{F_{\mu\nu} F^{\mu\nu}\} \right) = \int d^4x \text{Tr}\{\delta_\mu(F_{\mu\nu} F^{\mu\nu})\} \\ &= 2 \int d^4x \text{Tr}\{F^{\mu\nu} \delta_\mu F_{\mu\nu}\} \stackrel{(4.21)}{=} 2 \int d^4x \text{Tr}\{F^{\mu\nu} (-D_\nu \delta A_\mu)\} \\ &= 2 \left[\underbrace{\text{Tr}\left\{ - \int d\tau d^2\vec{x}_\perp d\eta \tau F^{\mu\nu} \partial_\nu \delta A_\mu \right\}}_0 + \right. \\ &\quad \left. \int d\tau d^2\vec{x}_\perp d\eta \delta A_\mu \partial_\nu (\tau F^{\mu\nu}) + \underbrace{\text{surface term}}_{-\text{Tr}\{[\tau F^{\mu\nu}, A_\nu] \delta A_\mu\}} \right. \\ &\quad \left. + ig \int d\tau d^2\vec{x}_\perp d\eta \underbrace{\text{Tr}\{\tau F^{\mu\nu} [\delta A_\mu, A_\nu]\}}_{D_\nu(\tau F^{\mu\nu})} \right] \\ &= 2 \int d\tau d^2\vec{x}_\perp d\eta \text{Tr}\left\{ \underbrace{[\partial_\nu(\tau F^{\mu\nu}) + ig[A_\nu, \tau F^{\mu\nu}]]}_{D_\nu(\tau F^{\mu\nu})} \delta A_\mu \right\}. \end{aligned}$$

Summarizing, we obtain

$$\delta_\mu \left(\int d^4x \text{Tr}\{F_{\mu\nu} F^{\mu\nu}\} \right) = 2 \int d\tau d^2\vec{x}_\perp d\eta \text{Tr}\{D_\nu(\tau F^{\mu\nu}) \delta A_\mu\}. \quad (4.22)$$

Hence, the variation of the action with respect to A_τ gives

$$\delta_\tau S = \delta_\tau \left(\int d\tau d^2\vec{x}_\perp d\eta \text{Tr} \left\{ \tau F_{\tau i} F_{\tau i} + \frac{1}{\tau} F_{\tau\eta} F_{\tau\eta} \right\} \right) \\ \stackrel{(4.22)}{=} 2 \int d\tau d^2\vec{x}_\perp d\eta \text{Tr} \left\{ \left(\tau D_i F_{\tau i} + \frac{1}{\tau} D_\eta F_{\tau\eta} \right) \delta A_\tau \right\},$$

which after imposing $\delta_\tau S = 0$ gives the Gauss constraint.³⁷

37: From Equation (4.20).

Therefore, this relation may equivalently be expressed in terms of the momenta as³⁸

$$D_i P^i + D_\eta P^\eta = 0. \quad (4.23)$$

Nevertheless, in the temporal gauge $A_\tau = 0$ and boost-invariant scenario³⁹ $\partial_\eta A_\mu = 0$, the action simplifies to

38: Using Equations (4.19) and (4.20).

$$S = \int d\tau d^2\vec{x}_\perp d\eta \text{Tr} \left\{ \tau \partial_\tau A_i \partial_\tau A_i + \frac{1}{\tau} \partial_\tau A_\eta \partial_\tau A_\eta - \frac{\tau}{2} F_{ij} F_{ij} - \frac{1}{\tau} D_i A_\eta D_i A_\eta \right\}. \quad (4.24)$$

This may easily be proven by noticing that⁴⁰

40: With $\mu = i, \eta$.

$$F_{\tau\mu} = \partial_\tau A_\mu - \partial_\mu \cancel{A}_\tau^0 - ig[A_\mu, \cancel{A}_\tau^0], \quad (4.25)$$

and similarly

$$F_{\eta i} = \partial_\eta \cancel{A}_i^0 - \partial_i \cancel{A}_\eta - ig[A_\eta, A_i] = -D_i A_\eta. \quad (4.26)$$

Plugging these results back in the action in (τ, η) coordinates⁴¹ immediately leads to the boost-invariant action.⁴²

41: From Equation (4.18).

Within this boost-invariant approximation, the Gauss constraint⁴³ reduces to

42: See Equation (4.24).

$$D_i P^i + \partial_\eta \cancel{P}^\eta + ig[A_\eta, P^\eta] = 0. \quad (4.27)$$

43: Written in terms of conjugate momenta in Equation (4.23).

The conjugate momenta further simplify to⁴⁴

44: After inserting the field strengths from Equations (4.25) and (4.26) back in Equation (4.19).

$$P^\eta = \frac{1}{\tau} \partial_\tau A_\eta, \quad (4.28a)$$

$$P^i = \tau \partial_\tau A_i. \quad (4.28b)$$

Varying this boost-invariant action with respect to the remaining gauge fields, namely A_η and A_i , provide us with the equations of motion

$$\begin{aligned}\partial_\tau P^i &= \tau D_j F_{ji} - \frac{ig}{\tau} [A_\eta, D_i A_\eta], \\ \partial_\tau P^\eta &= \frac{1}{\tau} D_i (D_i A_\eta).\end{aligned}\tag{4.29}$$

45: From Equation (4.18).

By varying the Yang-Mills action in (τ, η) coordinates⁴⁵ with respect to A_i gives

$$\begin{aligned}\delta_i S &= \delta_i \left(\int d\tau d^2 \vec{x}_\perp d\eta \text{Tr} \left\{ \tau F_{i\tau} F_{i\tau} - \frac{\tau}{2} F_{ij} F_{ij} - \frac{1}{\tau} F_{i\eta} F_{i\eta} \right\} \right) \\ &\stackrel{(4.22)}{=} 2 \int d\tau d^2 \vec{x}_\perp d\eta \text{Tr} \left\{ \left(D_\tau \tau F_{i\tau} - \frac{\tau}{2} D_j F_{ij} - \frac{1}{\tau} D_\eta F_{i\eta} \right) \delta A_i \right\}.\end{aligned}$$

Nevertheless, in the boost-invariant approximation, the above expression becomes

$$\begin{aligned}\delta_i S &\stackrel{(4.25)}{=} \stackrel{(4.26)}{=} 2 \int d\tau d^2 \vec{x}_\perp d\eta \text{Tr} \left\{ \left[(\partial_\tau - ig A_\tau) \tau (-\partial_\tau A_i) - \frac{\tau}{2} D_j (-F_{ji}) - \frac{1}{\tau} (\cancel{\partial_\eta} \cancel{D_i} A_\eta - ig [A_\eta, D_i A_\eta]) \right] \delta A_i \right\} \\ &\stackrel{(4.28a)}{=} -2 \int d\tau d^2 \vec{x}_\perp d\eta \text{Tr} \left\{ \underbrace{\left[\partial_\tau (\tau \partial_\tau A_i) - \tau D_j F_{ji} + \frac{ig}{\tau} [A_\eta, D_i A_\eta] \right]}_{P^i} \delta A_i \right\}.\end{aligned}$$

In a similar manner, the functional derivative of the Yang-Mills action in terms of A_η gives

$$\begin{aligned}\partial_\eta S &= \partial_\eta \left(\int d\tau d^2 \vec{x}_\perp d\eta \text{Tr} \left\{ \frac{1}{\tau} F_{\eta\tau} F_{\eta\tau} - \frac{1}{\tau} F_{\eta i} F_{\eta i} \right\} \right) \\ &\stackrel{(4.22)}{=} 2 \int d\tau d^2 \vec{x}_\perp d\eta \text{Tr} \left\{ \left(D_\tau \frac{1}{\tau} F_{\eta\tau} - \frac{1}{\tau} D_i F_{\eta i} \right) \delta A_\eta \right\},\end{aligned}$$

which in the boost-invariant case further simplifies to

$$\begin{aligned}\partial_\eta S &\stackrel{(4.25)}{=} \stackrel{(4.26)}{=} 2 \int d\tau d^2 \vec{x}_\perp d\eta \text{Tr} \left\{ \left[(\partial_\tau - ig A_\tau) \frac{1}{\tau} (-\partial_\tau A_\eta) - \frac{1}{\tau} D_i (-D_i A_\eta) \right] \delta A_\eta \right\} \\ &\stackrel{(4.28b)}{=} 2 \int d\tau d^2 \vec{x}_\perp d\eta \text{Tr} \left\{ \left[-\partial_\tau \underbrace{\left(\frac{1}{\tau} \partial_\tau A_\eta \right)}_{P^\eta} + \frac{1}{\tau} D_i (D_i A_\eta) \right] \delta A_\eta \right\}.\end{aligned}$$

Initial conditions

Equivalently, one may write the equations of motion for the unknown fields $\alpha^i(\tau, \vec{x}_\perp)$ and $\alpha^\eta(\tau, \vec{x}_\perp)$ as⁴⁶

$$\begin{aligned} \frac{1}{\tau} D_i \partial_\tau \alpha^i + ig\tau \alpha^\eta \partial_\tau \alpha^\eta &= 0, \\ \frac{1}{\tau} \partial_\tau \tau \partial_\tau \alpha^i - ig\tau^2 \alpha^\eta D_i \alpha^\eta - D_j F_{ji} &= 0, \\ \frac{1}{\tau^2} \partial_\tau \tau^2 \partial_\tau \alpha^\eta - D_i (D_i \alpha^\eta) &= 0. \end{aligned}$$

These boost-invariant Yang-Mills equations must be accompanied by initial conditions⁴⁷ at $\tau \rightarrow 0$

$$\alpha^i(\tau, \vec{x}_\perp) \Big|_{\tau=0} = \alpha_1^i(\vec{x}_\perp) + \alpha_2^i(\vec{x}_\perp), \quad (4.30a)$$

$$\alpha^\eta(\tau, \vec{x}_\perp) \Big|_{\tau=0} = \frac{ig}{2} [\alpha_1^i(\vec{x}_\perp), \alpha_2^i(\vec{x}_\perp)], \quad (4.30b)$$

along with

$$\partial_\tau \alpha^i(\tau, \vec{x}_\perp) \Big|_{\tau=0} = \partial_\tau \alpha^\eta(\tau, \vec{x}_\perp) \Big|_{\tau=0} = 0.$$

We are going to provide a sketch of this computation, borrowed from [44], by only looking at the terms⁴⁸ which have $\delta(x^\pm)$ as coefficients and afterwards cancel those terms. From the Yang-Mills equation for $\mu = i$ one obtains⁴⁹ :

$$\text{coefficient of } \delta(x^-)\delta(x^+) : \quad \alpha^i(\tau, \vec{x}_\perp) - \alpha_1^i(\vec{x}_\perp) - \alpha_2^i(\vec{x}_\perp),$$

which after integration over the x^\pm components lead to the initial condition⁵⁰ for α^i . In a similar manner, the Yang-Mills equation for $\mu = +$ gives⁵¹

$$\text{coefficient of } \delta(x^-)\theta(x^+) : \quad 2\alpha^\eta(\tau, \vec{x}_\perp) - ig[\alpha_1^i(\vec{x}_\perp), \alpha_2^i(\vec{x}_\perp)].$$

The initial conditions may also be expressed in terms of

$$\begin{aligned} A_i(\tau, \vec{x}_\perp) \Big|_{\tau=0} &= -\alpha^i(\tau, \vec{x}_\perp) \Big|_{\tau=0}, & P^i(\tau, \vec{x}_\perp) \Big|_{\tau=0} &= 0, \\ A_\eta(\tau, \vec{x}_\perp) \Big|_{\tau=0} &= 0, & P^\eta(\tau, \vec{x}_\perp) \Big|_{\tau=0} &= -2\alpha^\eta(\tau, \vec{x}_\perp) \Big|_{\tau=0}. \end{aligned}$$

Provided with initial values and evolution equations,⁵² one may discretize them on a lattice and solve them numerically.

46: These equations were originally proposed in [41, 42]. One may find a detailed derivation in [43], in which, as opposed to deriving the equations of motion directly from an action written in (τ, η) coordinates, one expresses all the components of the field strength tensor and then the Yang-Mills equations in these coordinates.

47: By inserting the ansatz from Equation (4.16) back in the Yang-Mills equations from Equation (3.14). The presence of the Heaviside functions will give rise, upon repeatedly applying derivatives, to Delta functions. By imposing that their coefficients vanish at $\tau = 0$, one obtains initial conditions for α^i and α^η .

48: Arising from inserting Equation (4.16) back in Equation (3.14).

49: That is $D_\mu F^{\mu i} = 0$, a term with $\delta(x^-)\delta(x^+)$ may arise from $\partial_- \partial_+ A^i$.

50: See Equation (4.30a).

51: That is $D_\mu F^{\mu +} = J^+$ give several contributions through the terms $\partial_- F^{-+}$ and $D_i(-\partial_- A^i)$. The latter one contains

$$-\partial_- \partial_i A^i = \underbrace{-\delta(x^-) \partial_i \alpha_1^i}_{J_1^+} \theta(x^+).$$

52: From Equation (4.29) with the additional Gauss constraint from Equation (4.27) which must be fulfilled at all proper times.

4.2 Lattice gauge theory

Gauge invariance

Nevertheless, a naive discretization of the Yang-Mills action⁵³ in which one replaces all the partial derivatives⁵⁴ with finite differences leads to the loss of gauge invariance [14, 21].

This is a consequence of imposing local gauge symmetry⁵⁵ of the fields

$$\phi(x) \mapsto U(x)\phi(x).$$

Fields at different space-time points cannot directly be compared.⁵⁶ By introducing a quantity which gauge transform as

$$W(x, y) \mapsto U(x)W(x, y)U^\dagger(y), \quad (4.31)$$

one may now properly define the covariant derivative as⁵⁷

$$D_\mu\phi(x) \triangleq \lim_{\delta\epsilon^\mu \rightarrow 0} \frac{W(x, x + \epsilon)\phi(x + \epsilon) - \phi(x)}{\epsilon^\mu}. \quad (4.33)$$

We choose $W(x, x) = 1$ and then write an expansion in terms of the gauge fields⁵⁸

$$W(x, x + \epsilon) = 1 + ig\epsilon^\mu A_\mu + \mathcal{O}(\epsilon^2).$$

This enables us to express the **Wilson line** as⁵⁹

$$W(x, y) = \mathcal{P} \exp \left\{ ig \int_y^x dz^\mu A_\mu(z) \right\}. \quad (4.34)$$

The **path-ordering** operator $\mathcal{P}\{\dots\}$ is necessary due to the non-Abelian nature of the fields. More clearly, after writing a Taylor expansion, the path-ordering operator acts as

$$\begin{aligned} W(x, y) = & 1 + ig \int_0^1 \frac{dz_\lambda^\mu}{d\lambda} A_\mu(z_\lambda^\mu) T^a d\lambda - \frac{1}{2} g^2 \int_0^1 d\lambda \int_0^1 d\tau \frac{dz_\lambda^\mu}{d\lambda} \frac{dz_\tau^\nu}{d\tau} \times \\ & \times A_\mu^\alpha(z_\lambda^\mu) A_\nu^\beta(z_\tau^\nu) [T^a T^b \theta(\lambda - \tau) + T^b T^a \theta(\tau - \lambda)] + \dots \end{aligned}$$

A Wilson line taken along a closed path γ is called a **Wilson loop** and it's given by

$$W_\gamma = \mathcal{P} \exp \left\{ ig \oint_\gamma dx^\mu A_\mu(x) \right\}. \quad (4.35)$$

It is important to emphasize that the trace of a Wilson loop is gauge invariant⁶⁰.

Real-time lattice gauge theory

Let us begin by discretizing the Minkowski space-time on a hypercubic lattice⁶¹ whose points are given by

$$\mathbb{X}^4 = \left\{ x \mid x = \sum_{\mu=0}^3 n_\mu \hat{a}^\mu, \quad n_\mu \in \mathbb{Z} \right\}.$$

A field $\phi(x)$ which resides on the lattice will be denoted⁶² as ϕ_x . The gauge transformation $U(x)$ will become, upon discretization, U_x . The discretized action and corresponding field equations written in terms of A_μ will not remain gauge invariant.

Nevertheless, a gauge invariant lattice action may be constructed. Instead of using the gauge fields⁶³ A_μ as the main degrees of freedom, one may simply seek for a more suitable quantity which is already gauge invariant and preserves gauge invariance upon discretization. An action built from such a quantity will inherently be gauge invariant. The simplest choice is the trace of a Wilson line.⁶⁴

A Wilson line taken between two neighbouring lattice points⁶⁵ is called a **gauge link** and it's given by⁶⁶

$$W_{x,\mu} = \overline{\mathcal{P}} \exp \left\{ ig \int_x^{x+\hat{a}^\mu} dx^\nu A_{x,\mu} \right\}.$$

In a similar manner, we may also introduce a gauge link along the opposite direction, which would yield

$$W_{x,\mu}^\dagger = W_{x+\mu,-\mu}. \quad (4.36)$$

60: This may easily be proven by inserting Equation (4.35) back in Equation (4.31) and using the invariance of the trace under cyclic permutations.

61: The lattice spacing along direction μ , with the unit vector is \hat{e}^μ , is a^μ . This enables us to write $\hat{a}^\mu = a^\mu \hat{e}^\mu$. More concisely, a^0 is the time step and a^i denote the spatial lattice spacings.

62: With $x \in \mathbb{X}^4$.

63: Along with the corresponding conjugate momenta P_μ .

64: As given in Equation (4.35). We already saw that such a construction is gauge invariant.

65: Namely x and $x + \hat{a}^\mu$.

66: Here $\overline{\mathcal{P}}\{\dots\}$ denotes the anti-path-ordering. We introduce the notation

$$W_{x,\mu} \triangleq W(x, x + \hat{a}^\mu)$$

and similarly for $A_{x,\mu}$.

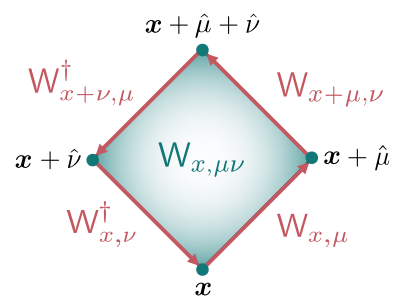


Diagram of a plaquette.

A gauge link transforms as

$$W_{x,\mu} \rightarrow U_x W_{x,\mu} U_{x+\mu}^\dagger.$$

One may express a gauge link and afterwards expand it as⁶⁷

67: See Equation (4.34).

$$W_{x,\mu} = \exp\{iga^\mu A_{x,\mu}\} \approx \mathbb{1} + ig a^\mu A_{x,\mu(x)} - \frac{1}{2} g^2 a^\mu a^\nu A_{x,\mu} A_{x,\nu} + \mathcal{O}(a^3). \quad (4.37)$$

68: The shortest Wilson line would just go back and forth between two neighbouring sites but such a combination would simply yield the trivial result

$$W_{x,\mu} W_{x+\mu,-\mu} \xrightarrow{(4.36)} \mathbb{1}.$$

which may further be expressed as

$$W_{x,\mu\nu} \approx \exp\{iga^\mu a^\nu F_{x,\mu\nu} + \mathcal{O}(a^3)\}.$$

69: Using the Campbell-Baker-Hausdorff formula

$$\begin{aligned} & \exp\{A\} \exp\{B\} \\ & \approx \exp\left\{A + B + \frac{1}{2}[A, B] + \dots\right\}. \end{aligned}$$

We may write the discretized Wilson loop as⁶⁹

$$\begin{aligned} W_{x,\mu\nu} \approx & \exp\left\{ig(A_{x,\mu} + A_{x+\mu,\nu} - A_{x+\nu,\mu} - A_{x,\nu}) + \right. \\ & + \frac{g^2}{2} \left([A_{x,\nu} + A_{x+\nu,\mu}, A_{x+\mu,\nu} + A_{x,\mu}] - \right. \\ & \left. \left. - [A_{x,\nu}, A_{x+\nu,\mu}] - [A_{x+\mu,\nu}, A_{x,\mu}] \right) \right\}. \end{aligned}$$

By making use of the expansion

$$A_{x+\mu,\nu} \approx A_{x,\nu} + a^\mu \partial_\mu A_{x,\nu} + \mathcal{O}(a^2),$$

we may then derive

$$W_{x,\mu\nu} \approx \exp\left\{iga^\mu a^\nu \underbrace{\left(\partial_\mu A_{x,\nu} - \partial_\nu A_{x,\mu} - ig[A_{x,\nu}, A_{x,\mu}]\right)}_{F_{x,\mu\nu}} + \mathcal{O}(a^3)\right\}.$$

70: In the limit of small lattice spacings.

This may further be approximated as⁷⁰

$$W_{x,\mu\nu} = \mathbb{1} + ig a^\mu a^\nu F_{x,\mu\nu} - \frac{1}{2} (ga^\mu a^\nu)^2 F_{x,\mu\nu}^2 + \mathcal{O}(a^5).$$

Therefore, we may construct a gauge invariant⁷¹ quantity under the discretized gauge transformation U_x as

$$\text{Tr}\{2 - W_{x,\mu\nu} - W_{x,\mu\nu}^\dagger\} \approx (ga^\mu a^\nu)^2 \text{Tr}\{F_{x,\mu\nu}^2\} + \mathcal{O}(a^6). \quad (4.38)$$

The Yang-Mills action⁷² may be split into an electric and a magnetic part

$$S = \underbrace{\int d^4x \sum_i \text{Tr}\{F_{0i}^2(x)\}}_{S_E} + \underbrace{\int d^4x \sum_{i,j} \frac{1}{2} \text{Tr}\{F_{ij}^2(x)\}}_{S_B}.$$

Upon discretization, they become⁷³

$$\begin{aligned} S_E &\approx V \sum_x \sum_i \frac{1}{(ga^0 a^i)^2} \text{Tr}\{2 - W_{x,0i} - W_{x,0i}^\dagger\}, \\ S_B &\approx V \sum_x \sum_{i,j} \frac{1}{2(ga^i a^j)^2} \text{Tr}\{2 - W_{x,ij} - W_{x,ij}^\dagger\}. \end{aligned}$$

Thus, the Yang-Mills action on the lattice is given by

$$S = V \sum_x \left(\sum_i \frac{1}{(ga^0 a^i)^2} \text{Tr}\{2 - W_{x,0i} - W_{x,0i}^\dagger\} - \sum_{i,j} \frac{1}{2(ga^i a^j)^2} \text{Tr}\{2 - W_{x,ij} - W_{x,ij}^\dagger\} \right).$$

Discretized boost-invariant action⁷⁴

One may deduce an expression for the discretized boost-invariant action⁷⁵ which after introducing the gauge-covariant forward and backward finite differences

$$\begin{aligned} D_i^F A_{x,\eta}(\tau) &\stackrel{\Delta}{=} \frac{1}{a^i} [W_{x,i}(\tau) A_{x+i,\eta}(\tau) W_{x+i,-i}(\tau) - A_{x,\eta}], \\ D_i^B A_{x,\eta}(\tau) &\stackrel{\Delta}{=} \frac{1}{a^i} [A_{x,\eta}(\tau) - W_{x,-i}(\tau) A_{x-i,\eta} W_{x-i,i}(\tau)], \end{aligned}$$

and the discretized conjugate momenta

$$\begin{aligned} P_x^\eta(\tau) &= \frac{1}{\tau} \partial_\tau A_{x,\eta}(\tau), \\ P_x^i(\tau) &= -i\tau \frac{1}{ga^i} [\partial_\tau W_{x,i}(\tau)] W_{x,i}^\dagger(\tau), \end{aligned}$$

71: Since in contains Wilson lines traced over.

72: From Equation (4.17).

73: By making the replacement

$$\int d^4x (\dots) \mapsto \underbrace{\prod_\mu}_{V} \underbrace{a^\mu}_{\sum_x} \sum_x (\dots)$$

and using the result from Equation (4.38).

74: All the results sketched in this section have detailed proofs in [45].

75: By taking the continuum action in (τ, η) coordinates from Equation (4.24), replacing the transverse gauge fields $A_i(\tau, \vec{x}_\perp)$ with transverse gauge links $W_{x,i}(\tau)$ and then discretizing the term which contains F_{ij}^2 with Equation (4.38).

Another approach [46] would be to use the Wilson action on the lattice and take the limits $a^0 \rightarrow \infty$ and $a^3 \rightarrow \infty$, which will yield an action discretized only in the transverse plane.

may be expressed as

$$S = \int d\tau d\eta \sum_x \left(\prod_i a^i \right) \text{Tr} \left\{ \frac{1}{\tau} \sum_i \left\{ [P_x^i(\tau)]^2 + \tau [P_x^\eta(\tau)]^2 - [\mathcal{D}_i^F A_{x,\eta}(\tau)]^2 \right\} - \tau \sum_{i,j} \frac{1}{2(ga^i a^j)^2} [2 - W_{x,ij}(\tau) - W_{x,ij}^\dagger(\tau)] \right\}.$$

76: This may be obtained by varying the Wilson action in (τ, η) coordinates with respect to A_τ a priori to fixing the gauge, that is imposing $A_\tau = 0$.

The discretized Gauss constraint becomes⁷⁶

$$\sum_i \mathcal{D}_i^B P_x^i + ig [A_{x,\eta}, P_x^\eta] = 0.$$

Varying the Yang-Mills action in the temporal gauge with respect to $A_{x,\eta}$ yields the equation of motion

$$\partial_\tau P_x^\eta = \frac{1}{\tau} \sum_i \mathcal{D}_i^2 A_{x,\eta},$$

77: Where $[...]_{\text{ah}}$ denotes the anti-hermitian traceless part of a matrix.

whereas the variation in terms of $W_{x,i}$ gives⁷⁷

$$\partial_\tau P_x^i = - \sum_j \frac{\tau}{ga^i(a^j)^2} [W_{x,ij} + W_{x,i-j}]_{\text{ah}} - \frac{ig}{\tau} [W_{x,i} A_{x+i,\eta} W_{x,i}^\dagger, \mathcal{D}_i^F A_{x,\eta}].$$

These equations may be discretized in the proper time and afterwards one may use a numerical scheme to integrate them numerically. For this particular set of differential equations, a suitable numerical scheme is provided by the [leapfrog algorithm](#).⁷⁸

78: More details in [43, 45]. The fields and associated momenta are successively computed at integer and fractional proper times.

4.3 Numerical simulation

Numerical implementation

79: Where $a_T \triangleq a^1 = a^2$ is the transverse lattice spacing and N_T the number of cells.

In the transverse plane, the fields are discretized on a square lattice of size⁷⁹ $L_T = N_T a_T$. Since in the MV model, the nuclei extend infinitely in the transverse plane, one needs to impose periodic boundary conditions at the edges of the cells. The Glasma may be implemented numerically with the following prescription:

Randomly distribute color charges in the transverse plane according to a Gaussian distribution.

Step 1

The two-point function of the charges becomes⁸⁰

$$\langle \rho_{x,n}^a \rho_{y,m}^b \rangle = \frac{g^2 \mu^2}{N_s a_T^2} \delta_{nm} \delta^{ab} \delta_{xy}.$$

Thus, the color charge $\rho_{x,n}^a$ at each lattice point x belonging to a certain color sheet n and having a color index a may be generated as a random number from a Gaussian distribution, such that the mean value is null and the variance is given by $g^2 \mu^2 a_T^2 / N_s$.

Perform a Fast Fourier Transform to obtain the Fourier transformed color charge.

Step 2

One may define⁸¹ the discrete Fourier transform of the lattice color charge as

$$\tilde{\rho}_{k,x}^a \triangleq \left(\frac{2\pi}{L_T} \right)^2 \sum_{\vec{\kappa}_\perp} \rho_{x,n}^a \exp\{-i\vec{\kappa}_\perp \cdot \vec{x}_\perp\},$$

where $\vec{\kappa}_\perp$ is the discretized transverse momentum. This may be achieved by using already implemented FFT routines.

Solve a Poisson equation in momentum space and obtain the Fourier transformed fields.

Step 3

The fields in the covariant gauge satisfy a Poisson equation which in momentum space may be written as⁸²

$$\tilde{k}_\perp^2 \tilde{\alpha}_{k,n}^a = \tilde{\rho}_{k,n}^a,$$

from which one may extract a regularized solution⁸³

$$\tilde{\alpha}_{k,n}^a = \frac{\tilde{\rho}_{k,n}^a}{\tilde{k}_\perp^2 + m^2} \Big|_{\tilde{k}_\perp^2 < \Lambda_{UV}^2}.$$

Obtain the solution via an Inverse Fast Fourier Transform.

80: This is just the discretized version of the correlator from Equation (4.5). Recall that $n, m \in \overline{1, N_s}$ represent color sheet indices and N_s the total number of color sheets.

Step 2

81: By introducing the notation

$$\vec{\kappa}_\perp \cdot \vec{x}_\perp \triangleq \frac{2\pi}{L_T} (\kappa^1 x^1 + \kappa^2 x^2),$$

and also

$$\sum_{\vec{\kappa}_\perp} \triangleq \sum_{\kappa^1} \sum_{\kappa^2},$$

with $\kappa^1, \kappa^2 \in \overline{0, N_T^2 - 1}$.

Step 3

82: See Equation (4.12).

83: In which m is an infrared regulator which acts as a screening mass and Λ_{UV} a ultra-violet regulator for high-momentum modes.

Step 4

Once a solution is obtained in the momentum space, one may perform an inverse FFT and get

$$\alpha_{x,n}^a = \frac{1}{L_T^2} \sum_{\vec{\kappa}_\perp} \tilde{\alpha}_{k,n}^a \exp\{i\vec{\kappa}_\perp \cdot \vec{x}_\perp\}.$$

Step 5

Gauge transform back to the light-cone gauge and compute the transverse gauge links.

84: Which is just the discretized version of Equation (4.7).

85: For each of the nuclei denoted with 1 and 2.

Equipped with a solution for the gauge field in the covariant gauge, one may compute the Wilson line of a nucleus as⁸⁴

$$V_x^\dagger = \prod_{n=1}^{N_s} \exp\{-ig\alpha_{x,n}^a t^a\},$$

and then obtain the gauge links⁸⁵ by gauge transforming back to the light-cone gauge

$$W_{x,i} = V_{A,x} V_{A,x+i}^\dagger.$$

Step 6

Calculate the gauge fields $A_{x,\eta}$, transverse gauge links $W_{x,i}$ and conjugate momenta P_x^η and P_x^i using the leapfrog algorithm.

Computing observables

The aim is to extract the energy-momentum tensor of the plasma and further evaluate some of its components. For the CGC Lagrangian,⁸⁶ it reads

$$T^{\mu\nu} = \text{Tr}\left\{ -F^{\mu\rho}F_\rho^\nu + \frac{1}{2}g^{\mu\nu}F^{\rho\sigma}F_{\rho\sigma} \right\}. \quad (4.39)$$

86: See the Yang-Mills action from Equation (4.17).

87: It is given by

$$L_{\text{CGC}} = -\frac{1}{2}\text{Tr}\{F_{\mu\nu}F^{\mu\nu}\}.$$

88: By using

$$\frac{\delta L_{\text{CGC}}}{\delta(\partial_\mu A_\rho)} = -F^{\mu\rho}.$$

This result is not obvious. By directly applying Noether's theorem for invariance under space-time translation one gets the conserved quantity

$$T^{\mu\nu} = \frac{\delta L}{\delta(\partial_\mu A_\rho)} \partial^\nu A_\rho - L \delta^{\mu\nu},$$

which applied for to the CGC Lagrangian⁸⁷ yields⁸⁸

$$T^{\mu\nu} = -\text{Tr}\left\{ F^{\mu\rho}\partial^\nu A_\rho + \frac{1}{2}g^{\mu\nu}F_{\rho\sigma}F^{\rho\sigma} \right\}.$$

This expression is neither symmetric nor gauge invariant. Nevertheless, adding a surface term of the form $\partial_\rho F^{\mu\rho} A^\nu$ fixes this problems and yields a more suitable expression for the energy momentum tensor.⁸⁹

89: From Equation (4.39).

Let us begin by computing the diagonal component

$$T^{\tau\tau} = \text{Tr} \left\{ \frac{1}{\tau^2} P^i P^i + (P^\eta)^2 + F_{ij}^2 + \frac{1}{\tau^2} D_i A_\eta D_i A_\eta \right\}. \quad (4.40)$$

The first diagonal component of the energy-momentum tensor⁹⁰ may be evaluated on color components as

90: For $\mu = \nu = \tau$.

$$\begin{aligned} T^{\tau\tau} &\stackrel{(4.39)}{=} -F^{a,\tau\rho} F_{\rho}^{a,\tau} + \frac{1}{4} F^{a,\rho\sigma} F_{\rho\sigma}^a \\ &= -\left(\underbrace{F_{\tau i}^{a,\tau i} F_{\tau i}^a}_{-\overbrace{F_{\tau i}^a F_{\tau i}^a}^{\frac{1}{\tau^2}}} + \underbrace{F_{\tau\eta}^{a,\tau\eta} F_{\tau\eta}^a}_{-\overbrace{F_{\tau\eta}^a F_{\tau\eta}^a}^{\frac{1}{\tau^2}}} \right) + \frac{1}{2} \left(\underbrace{F_{\tau i}^{a,\tau i} F_{\tau i}^a}_{-\overbrace{F_{\tau i}^a}^{\frac{1}{\tau^2}}} + \underbrace{F_{\tau\eta}^{a,\tau\eta} F_{\tau\eta}^a}_{-\overbrace{F_{\tau\eta}^a}^{\frac{1}{\tau^2}}} + \underbrace{F_{ij}^{a,ij} F_{ij}^a}_{\overbrace{F_{ij}^a}^{\frac{1}{\tau^2}}} + \underbrace{F_{in}^{a,in} F_{in}^a}_{\overbrace{F_{in}^a}^{\frac{1}{\tau^2}}} \right) \\ &= \text{Tr} \left\{ F_{\tau i} F_{\tau i} + \frac{1}{\tau^2} F_{\tau\eta} F_{\tau\eta} + F_{ij} F_{ij} + \frac{1}{\tau^2} F_{in} F_{in} \right\}. \end{aligned}$$

By making use of the expression for the components of the field strength tensor in the boost-invariant case,⁹¹ we eventually derive

$$T^{\tau\tau} \stackrel{(4.25)}{=} \text{Tr} \left\{ \underbrace{\left(F_{\tau i}^a \right)^2}_{\partial_\tau A_i} + \frac{1}{\tau^2} \underbrace{\left(F_{\tau\eta}^a \right)^2}_{\partial_\tau A_\eta} + F_{ij} F_{ij} + \frac{1}{\tau^2} \underbrace{\left(F_{in}^a \right)^2}_{D_i A_\eta} \right\},$$

which expressed in terms of conjugate momenta⁹² gives the desired result.⁹³

91: See the relations derived in Equations (4.25) and (4.26).

By introducing the following notations for the longitudinal and transverse electric and magnetic fields as

$$\begin{aligned} E_L &\triangleq E_3 = P^\eta \stackrel{(4.28a)}{=} \frac{1}{\tau} \partial_\tau A_\eta, & E_i &\triangleq \frac{1}{\tau} P^i \stackrel{(4.28b)}{=} \partial_\tau A_i, \\ B_L &\triangleq B_3 = -F_{ij}, & B_i &\triangleq -\epsilon_{ij} \frac{1}{\tau} D_j A_\eta, \end{aligned}$$

92: From Equations (4.28a) and (4.28b).

one may equivalently write⁹⁴

$$T^{\tau\tau} = \text{Tr} \left\{ E_L^2 + E_T^2 + B_L^2 + B_T^2 \right\}.$$

The energy density of the Glasma may be split intro the following contributions⁹⁵

93: Written in Equation (4.40).

94: After introducing the notations

$$\begin{aligned} E_T^2 &\triangleq E_1^2 + E_2^2, \\ B_T^2 &\triangleq B_1^2 + B_2^2. \end{aligned}$$

This expression is similar with the energy density of the electromagnetic field.

95: Where $\langle \dots \rangle$ denotes averaging over many color charge configurations.

$$\varepsilon = \langle T^{\tau\tau} \rangle = \underbrace{\langle \text{Tr}\{E_L^2\} \rangle}_{\varepsilon_{E,L}} + \underbrace{\langle \text{Tr}\{E_T^2\} \rangle}_{\varepsilon_{E,T}} + \underbrace{\langle \text{Tr}\{B_L^2\} \rangle}_{\varepsilon_{B,L}} + \underbrace{\langle \text{Tr}\{B_T^2\} \rangle}_{\varepsilon_{B,T}}.$$

One may define the longitudinal and transverse components of the pressure as

$$\begin{aligned} p_L &\stackrel{\Delta}{=} \langle T^{11} \rangle = \langle T^{22} \rangle, \\ p_T &\stackrel{\Delta}{=} \langle T^{33} \rangle = \langle \tau^2 T^{\eta\eta} \rangle, \end{aligned}$$

which after performing similar computations may be expressed as⁹⁶

96: Notice that

$$\epsilon = 2p_T + p_L,$$

which comes from the fact that the energy-momentum tensor is traceless.

$$\begin{aligned} p_L &= \varepsilon_{E,T} + \varepsilon_{B,T} - \varepsilon_{E,L} - \varepsilon_{B,L}, \\ p_T &= \varepsilon_{E,L} + \varepsilon_{B,L}. \end{aligned}$$

These will be the main Glasma observables which will be extracted from the numerical simulations.

97: Since the nuclear radius may be parametrized as

$$R_A \approx R_0 A^{1/3} \approx 7.27 \text{ fm},$$

for $A = 197$, where $R_0 \approx 1.25$ fm.

98: The averaged color charge density per unit of transverse area μ may roughly be obtained by multiplying the total number of quarks in the transverse area

$$n_q = 3 \frac{A}{\pi R_A^2} \approx 0.8 A^{1/3} \text{ fm}^{-2},$$

with the average color charge squared of a single quark

$$\langle Q^2 \rangle = \sum_a t^a = \frac{4}{3}.$$

99: We shall see that such a dependence is not exact and is influenced by the choice of the other parameters, namely m and N_s .

100: Which is also $m \approx 1 \text{ fm}^{-1}$, thus assuring color neutrality at nucleonic level.

Simulation parameters

In this section, we will focus on central Au-Au collisions at center of mass energy $\sqrt{s_{\text{NN}}} = 200 \text{ GeV}$. In order to enclose in the simulation box the whole overlapping region of the colliding nuclei, we shall choose the transverse length to be⁹⁷ $L_T = \sqrt{\pi R_A^2} \approx 12.9 \text{ fm}$.

The only phenomenological parameter of the MV model is the MV parameter μ . One may directly estimate it as⁹⁸

$$\mu^2 \approx 1.1 A^{1/3} \text{ fm}^{-2}.$$

For a Au nucleus, this would yield the value $\mu \approx 0.5 \text{ GeV}$. A similar value may be obtained from a different estimation. At energies of $\sqrt{s_{\text{NN}}} = 200 \text{ GeV}$, the saturation momentum takes the value [47] $Q_s \approx 2 \text{ GeV}$. At this scale, the running of the coupling constant yields $\alpha_s(Q_s) \approx 0.3$, hence the coupling constant is roughly $g \approx 2$. Using the approximation⁹⁹ $Q_s \approx g^2 \mu$ thus gives $\mu \approx 0.5 \text{ GeV}$.

We set the IR regulator at¹⁰⁰ $m = 0.2 \text{ GeV}$ and the UV one at a large enough value of $\Lambda_{\text{UV}} = 10 \text{ GeV}$.

Most of the results will be obtained using SU(3). The rest of the numerical parameters, such as the number of color sheets N_s , the number of cells in the transverse size N_T or the time step in the leapfrog algorithm $\Delta\tau$, may vary for different simulations but will be individually specified.

Results

The results in this section are obtained using **Curraun**.¹⁰¹ It has implemented both **SU(2)** or **SU(3)** gauge groups and may run on **CUDA**-enabled graphics units. We first look at the energy density $\varepsilon(\tau, \vec{x}_\perp)$ in the transverse plane at different τ values.

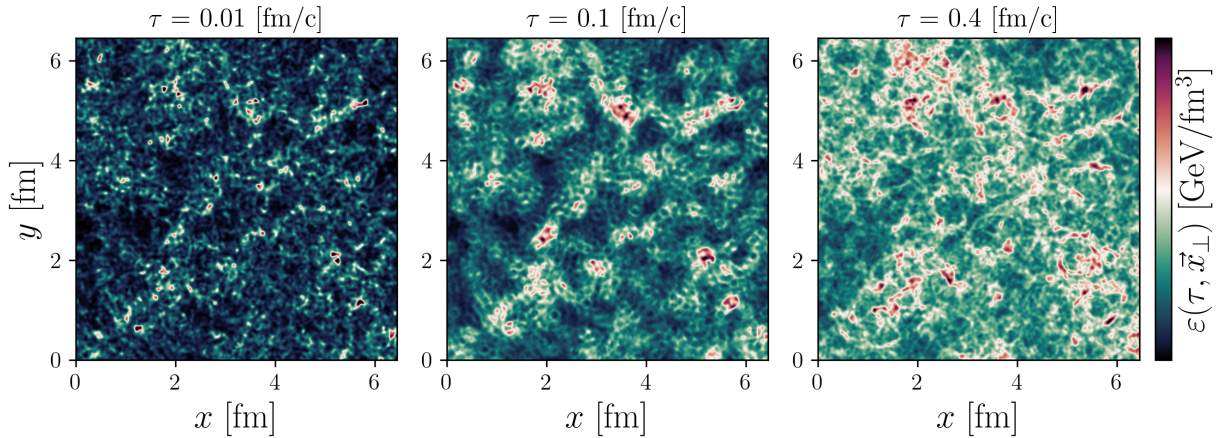
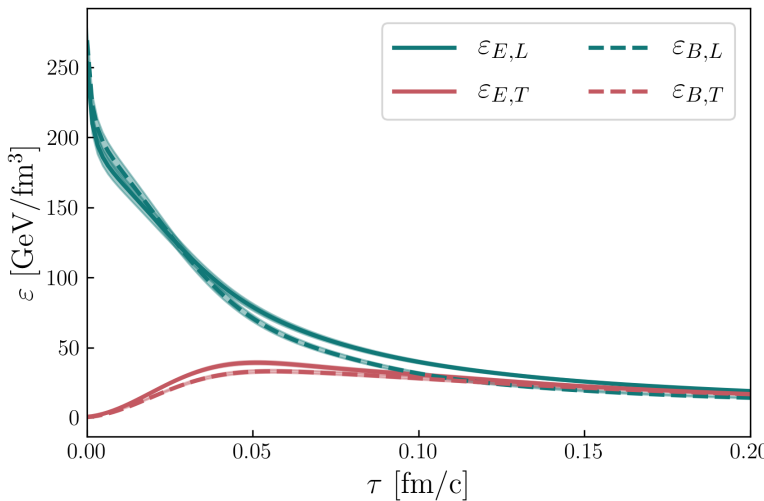


Figure 4.2: Energy density in the transverse plane at various values of the proper time. Simulation parameters: $N_s = 1$, $N_T = 1024$ and $\Delta\tau = a_T/8$. In this plot, only a quarter of the simulation box is showed.



The picture that emerges is the following: initially,¹⁰² the Glasma is mainly composed of longitudinal colored electric and magnetic fields, commonly referred to as **flux tubes**. Once the Glasma evolves,¹⁰³ these flux tubes begin to expand in the transverse plane and circular patterns form. The longitudinal components of the energy density start to decrease while the transverse ones increase. This takes place until¹⁰⁴ all these

¹⁰¹: Which is publicly available at <https://gitlab.com/openpixi/curraun>.

Figure 4.3: Longitudinal and transverse, electric and magnetic contributions to the energy density as a function of proper time, averaged over the transverse plane and over multiple events. Simulation parameters: $N_s = 1$, $N_T = 512$, $\Delta\tau = a_T/8$ and $N_{\text{events}} = 30$. After $\tau \approx Q_s^{-1}$, all the components of the energy density become equal.

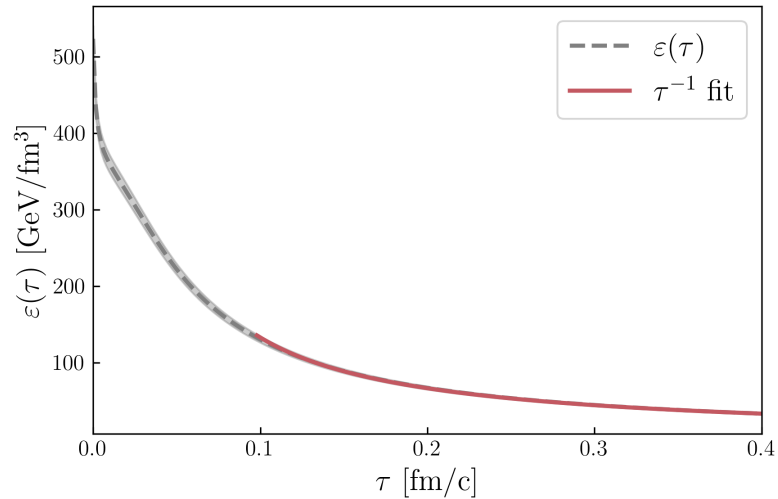
¹⁰²: See the plot at $\tau = 0.01$ fm/c.

¹⁰³: At $\tau = 0.1$ fm/c $\approx Q_s^{-1}$.

¹⁰⁴: Look at the plot captured at $\tau = 0.4$ fm/c.

components become equal and the system homogenizes. This description of the Glasma evolution may further be supported by looking at how the energy density and its components evolve with respect to the proper time.

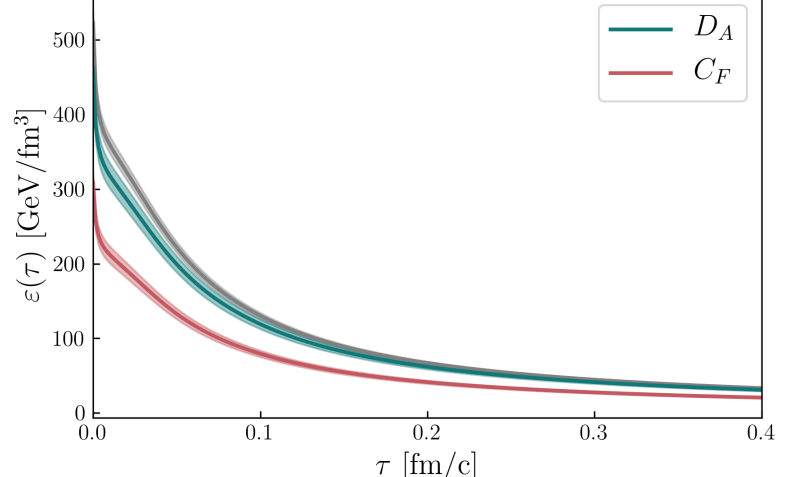
Figure 4.4: Energy density as a function of proper time, averaged over the transverse plane and over multiple events. Simulation parameters: $N_s = 1$, $N_T = 512$, $\Delta\tau = a_T/8$ and $N_{\text{events}} = 30$. After $\tau \approx Q_s^{-1}$, the energy density becomes that of a Bjorken type boost-invariant expansion, namely $\tau\varepsilon(\tau) \approx \text{const.}$



One may extract $\varepsilon(\tau = 0.01 \text{ fm}/c) \approx 134 \text{ GeV}/\text{fm}^3$, which is comparable with the value $\varepsilon(\tau = 0.01 \text{ fm}/c) \approx 130 \text{ GeV}/\text{fm}^3$ obtained in [48].

¹⁰⁵: See the plots from [45] obtained with a previous version of Curraun which may be found at https://gitlab.com/dmueller/curraun_cy.

Figure 4.5: Comparison between the energy density obtained using $SU(3)$ gauge group and $SU(2)$ respectively, but scaled with either the Casimir in the fundamental representation $C_F(3)/C_F(2) = 16/9$, or with the dimension of the adjoint representation $D_A(3)/D_A(2) = 8/3$ with $D_A(N_c) = N_c^2 - 1$.



One may also study the dependence of the energy density on some numerical parameters, namely N_s and m . The continuum limit of the generalized MV model¹⁰⁶ may numerically be chosen at $N_s = 50$ since for values of $m \approx 0.2 \text{ GeV}$ and

¹⁰⁶: Which is analytically taken as $N_s \rightarrow \infty$.

greater, increasing N_s will not bring any significant differences.

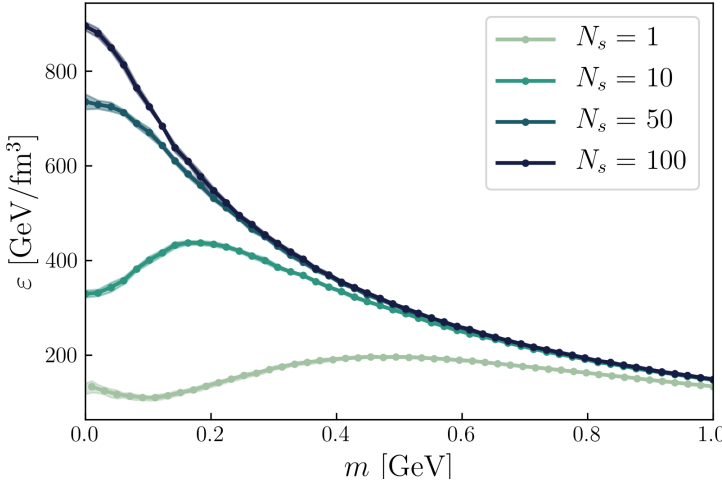


Figure 4.6: Energy density at $\tau = 0.1$ fm/c as a function of m for various values of N_s , averaged over multiple events. Simulation parameters: $N_T = 512$, $\Delta\tau = a_T/8$ and $N_{\text{events}} = 30$.

The longitudinal and transverse pressure components reveal yet another peculiar aspect of the Glasma, namely **pressure anisotropy**. The Yang-Mills fields of the Glasma generate pressures which satisfy¹⁰⁷

$$\lim_{\tau \rightarrow \infty} p_L = 0, \quad \lim_{\tau \rightarrow \infty} p_T = \frac{\varepsilon}{2}.$$

107: As opposed to an isotropic system, for which the pressures should reach

$$\lim_{\tau \rightarrow \infty} p_L = \lim_{\tau \rightarrow \infty} p_T = \frac{\varepsilon}{3}.$$

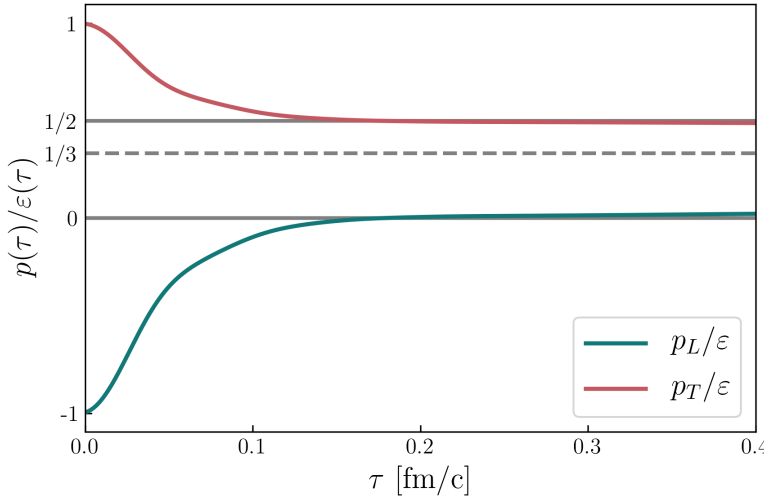


Figure 4.7: Longitudinal and transverse pressure to energy density ratio as a function of proper time, averaged over multiple events. Simulation parameters: $N_s = 1$, $N_T = 512$, $\Delta\tau = a_T/8$ and $N_{\text{events}} = 30$. The Glasma never reaches pressure isotropy.

This feature of the Glasma is problematic since it doesn't allow a smooth coupling to ideal or viscous hydrodynamics, in which the system is assumed to be at local equilibrium and isotropic. There exist various workarounds to surpass this problem: add quantum fluctuations on top of the classic field, which would then bring the system towards a state

109: Such an approach is described in [50, 51].

110: Reviews of this topic may be found at [52, 53].

were hydrodynamics becomes applicable¹⁰⁸; use an intermediate stage between the classic description of the Glasma and the hydrodynamic evolution of the QGP, based on an effective kinetic theory;¹⁰⁹ apply anisotropic hydrodynamics,¹¹⁰ a modified version of relativistic hydrodynamics which accommodates large momentum anisotropies, as those generated in heavy-ion collisions.

HYDRODYNAMIC EVOLUTION

5

COUPLE TO HYDRODYNAMICS

PREVIEW

Impact parameter dependence is implemented in the MV model. The Landau matching is explained and resulting the local rest frame energy density and flow velocity are studied. The centrality selection procedure is then presented. The DNMR relativistic viscous equations and the Cooper-Fryer formalism with viscous corrections are briefly introduced. A simple parameter search is performed, with shear and w/o bulk viscosity. Best fit to final multiplicities results are shown for a few observables, including elliptic flow.

5.1 Landau matching	59
5.2 Centrality selection	64
5.3 Relativistic viscous hydrodynamics	66

5.1 Landau matching

Improved MV model

Instead of providing approximate values for the phenomenological parameters, one may use results borrowed from DIS and express all the relevant parameters in terms $\sqrt{s_{\text{NN}}}$ and A for a given system. More concisely, we are going to make use of **geometrical scaling** which relates the saturation momentum of the proton $Q_{s,p}$ to the x value of a parton belonging to the proton as¹

$$Q_{s,p}^2 = Q_0^2 \left(\frac{x_0}{x} \right)^\lambda,$$

with $x_0 = 3.04 \cdot 10^{-4}$, $\lambda = 0.288$ and $Q_0 = 1 \text{ GeV}$, as extracted from fits to HERA data² [54]. If the momentum fraction x is chosen to take an effective value as

$$x = x_{\text{eff}} \approx \frac{Q_{s,p}}{\sqrt{s_{\text{NN}}}},$$

1: This parametrization is used in the GWB model of saturation [54]. There exist more sophisticated models which incorporate the physics of saturation, see [55] for a schematic overview.

2: Fits including charm quarks lead to different values for these parameters, resulting in a larger saturation scale [56].

one may deduce a parametrization of the saturation momentum in terms of energy as

$$Q_{s,p}^2(\sqrt{s_{\text{NN}}}) \approx 0.13 \sqrt{s_{\text{NN}}}^{0.25} \text{ GeV}^2.$$

The saturation scale of a nucleus $Q_{s,A}$ with a given A may be obtained from the saturation scale of the proton $Q_{s,p}$ through scaling with a geometric factor g_A which is chosen to take the simple form³

$$Q_{s,A}^2 = g_A Q_{s,p}^2 \approx A^{1/3} Q_{s,p}^2.$$

This eventually leads to the following parametrization of the saturation scale⁴

$$Q_{s,A}^2 \approx 0.13 A^{1/3} \sqrt{s_{\text{NN}}}^{0.25} \text{ GeV}^2.$$

Once the saturation scale is fixed, the coupling constant may be computed from

$$g^2 = \frac{\alpha_s(Q_{s,A})}{4\pi},$$

where the running coupling constant is given by⁵

$$\alpha_s(Q_{s,A}^2) = \frac{1}{\frac{33 - 3N_f}{12\pi} \ln \frac{Q_{s,A}^2}{\Lambda_{\text{QCD}}^2}}.$$

The relation between the saturation scale $Q_{s,A}$ and MV model parameter μ is influenced in a non-trivial manner by the number of color sheets N_s and IR regulator m . In [56], it yields⁶ $Q_{s,A} \approx 0.8g^2\mu$ for $N_s = 50$ and $m = 0.1g^2\mu$.

Impact parameter dependence

Until now only central collisions were taken into consideration. In order to simulate non-central collisions, one simply employs the color charge density of the MV model as⁷

$$\rho^a(\vec{x}_\perp) \mapsto \sigma(r_\perp)\rho^a(\vec{x}_\perp),$$

modulated by a Woods-Saxon distribution given by⁸

$$\sigma(r_\perp) \triangleq \frac{1}{1 + \exp\left\{\frac{r_\perp - r_0}{a}\right\}}.$$

3: See [56] for other possible extrapolations of the DIS data on protons to nuclei.

4: For a Au nucleus with $A = 197$ at RHIC energies of $\sqrt{s_{\text{NN}}} = 200$ GeV, the saturation scale yields $Q_{s,A} \approx 1.68$ GeV.

5: With the number of flavours $N_f = 3$ and the QCD scale $\Lambda_{\text{QCD}} \approx 200$ GeV for SU(3). For $Q_{s,A} \approx 1.68$ GeV, this yields a coupling constant of $g \approx 2.15$.

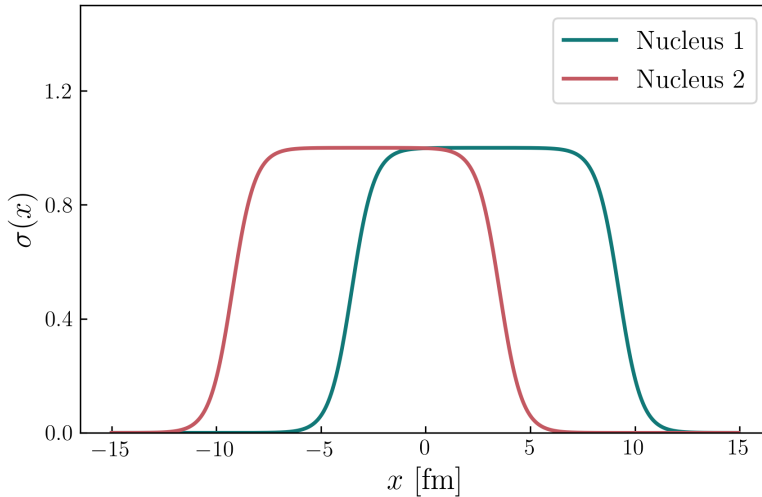
6: This results in $\mu \approx 0.45$ GeV MV parameter for a regulator $m \approx 0.21$ GeV.

7: With the notation

$$r_\perp \triangleq \sqrt{\left(x \pm \frac{b}{2}\right)^2 + \left(y \pm \frac{b}{2}\right)^2},$$

where $\vec{x}_\perp = (x, y)$.

8: For a Au nucleus, the radius is $r_0 = 6.38$ fm and the surface thickness $a = 0.535$ fm [57].



Off-central collisions are thus obtained by shifting the transverse radius⁹ with $\pm b/2$.

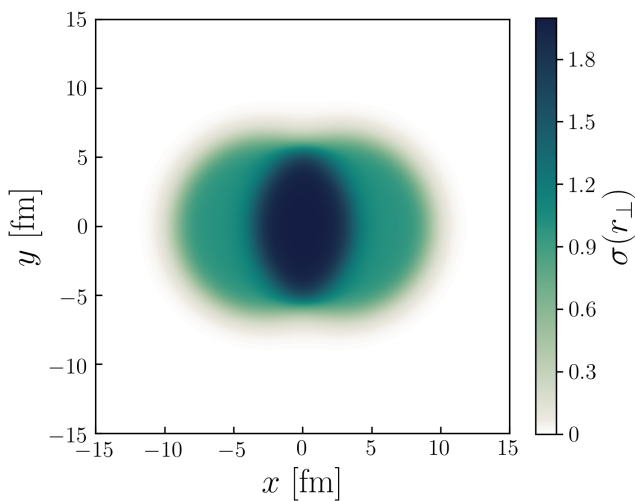


Figure 5.1: Woods-Saxon distribution $\sigma(x, y)$ as a function of x at $y = 0$ for a 10-20% centrality event having $b = 5.7$ fm.

9: For example, with $b/2$ for nucleus 1 and $-b/2$ for nucleus 2.

Landau matching

The Glasma exhibits pressure anisotropy and within a classical description,¹⁰ it may never reach isotropy. Nevertheless, the produced QGP may very well be described by employing an ideal hydrodynamics evolution [58, 59], during which the medium is assumed to be isotropic. In order to match this distinct and irreconcilable scenarios, we are going to discard information from the Glasma energy-momentum tensor.¹¹ One may construct an ideal energy-momentum tensor through a procedure named **Landau matching** as¹²

$$\mathcal{T}^{\mu\nu} = (\varepsilon_{\text{LRL}} + P)u^\mu u^\nu - Pg^{\mu\nu} = \text{Diag}\{\varepsilon_{\text{LRL}}, P, P, P\},$$

10: Using non-Abelian Yang-Mills theory.

11: By neglecting the components which would deviate the system from equilibrium.

12: Here P represents the pressure and may be computed once an equation of state is provided, namely $P = P(\varepsilon, T)$.

- 13: Where $T^{\mu\nu}$ is the energy-momentum tensor of the Glasma. One must only choose time-like flow vectors $u^\mu u_\mu = 1$.

where the local rest frame (LRF) energy density ε_{LRL} and the flow velocity u^μ may be obtained by solving¹³ the eigenequation

$$T_\nu^\mu u^\nu = \varepsilon_{\text{LRL}} u^\mu. \quad (5.1)$$

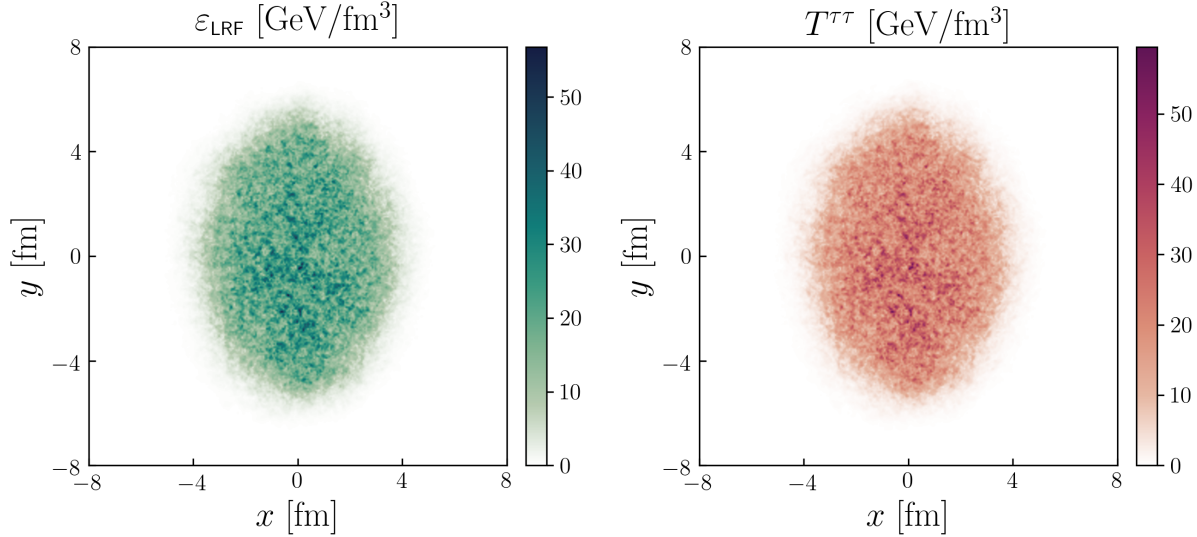


Figure 5.3: Qualitative comparison between the local rest frame ε_{LRL} and $T^{\tau\tau}$ component of the Glasma energy-momentum tensor, evaluated at $\tau_{\text{switch}} = 0.4$ fm/c for a 10-20% centrality event with $b = 5.7$ fm.

- 14: Once dissipation exhibits itself, thermodynamic quantities, which were well defined only for a fluid at local thermal equilibrium, may no longer be used.
15: Valid for an arbitrary u^μ .

- 16: In this way, the equilibrium component of $T^{\mu\nu}$ may be constructed from the local rest frame energy ε_{LRL} .

- 17: For the ideal fluid, a LRF was simply the frame in which the fluid volume element was at rest and both the energy and particle flows were null.

- 18: This choice is more appropriate for ultrarelativistic heavy-ion collisions since they take place at negligible net baryon current.

For a dissipative fluid which is near equilibrium, one may decompose the energy-momentum tensor as¹⁴

$$T^{\mu\nu} = T_{\text{ideal}}^{\mu\nu} + \delta T^{\mu\nu}.$$

Nevertheless, one may artificially assure local equilibrium by imposing the Landau matching condition¹⁵ through

$$u_\mu u_\nu \delta T^{\mu\nu} = 0,$$

which further yields¹⁶

$$\varepsilon_{\text{LRL}} = u_\mu u_\nu T^{\mu\nu}.$$

For a dissipative system in which both energy and particle diffusion coexist, one may define the LRL¹⁷ in multiple ways. Nevertheless, there exist two simple choices: the Eckart frame, where the energy flow is null, and the Landau frame, in which particle flow vanishes.¹⁸ In the Landau frame, the flow velocity u^μ is chosen to be along the energy flow velocity

$T^{\mu\nu}u_\nu$, that is

$$u_\nu T^{\mu\nu} = \varepsilon_{\text{LRL}} u^\mu.$$

In the boost-invariant approximation, one may further neglect the longitudinal flow component¹⁹ $u^\eta = 0$. Hence, the problem reduces to finding the eigenvalues ε_{LRL} and eigenvectors (u^τ, u^x, u^y) of a 3×3 sub-matrix of $T^{\mu\nu}$.

One may define flow velocities weighted with respect to the energy density as²⁰

$$w^\perp \triangleq \frac{\varepsilon_{\text{LRL}}}{\langle \varepsilon_{\text{LRL}} \rangle} u^\perp.$$

19: As emphasized in [43] and showed in [60], this component turns out to also be of relevance.

20: Where $w^\perp \triangleq (w^x, w^y)$ and similarly for u^\perp .

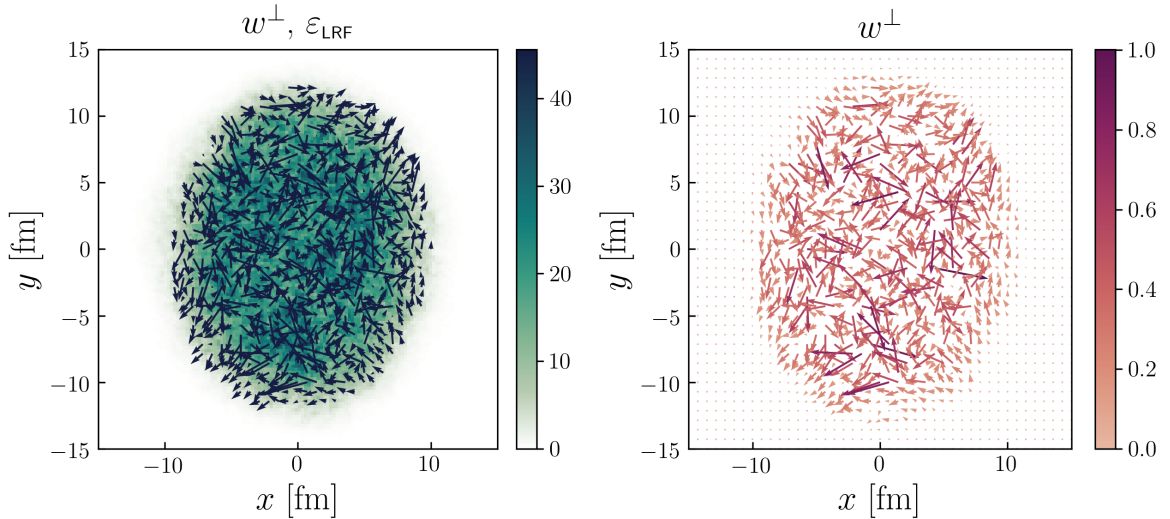


Figure 5.4: Weighted flow velocity w^\perp superimposed over the local rest frame ε_{LRL} , evaluated at $\tau_{\text{switch}} = 0.4$ fm/c for a 5-10% centrality event with $b = 3.7$ fm.

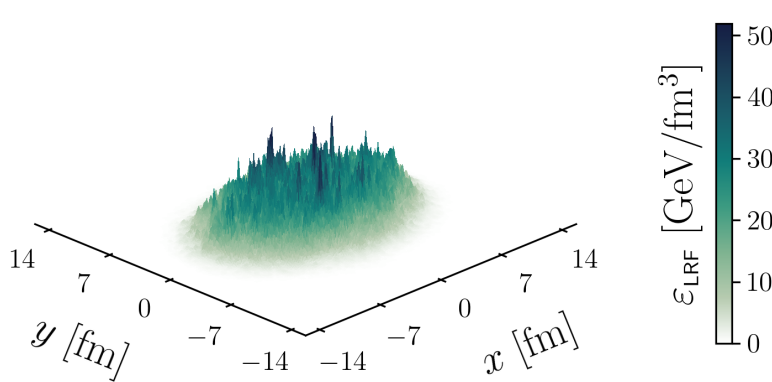


Figure 5.5: Energy density in the local rest frame ε_{LRL} as a function of the transverse coordinates, evaluated at $\tau_{\text{switch}} = 0.4$ fm/c for a 10-20% centrality event with $b = 5.7$ fm. One may notice spikes arising from the highly dense regions of the Glasma.

5.2 Centrality selection

21: We simulated $5 \cdot 10^4$ events.

22: In the range $b \in (0, 3r_0)$, that is $b \approx 0 \div 18$ fm.

23: We are going to make use of the fact that there exists a good correlation between the initial energy in the central pseudorapidity region and the final charged multiplicity.

Each event requires an impact parameter as input. In order to mimic the minimum bias centrality selection, one needs to simulate many events²¹ with impact parameters²² randomly distributed according to

$$P(b)db = \frac{bdb}{b_{\max}^2/2}.$$

The centrality selection should be performed in terms of the final charged particle multiplicity $dN_{\text{ch}}/d\eta$ but we are going to apply the centrality cuts before the hydrodynamic evolution²³ since performing hydrodynamics simulations on such a large number of events is computationally expensive and time consuming.

The Glasma fields are evolved until $\tau_{\text{switch}} = 0.4$ fm/c. We already observed that for proper times $\tau > 0.1$ fm/c the expansion of the system is of Bjorken type. Hence, the energy density at mid-pseudorapidity of the Glasma may be expressed as [61]

$$\varepsilon(\tau) \approx \frac{1}{S_{\perp}} \left(\frac{1}{\tau} \frac{dE_{\perp}}{d\eta} \right).$$

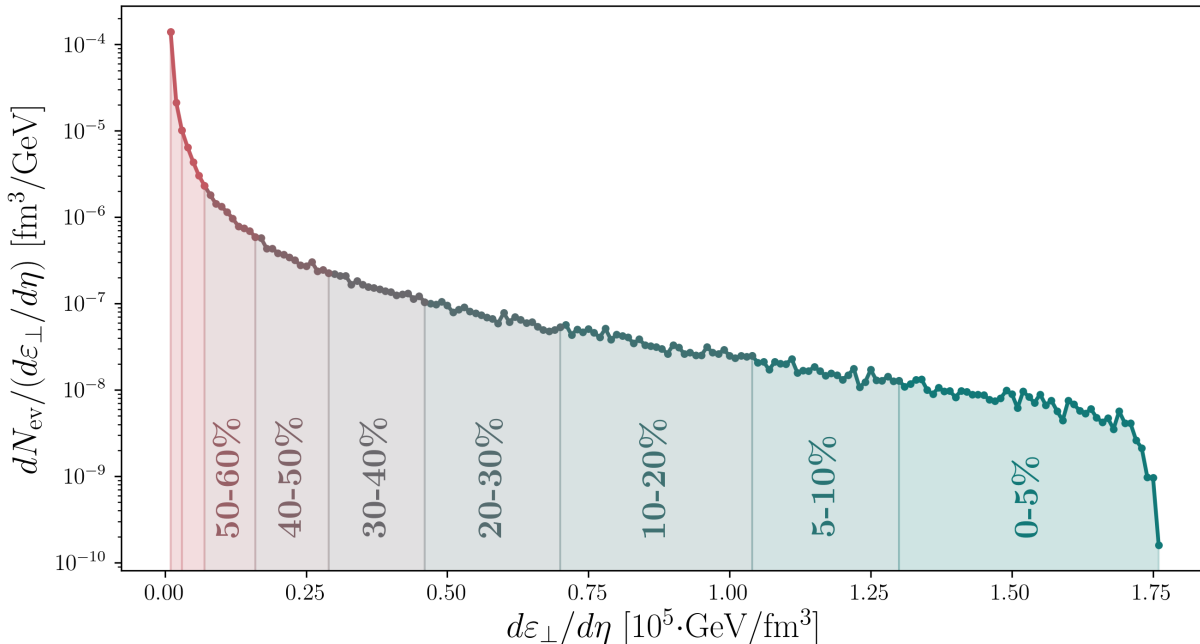
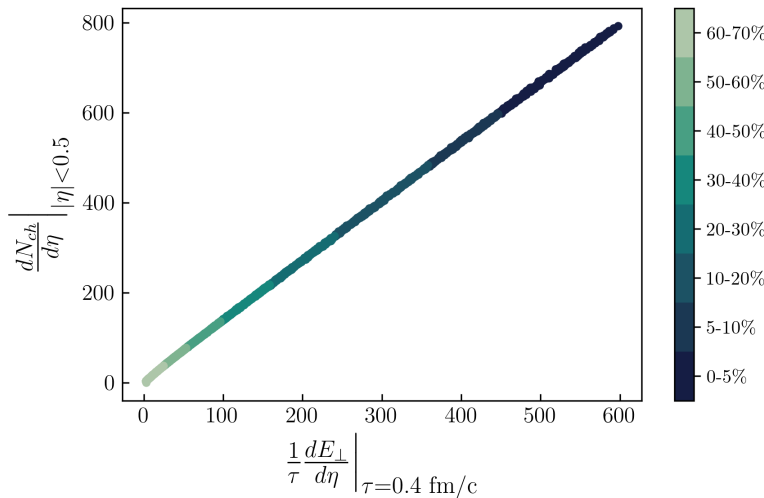


Figure 5.6: Minimum bias centrality selection using $5 \cdot 10^4$ events simulated with Curraun, divided in centrality classes according to their total energy density in the transverse plane $d\varepsilon_{\perp}/d\eta$.

Therefore, we shall split the events resulting from Curraun in terms of the total energy density²⁴ $d\varepsilon_{\perp}/d\eta$. Nevertheless, such an approach turns out to be problematic since, within a model constructed with fields, one may not provide a clear criteria whether a collision event occurs or not.

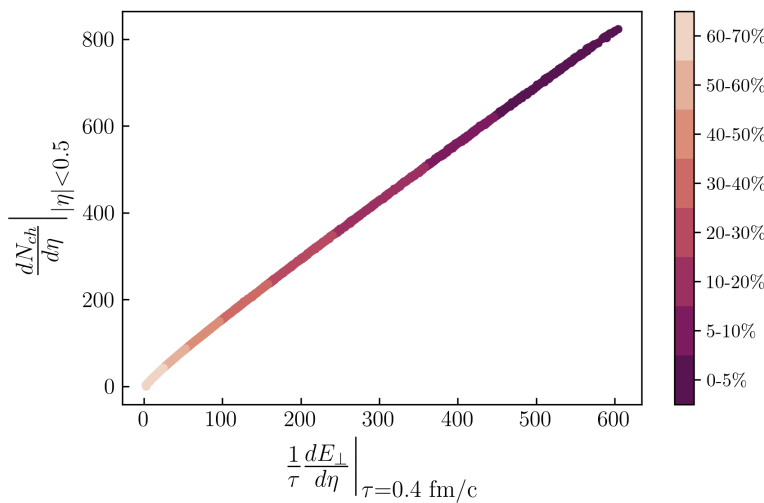
Thus, the 100% centrality cut must be chosen by hand. We shall attempt to guess it through an iterative procedure. Since $d\varepsilon_{\perp}/d\eta$ is correlated with $dN_{\text{ch}}/d\eta$, one may vary this cut until the ratios between the total energy density in different centrality cuts match the corresponding experimental multiplicity ratios. A later scaling of the energy density should not affect this centrality selection. It is important to mention that²⁵ some events may end up in a different centrality class after the hydrodynamic evolution.



24: It's not possible to directly evaluate the overlapping area in the transverse plane S_{\perp} but one may numerically extract

$$\frac{1}{\tau} \frac{dE_{\perp}}{d\eta} \Big|_{\tau} = (a_T)^2 \frac{d\varepsilon_{\perp}}{d\eta} \Big|_{\tau},$$

evaluated at $\tau = 0.4$ fm/c, where $d\varepsilon_{\perp}/d\eta$ is the total energy density in the transverse plane.



25: Since the previously mentioned correlation is only approximate.

Figure 5.7: Correlation between the initial $d\varepsilon_{\perp}/d\eta$ and the final $dN_{\text{ch}}/d\eta$ for a subset of 2700 events with 300 events per centrality. Main simulation parameters: $\eta/s = 0.24$ and $T_{\text{fo}} = 180$ MeV. A power law fit yields

$$\frac{dN_{\text{ch}}}{d\eta} \approx 2.1 \left(\frac{1}{\tau} \frac{dE_{\perp}}{d\eta} \right)^{0.93}.$$

Figure 5.8: Correlation between the initial $d\varepsilon_{\perp}/d\eta$ and the final $dN_{\text{ch}}/d\eta$ for a subset of 2700 events with 300 events per centrality. Main simulation parameters: $\eta/s = 0.1$ and $T_{\text{fo}} = 180$ MeV and hard-coded $\zeta(T)$. A power law fit yields

$$\frac{dN_{\text{ch}}}{d\eta} \approx 1.56 \left(\frac{1}{\tau} \frac{dE_{\perp}}{d\eta} \right)^{0.96}.$$

26: And obtain a parametrization of the type

$$\frac{dN_{\text{ch}}}{d\eta} = \text{const} \left(\frac{1}{\tau} \frac{dE_{\perp}}{d\eta} \right)^{\text{power}}.$$

27: Where $\Delta^{\mu\nu}$ acts as a projector operator onto the space perpendicular to u^μ . This may be inferred from its properties, namely $\Delta^{\mu\nu}u_\mu = \Delta^{\mu\nu}u_\nu = 0$ and $\Delta^{\mu\nu}\Delta_\nu^\alpha = \Delta^{\mu\alpha}$.

28: This form is only valid in the Landau frame $T^{\mu\nu}u_\nu = \varepsilon u^\mu$.

29: This should be accompanied by the conservation of the charge current but we shall work with null baryon current.

30: Which would result in

$$\begin{aligned} \Pi &= -\zeta \partial_\mu u^\mu, \\ \pi^{\mu\nu} &= 2\eta \nabla^{\langle\mu} u^{\nu\rangle}, \end{aligned}$$

with ζ and η being transport coefficients. More details in [63].

31: See [64] for a more in depth review.

32: Adding deviations from equilibrium to the entropy current.

33: Considering small deviations from the equilibrium Boltzmann equation.

An alternative approach [62] would be to take a subset from the total events, pass them through the hydrodynamic simulation, extract the final multiplicities and then map²⁶ $dN_{\text{ch}}/d\eta$ as a function of $d\varepsilon_{\perp}/d\eta$. Afterwards, one may perform a centrality selection using this map. The disadvantage would be that such a map and hence the centrality selection depends on the parameters from the hydrodynamic simulation.

5.3 Relativistic viscous hydrodynamics

Viscous hydrodynamics primer

Starting from the energy-momentum tensor for the ideal fluid²⁷

$$T_{\text{eq}}^{\mu\nu} = \varepsilon u^\mu u^\nu - P \Delta^{\mu\nu},$$

one may add dissipative corrections²⁸

$$T^{\mu\nu} = T_{\text{eq}}^{\mu\nu} - \Pi \Delta^{\mu\nu} + \pi^{\mu\nu}.$$

Since the conservation of the energy momentum tensor²⁹

$$\partial_\mu T^{\mu\nu} = 0,$$

along with an equation of state $P = P(\varepsilon, T)$ provide $4 + 1 = 5$ equations for a system with $1 + 1 + 3 + 1 + 5 = 11$ unknowns, additional information is needed to construct the viscous corrections.

One may attempt to use a relativistic version of the Navier-Stokes equations³⁰ but such an equation suffers from acausality: adding a small perturbation of energy density and flow velocity gives a parabolic dispersion relation and thus faster than light propagation. A solution is provided within the Israel-Stewart³¹ formulation by either using the second law of hydrodynamics³² or using kinetic theory.³³

In kinetic theory, all information is encoded in the microscopic distribution function $f(t, \vec{x}, \vec{p})$. Within the Boltzmann approximation, it satisfies the equation

$$p^\mu \partial_\mu f(t, \vec{x}, \vec{p}) = \mathcal{C}[f(t, \vec{x}, \vec{p})],$$

where $\mathcal{C}[f]$ represents the collision integral. One may construct the macroscopic energy-momentum tensor as

$$T^{\mu\nu}(t, \vec{x}, \vec{p}) = \sum_i g_i \int \frac{d^3 \vec{p}}{(2\pi)^3 E_{\vec{p}}} p^\mu p^\nu f_i(t, \vec{x}, \vec{p}),$$

with g_i denoting the degeneracy of the species i .

Dissipation may be added by considering small deviations of the distribution function $f = f_{\text{eq}} + \delta f$, with the equilibrium distribution given by³⁴

$$f_{\text{eq}}(x, \vec{p}) = \frac{1}{\exp\left\{\frac{p \cdot u}{T}\right\} \mp 1}.$$

Further, one may deduce an evolution equation for δf which, by making use of the energy-momentum conservation, leads to a set of equations for Π and $\pi^{\mu\nu}$. They will turn out to depend on the collision kernel. Nevertheless, by employing Grad's 14 momentum approximation³⁵

$$\delta f(\vec{p}) = f_{\text{eq}}(\vec{p}) [A_0 + A_1(p \cdot u) + A_2(p \cdot u)^2] \Pi + B_0 \pi_{\mu\nu} p^\mu p^\nu,$$

they may be reduced to a closed form³⁶

$$\begin{aligned} \tau_\pi \dot{\pi}^{\langle\mu\nu\rangle} + \pi^{\mu\nu} &= 2\eta \sigma^{\mu\nu} + 2\tau_\pi \pi_\alpha^{\langle\mu} \omega^{\nu\rangle\alpha} - \delta_{\pi\pi} \pi^{\mu\nu} \theta + \varphi_7 \pi_\alpha^{\langle\mu} \pi^{\nu\rangle\alpha} - \tau_{\pi\pi} \pi_\alpha^{\langle\mu} \sigma^{\nu\rangle\alpha} + \lambda_{\pi\Pi} \Pi \sigma^{\mu\nu}, \\ \tau_\Pi \dot{\Pi} + \Pi &= -\zeta \theta - \delta_{\Pi\Pi} \Pi \theta + \lambda_{\Pi\pi} \pi^{\mu\nu} \sigma_{\mu\nu}. \end{aligned}$$

The second order transport coefficients become, in the small mass limit³⁷

$$\begin{aligned} \tau_\pi &= \frac{5\eta}{(\varepsilon + P)}, & \tau_{\Pi\Pi} &= \zeta / \left[15 \left(\frac{1}{3} - c_s^2 \right)^2 (\varepsilon + P) \right], \\ \delta_{\pi\pi} &= \frac{4}{3} \tau_\pi, & \delta_{\Pi\Pi} &= \frac{2}{3} \tau_\Pi, \\ \varphi_7 &= \frac{9}{70P}, & \lambda_{\pi\Pi} &= \frac{6}{5}, \\ \tau_{\pi\pi} &= \frac{10}{7} \tau_\pi, & \lambda_{\Pi\pi} &= \frac{8}{5} \left(\frac{1}{3} - c_s^2 \right) \tau_\pi. \end{aligned}$$

Cooper-Fryer prescription

As the QGP expands, the medium becomes more dilute and its temperature decreases, eventually leading to a phase transition from a state of deconfined quarks and gluons to a

34: That is Bose-Einstein or Fermi-Dirac distributions.

35: In which the dissipative corrections are expanded up to quadratic terms in momentum.

36: See [65] for complete computations.

37: They were originally derived in [66–68].

38: The hadronization begins at the edge of the medium and gradually reaches the central region.

39: Usually referred to as particlization.

40: Which is the freeze-out temperature, denoted as T_{fo} .

41: Where n_i^μ represents the number current, $E_{\vec{p}}$ obeys the relation $E_{\vec{p}}^2 = \vec{p}^2 + m^2$ and $d^3\Sigma_\mu$ is the surface element oriented along the orthogonal direction from the hypersurface Σ .

42: This conversion of the hydrodynamic energy-momentum tensor to particles conserves the energy and the number of particles.

43: The shear correction must be a scalar constructed with $\pi^{\mu\nu}$.

hadron gas and then to reconfinement into hadrons.³⁸ The transition between a hydrodynamic description in terms of the energy-momentum tensor and the subsequent produced particles,³⁹ is assumed to take place at a given temperature⁴⁰ for all species.

The points at which the particlization temperature is reached form a 4-dimensional hypersurface Σ . Equipped with a microscopic distribution function, one may compute the number of points crossing this hypersurface as⁴¹

$$N_i = \int_{\Sigma} d^3\Sigma_\mu(x) \underbrace{\frac{g_i}{(2\pi)^3} \int \frac{d^3\vec{p}}{E_{\vec{p}}} p^\mu f_i(x, \vec{p})}_{n_i^\mu(x)}.$$

From this one may deduce the **Cooper-Fryer** formula⁴² [69]

$$\frac{dN_i}{d^3\vec{p}} = \frac{g_i}{(2\pi)^3} \int_{\Sigma} \frac{d^3\Sigma_\mu p^\mu}{E_{\vec{p}}} f_i(x, \vec{p}),$$

with the distribution function given by

$$f(x, \vec{p}) = f_{\text{eq}}(x, \vec{p}) + \delta f_{\text{shear}}(x, \vec{p}) + \delta f_{\text{bulk}}(x, \vec{p}).$$

The shear correction is chosen to take the quadratic form [70] for all hadron species⁴³

$$\delta f_{\text{shear}}(x, \vec{p}) = f_{\text{eq}}(1 \pm f_{\text{eq}}) \frac{\pi_{\mu\nu} p^\mu p^\nu}{2(\varepsilon_0 + P_0) T^2},$$

whereas the bulk correction, derived using the first-order Chapman-Enskog theory within the relaxation time approximation [71, 72], is species dependent

$$\delta f_{\text{bulk}}(x, \vec{p}) = -f_{\text{eq}}(1 \pm f_{\text{eq}}) \frac{C_{\text{bulk}}}{T} \left[\frac{m^2}{3(p \cdot u)} - \left(\frac{1}{3} - c_s^2 \right) (p \cdot u) \right] \Pi,$$

with the bulk coefficient expressible as

$$\frac{T}{C_{\text{bulk}}} = \frac{1}{3} \sum_i g_i m_i^2 \int \frac{d^3\vec{k}}{(2\pi)^3 E_{\vec{k}}} f_{i,\text{eq}}(1 \pm f_{i,\text{eq}}) \left[\frac{m_i^2}{3E_{\vec{k}}} - \left(\frac{1}{3} - c_s^2 \right) E_{\vec{k}} \right].$$

Afterwards, the number of particles in each cell is sampled according to a Poisson distribution.⁴⁴ The particle spectra resulting from Cooper-Fryer may not directly be compared to experimental data since after particilization, the resulting particles may decay or suffer rescatterings.

44: More details about the sampling procedure and a pedagogical derivation for the dissipative corrections to the distribution function may be found at [65].

General setup

The events resulting from **Curraun**, a Python based code for computing Glasma fields, are coupled, via energy density and flow velocity obtained from the Landau matching, to **MUSIC** [71, 73, 74], a code⁴⁵ for simulating relativistic heavy-ion collisions, using relativistic second-order viscous hydrodynamics, written in C++.

Recent hybrid simulations with CGC based initial conditions given as input to **MUSIC** also include a post-particilization stage⁴⁶ simulated with **UrQMD**. Nevertheless, in this work, only the decays of unstable particles shall be considered.⁴⁷

The most important parameters which were provided to **MUSIC** as input shall be summarized below. Some parameters have fixed values throughout this study:

The proper time at which the initial stage is stopped and the hydrodynamic evolution begins. In the current work, it is fixed at $\tau_{\text{switch}} = 0.4 \text{ fm/c}$.

τ_{switch}

The equation of state for the QGP. We shall employ "s95p-v1-PCE", constructed by interpolating between HRG at low temperatures and lattice QCD EoS [77], with partial chemical equilibrium at $T_{\text{chem}} = 150 \text{ MeV}$.

EoS

The specific bulk viscosity. It is hard-coded in **MUSIC** and parametrized with respect to temperature [5, 75], with a maximum around the QCD phase transition temperature $T_{\text{peak}} = 180 \text{ MeV}$.

ζ/s

whereas others are allowed to run freely in a certain range:

45: Publicly available at <https://github.com/MUSIC-fluid/MUSIC> with an user manual at https://webhome.phy.duke.edu/~jp401/music_manual/index.html

46: In [75] it was emphasized that including rescatterings bring improvements for protons and multi-strange particles.

47: **MUSIC** is also equipped with resonance decay routines fetched from **AZHYDRO** [76].

s_{factor}	The normalization factor for the initial energy density. This parameter is allowed to vary within the range $s_{\text{factor}} = 0.5 \div 2.0$.
η/s	The specific shear viscosity. We assume a temperature independent value tuned between $\eta/s = 0.08 \div 0.24$ when only shear viscosity corrections are considered and $\eta/s = 0.02 \div 0.1$ when bulk viscosity is also included.
T_{fo}	The kinetic freeze-out temperature, at which the Cooper-Fryer formula is applied for conversion to particles, allowed to take values within $T_{\text{fo}} = 100 \div 180$ MeV.

The strategy for extracting relatively realistic values for the free parameters is the following: firstly, we average all the events from a certain centrality class, as obtained from **Curraun**, since performing an event-by-event search for optimal parameters would be time expensive and using averaged initial conditions should provide reasonable results for spectra and final multiplicities; next, the averaged initial distributions⁴⁸ are provided as input for **MUSIC** with sufficiently many values for s_{factor} , η/s and T_{fo} ; afterwards, the set of parameters which best fit⁴⁹ the finally measured multiplicities⁵⁰ are chosen; these values are then used to perform event-by-event simulations for all centralities;⁵¹ lastly, we compare the results from this hybrid approach to experimental data. Among experimentally measured observables such as p_T spectra and particle multiplicities, it is also instructive to study the flow coefficients⁵² which arise from such an hybrid approach. From the Fourier expansion⁵³

$$\frac{dN}{d\Phi} = \frac{N}{2\pi} \left[1 + 2 \sum_n v_n \cos [n(\Phi - \Psi_n)] \right],$$

one may extract flow coefficients as⁵⁴

$$v_n \triangleq \langle \cos [n(\Phi - \Psi_n)] \rangle.$$

Event-by-event fluctuations in the initial energy density profile, which may display higher deformations, gives rise to higher order harmonics.⁵⁵ The study of flow coefficients enables the extraction of fundamental properties of the QGP, such as transport coefficients or the equation of state.

48: More concisely, averaged input files with energy density and flow velocity for 0-5%, 5-10%, 10-20%, 20-30% and 30-40%.

49: Which give the smallest χ^2 .

50: For pions, kaons and protons.

51: With 300 events per centrality class.

52: We shall focus on the elliptic flow v_2 , which is considered to be an important signature of QGP.

53: Where Φ is the azimuthal angle and Ψ_n denotes the event-plane angle.

54: They reflect the final momentum anisotropy, which may be caused by initial spatial anisotropies.

55: As showed in [78], where high order flow coefficients are well described by employing EoS fluctuating initial conditions.

Results

Shear viscosity

The minimal bayesian study previously described leads to the best fit parameters $s_{\text{factor}} = 1.6$, $\eta/s = 0.24$ and $T_{\text{fo}} = 180$ MeV for the case when only the shear dissipative corrections are taken into account. Before looking at the final results, it is perhaps instructive to see how varying⁵⁶ the shear viscosity or freeze-out temperature affects the spectra.

56: By keeping all the other parameters at the best fit values.

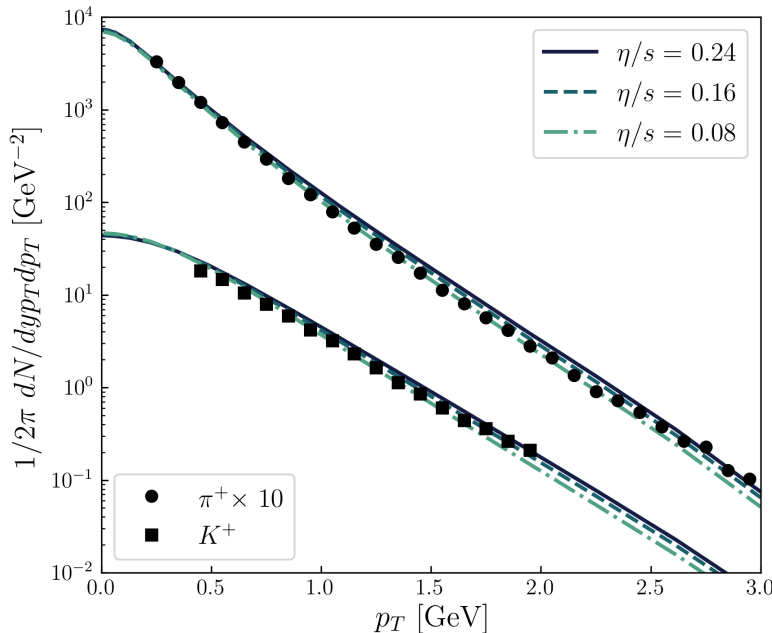


Figure 5.9: Transverse momentum spectra for positively charged pions and kaons of 0-5% centrality, with fixed $s_{\text{factor}} = 1.6$ and $T_{\text{fo}} = 180$ MeV but varying η/s . The results are compared to PHENIX data [79]. The shear viscosity correction δf_{shear} is included. Increasing η/s leads to flatter spectra.

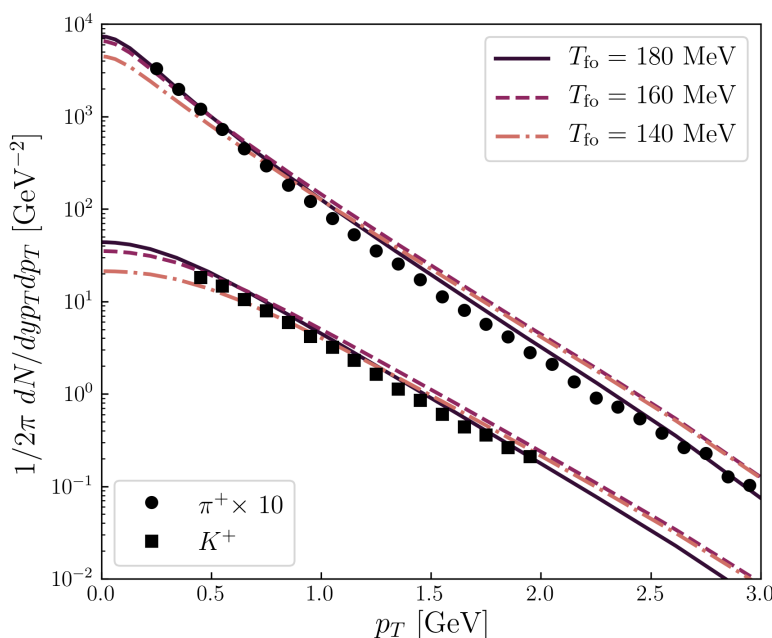


Figure 5.10: Transverse momentum spectra for positively charged pions and kaons of 0-5% centrality, with fixed $s_{\text{factor}} = 1.6$ and $\eta/s = 0.24$ MeV but varying T_{fo} . The results are compared to PHENIX data [79]. The shear viscosity correction δf_{shear} is included. Increasing T_{fo} leads to steeper spectra.

Figure 5.11: Charged particle multiplicity for all hadrons and positively charged pions, kaons and protons at different centralities. Data is taken from the tables provided in [80]. The proton multiplicity is not well reproduced. In [75] coupling MUSIC to UrQMD fixes this issue.

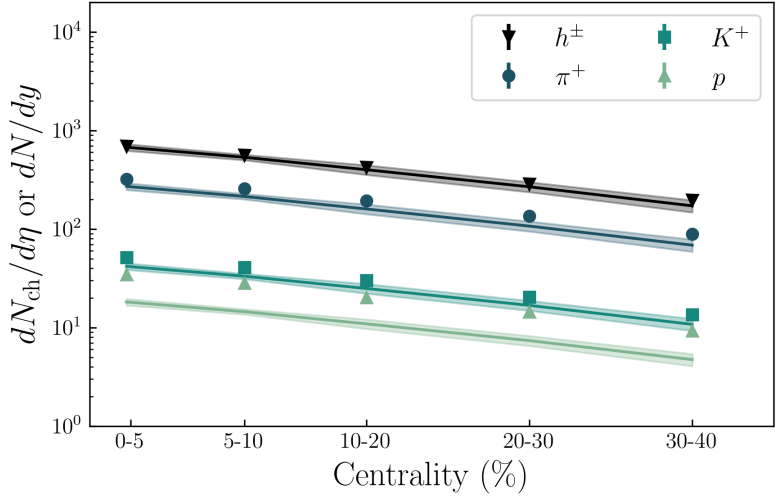


Figure 5.12: Transverse momentum integrated elliptic flow of charged hadrons as a function of centrality. Data is taken from [81].

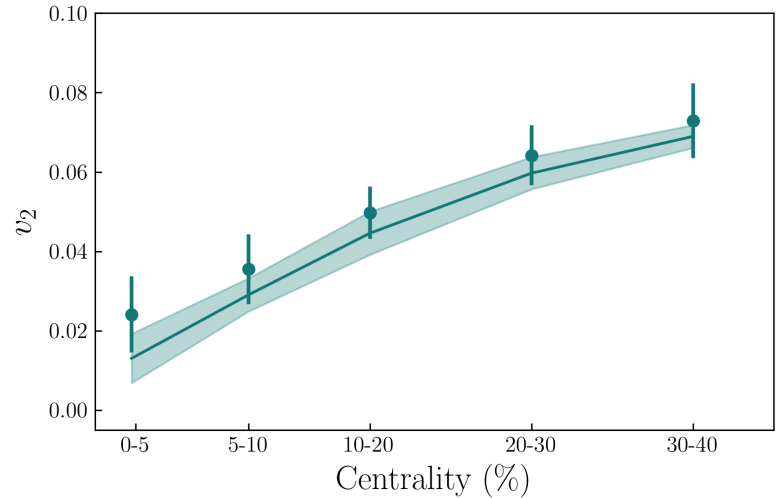
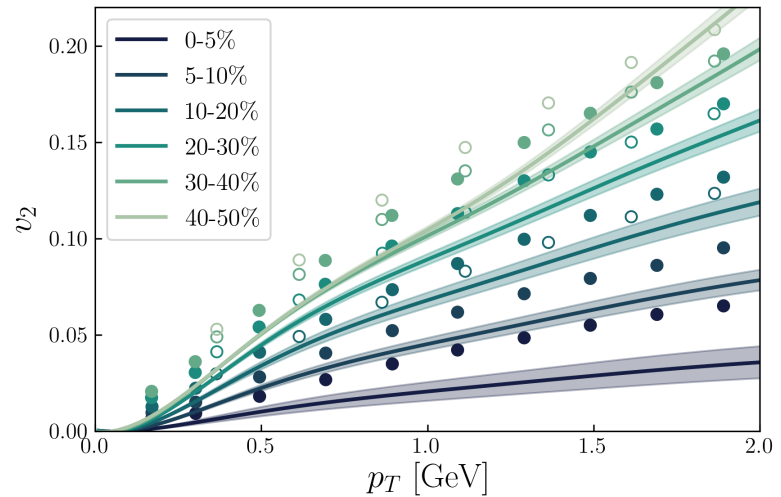


Figure 5.13: Differential elliptic flow for charged hadrons at different centralities. The open symbols represent PHENIX data points [82] whereas the filled correspond to STAR data [83].



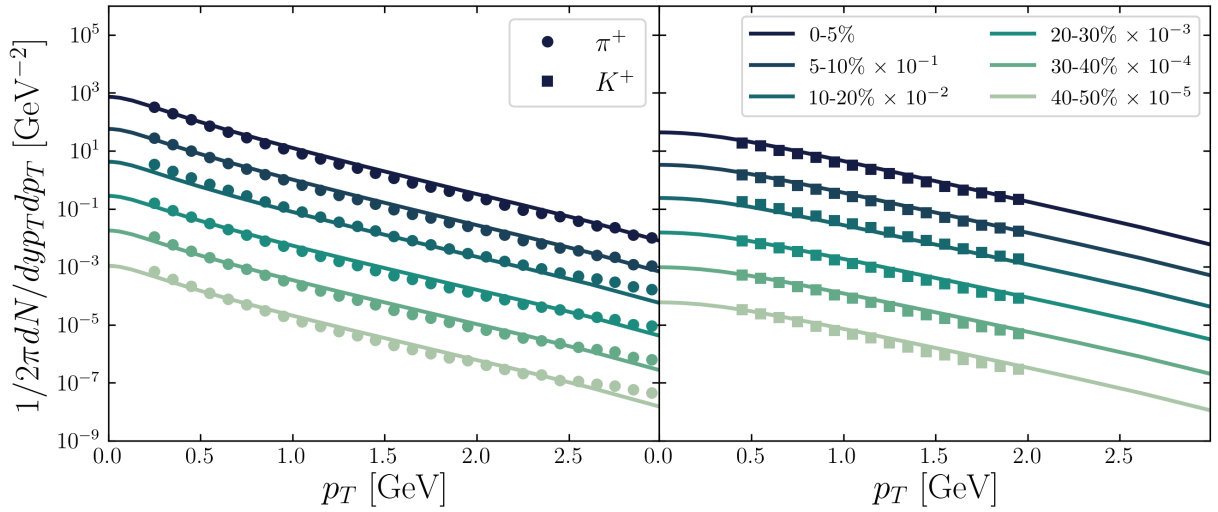


Figure 5.14: Transverse momentum spectra for positively charged pions and hadrons at different centralities. The results are compared to PHENIX data [79].

Shear and bulk viscosities

The minimal bayesian study described previously lead to the best fit parameters $s_{\text{factor}} = 1.6$, $\eta/s = 0.1$ and $T_{\text{fo}} = 180$ MeV when bulk viscosity is also considered.

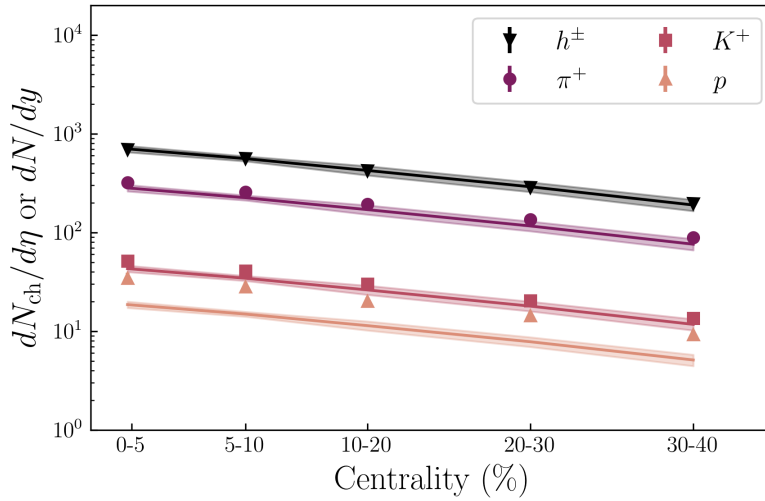


Figure 5.15: Charged particle multiplicity for all hadrons and positively charged pions, kaons and protons at different centralities. Data is taken from the tables provided in [80].

Figure 5.16: Transverse momentum integrated elliptic flow of charged hadrons as a function of centrality. Data is taken from [81].

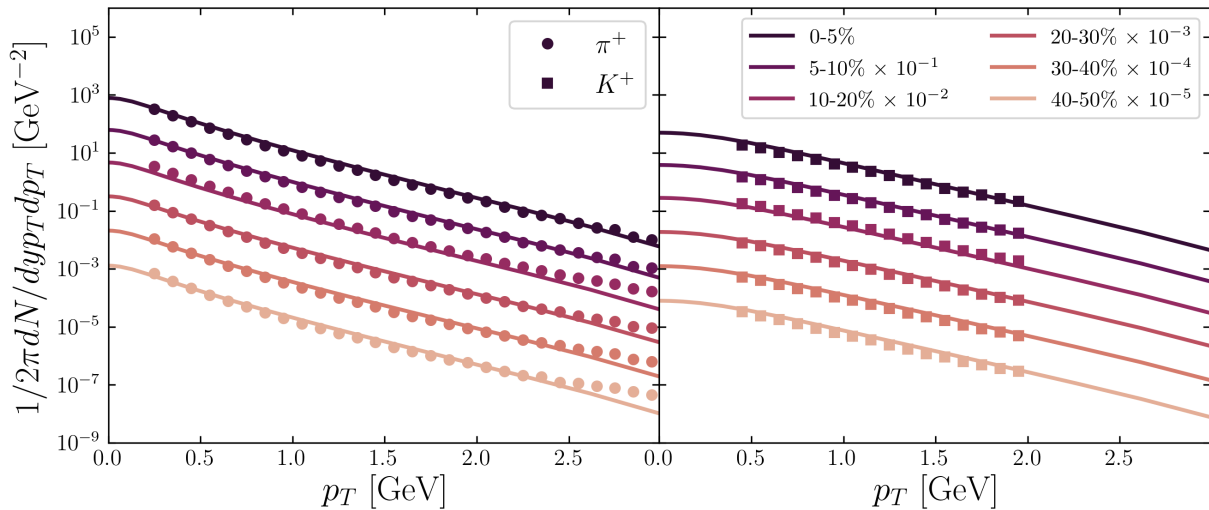
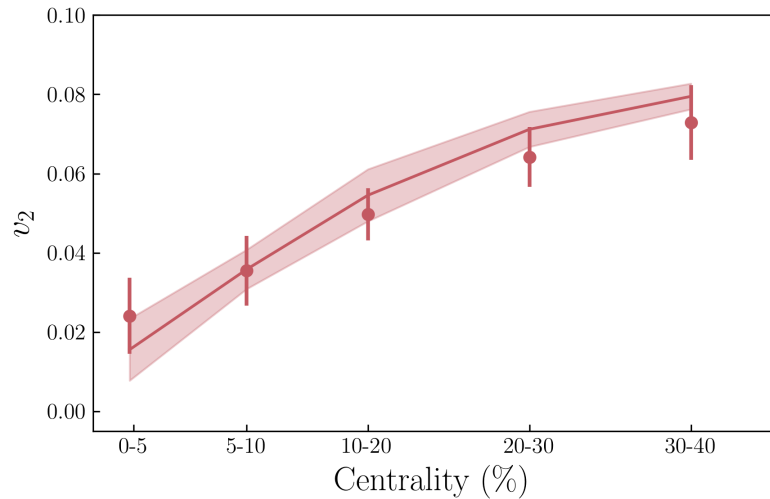
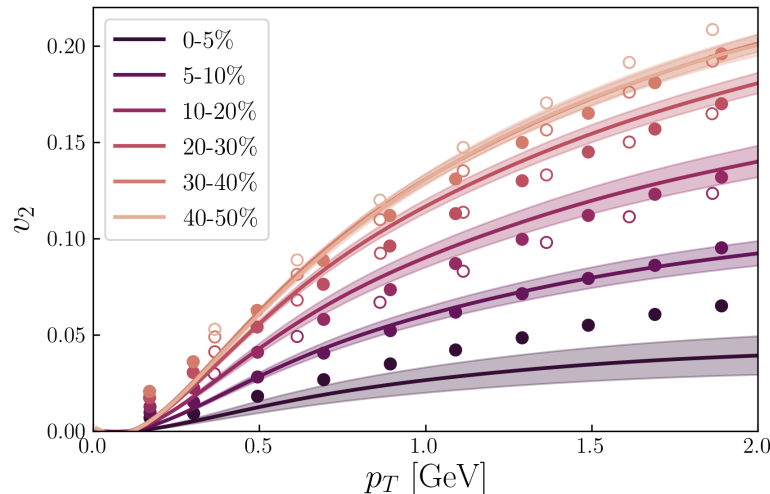


Figure 5.17: Transverse momentum spectra for positively charged pions and hadrons at different centralities. The results are compared to PHENIX data [79].

Figure 5.18: Differential elliptic flow for charged hadrons at different centralities. The open symbols represent PHENIX data points [82] whereas the filled correspond to STAR data [83].



CONCLUSIONS 6

This thesis aims to be an overview of the MV model along with the gluon saturation which emerges within its framework, and of some basic notions from relativistic viscous hydrodynamics. These approaches are numerically implemented in simulation codes publicly available. The initial conditions arising from CGC initial conditions are coupled to viscous hydrodynamics and the final results are compared to experimental data from RHIC for Au+Au collisions at $\sqrt{s_{NN}} = 200$ GeV, providing satisfactory results when both shear and bulk viscosities are taken into account. This is of course a minimal hybrid approach and more stages must be included for a better description of heavy-ion collisions.

“He had once tasted the experience that the Game could be played in a supreme and sacred sense; but he had also seen that the majority of players and students of the Game, and even some of the leaders and teachers, by no means shared that lofty and sacramental feeling for the Game. They did not regard the Game language as a lingua sacra, but more as an ingenious kind of stenography. They practiced the Game as an interesting or amusing specialty, an intellectual sport or an arena for ambition.[...] In short, he had doubts and divided feelings; the Game was a vital question for him, had become the chief problem of his life, and he was by no means disposed to let well-meaning spiritual guides ease his struggles or benignly smiling teachers dismiss them as trivial.“

Hermann Hesse, [The Glass Bead Game](#)

APPENDIX

A

LIGHT-CONE QUANTIZATION

A.1 Light-front form

Let us begin by choosing an appropriate coordinate system, that is one which would naturally allow for both a relativistic and quantum mechanical treatment. In [23], Dirac identified three possible manners of constructing such a formulation: the **instant form**, the **front form** and the **point form**.

The starting point for their derivation consists of the fact that a relativistic quantum system must, in an intrinsic way, possess invariance under inhomogeneous infinitesimal Lorentz transformations and also a Hamiltonian formulation. The first condition may simply be equivalently expressed as invariance under the action of the generators belonging to the Poincaré group, whereas the second one imposes particular transformation laws for the quantum Poisson bracket of any two dynamical variables.

The instant form

Given the Minkowski space-time equipped with a metric

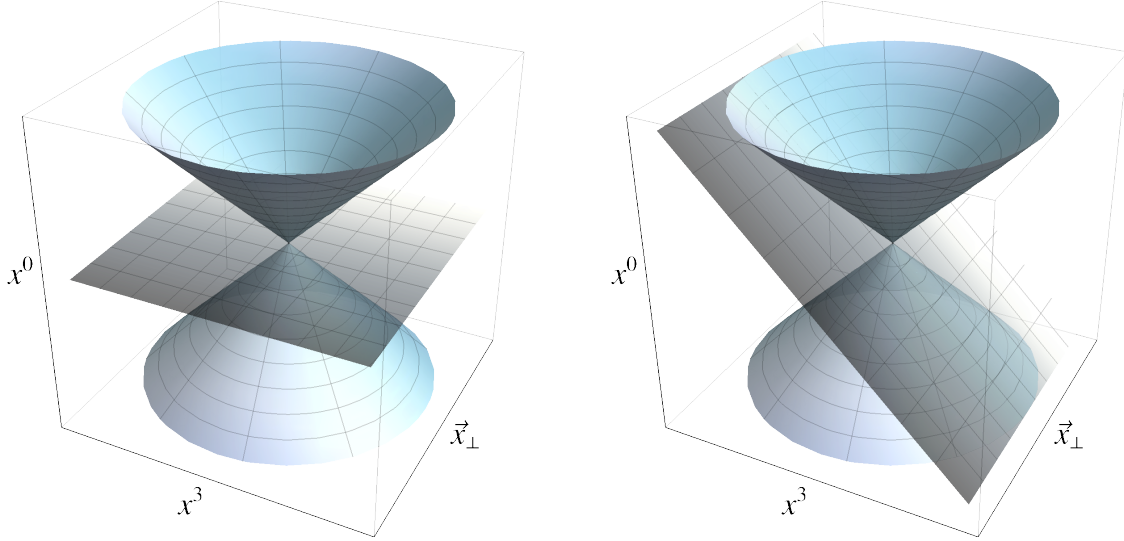
$$g_{\mu\nu} = g^{\mu\nu} = \begin{pmatrix} 1 & 0 & 0 & 0 \\ 0 & -1 & 0 & 0 \\ 0 & 0 & -1 & 0 \\ 0 & 0 & 0 & -1 \end{pmatrix},$$

the instant form is simply characterized by the usual covariant coordinates

$$x^\mu = (x^0, \underbrace{x^1, x^2}_{\triangleq \vec{x}_\perp}, x^3) = (x^0, \vec{x}_\perp, x^3).$$

Using a similar notation, the contravariant $x_\mu = (x_0, \vec{x}_\perp, x_3)$ may be expressed as $x_\mu = g_{\mu\nu}x^\nu = (x^0, -\vec{x}_\perp, -x^3)$. The scalar product is simply given by

$$x \cdot y = x_\mu y^\mu = g_{\mu\nu}x^\mu y^\mu = x^0 y^0 - \underbrace{(x^1 y^1 + x^2 y^2)}_{\vec{x}_\perp \cdot \vec{y}_\perp} - x^3 y^3.$$

The instant form initialized at $x^0 = 0$.The front form initialized at $x^+ = 0$.

Transition to other forms

Let us enforce a clear separation between the time and spatial coordinates by introducing the notation

$$x^\mu = (x^0 = t, \underbrace{x^1, x^2, x^3}_{\triangleq \mathbf{x}}) = (t, \mathbf{x}).$$

The evolution of a system characterized by a wavefunction $\Psi(t, \mathbf{x})$ is given by the Schrödinger equation

$$H_0 \Psi(t, \mathbf{x}) = i \frac{\partial}{\partial t} \Psi(t, \mathbf{x}),$$

where the free Hamiltonian H_0 represents the generator of spatial translations along \mathbf{x} in the time t . The solution for the above equation is obtained after imposing initial conditions $\Psi(t_0, \mathbf{x}_0)$ on a space-like hypersurface at $t = 0$.

One may adopt a more general approach and use generic coordinates $\tilde{x}^\mu = (\tilde{x}^0, \tilde{\mathbf{x}})$. A similar evolution equation for the state $\Psi(\tilde{x}^0, \tilde{\mathbf{x}})$ may also be written as

$$\tilde{H}_0 \Psi(\tilde{x}^0, \tilde{\mathbf{x}}) = i \frac{\partial}{\partial \tilde{x}^0} \Psi(\tilde{x}^0, \tilde{\mathbf{x}}),$$

with the initial conditions $\Psi(\tilde{x}^0, \tilde{\mathbf{x}})$ expressed on a null-time hypersurface $\tilde{x}^0 = 0$.

Each specific choice of coordinates provides a certain equation for the null-time hypersurface, which then describes a certain form of relativistic quantum mechanics. These choices of coordinates must be independent of each other, in the sense that one may not obtain a parametrization from another via a Lorentz transformation [84].

Besides the three forms of relativistic dynamics identified by Dirac, there are another two, chosen such that they satisfy the requirements: there exist a subgroup from the Poincaré

generators which leave the hypersurface invariant; they act in such a way that any points from the hypersurface may be connected via a transformation from the group of these generators [85]. In the following, we shall focus on the light-front form.

The front form

Let us perform a change of variables $(x^0, \vec{x}_\perp, x^3) \mapsto (x^+ \vec{x}_\perp, x^-)$ and introduce the light-cone coordinates

$$x^\pm \triangleq \frac{1}{\sqrt{2}} (x^0 \pm x^3),$$

A simple manipulation lead to an expression for the scalar product

$$\begin{aligned} x \cdot y &= x^0 y^0 - x^3 y^3 - \vec{x}_\perp \cdot \vec{y}_\perp \\ &= \frac{1}{2} [(x^0 + x^3)(y^0 - y^3) + (x^0 - x^3)(y^0 + y^3)] - \vec{x}_\perp \cdot \vec{y}_\perp \\ &= x^+ y^- + x^- y^+ - \vec{x}_\perp \cdot \vec{y}_\perp. \end{aligned}$$

We may easily conclude that the metric tensor becomes non-diagonal

$$\tilde{g}_{\mu\nu} = \tilde{g}^{\mu\nu} = \begin{pmatrix} 0 & 0 & 0 & 1 \\ 0 & -1 & 0 & 0 \\ 0 & 0 & -1 & 0 \\ 1 & 0 & 0 & 0 \end{pmatrix}.$$

When performing integrals, the volume element only acquires a unity factor from the Jacobian associated to the change of coordinates:

$$\int d^4x = \int dx^+ dx^- d^2\vec{x}_\perp.$$

Even though straight-forward, let us explicitly write down how the spatial and time partial derivatives look like. For simplicity, we are going to introduce the notations

$$\partial_\alpha \triangleq \frac{\partial}{\partial x^\alpha}, \quad \partial^\alpha \triangleq \frac{\partial}{\partial x_\alpha},$$

where the index $\alpha = \{+, -, \perp\}$. Hence, we have

$$\begin{aligned} \partial_+ &= \tilde{g}^{+-} \partial^- = \partial^-, \\ \partial_- &= \tilde{g}^{-+} \partial^+ = \partial^+, \\ \partial_i &= \tilde{g}^{ij} \partial^j = -\partial^i, \text{ where } i, j = 1, 2. \end{aligned}$$

Kinematic comparison between the instant and light-front forms

time coordinate	x^0	x^+
spatial coordinates	(\vec{x}_\perp, x^3)	(\vec{x}_\perp, x^-)
metric tensor	$g^{00} = 1,$ $g^{11} = g^{22} = g^{33} = -1$	$\tilde{g}^{+-} = \tilde{g}^{-+} = 1,$ $\tilde{g}^{11} = \tilde{g}^{22} = -1$
scalar product	$x^0 y^0 - x^3 y^3 - \vec{x}_\perp \cdot \vec{y}_\perp$	$x^+ y^- + x^- y^+ - \vec{x}_\perp \cdot \vec{y}_\perp$
time derivative	$\partial_0 = \partial^0$	$\partial_+ = \partial^-$
spatial derivatives	$\partial_i = -\partial^i, i = 1, 2, 3$	$\partial_- = \partial^+, \partial_i = -\partial^i, i = 1, 2$

A.2 Poincaré on the light-cone

Any form of relativistic quantum mechanics is constructed using the Poincaré group $\mathbb{R} \times \mathcal{SO}(1, 3)$. The associated Lie algebra is given by the commutation relations

$$\begin{aligned} [P^\nu, P^\mu] &= 0, \\ [M^{\nu\mu}, P^\rho] &= i(g^{\nu\rho} P^\mu - g^{\nu\mu} P^\rho), \\ [M^{\nu\mu}, M^{\rho\sigma}] &= i(g^{\nu\sigma} M^{\mu\rho} - g^{\nu\rho} M^{\mu\sigma} + g^{\mu\rho} M^{\nu\sigma} - g^{\mu\sigma} M^{\nu\rho}), \end{aligned} \tag{A.1}$$

where P^ν are spatial translations and $M^{\nu\mu}$ Lorentz transformations. If we introduce

$$J^i \triangleq \epsilon^{ijk} M^{jk}, \quad K^i \triangleq M^{0i},$$

the expressions written in Equation (A.1) become

$$\begin{aligned} [J^i, P^j] &= i\epsilon^{ijk} P^k, & [J^i, J^j] &= i\epsilon^{ijk} J^k, \\ [J^i, P^0] &= 0, & [J^i, K^j] &= i\epsilon^{ijk} K^k, \\ [K^i, P^j] &= -i\delta^{ij} P^0, & [K^i, K^j] &= -i\epsilon^{ijk} J^k, \\ [K^i, P^0] &= -iP^i, \end{aligned}$$

from which we may infer that J^i generate rotations, whereas K^i is a boost operator. In light-cone coordinates, the generators of the Poincaré algebra are [86]

$$\tilde{P}^\mu = (P^+, P^1, P^2, P^-), \quad \tilde{M}^{\nu\mu} = \begin{pmatrix} 0 & -S^1 & -S^2 & K^3 \\ S^1 & 0 & J^3 & B^1 \\ S^2 & -J^3 & 0 & B^2 \\ -K^3 & -B^1 & -B^2 & 0 \end{pmatrix}, \tag{A.2}$$

where we introduced the notations

$$\begin{aligned} P^+ &\triangleq \frac{P^0 + P^3}{\sqrt{2}}, & B^1 &\triangleq \frac{K^1 + J^2}{\sqrt{2}}, & S^1 &\triangleq \frac{K^1 - J^2}{\sqrt{2}} \\ P^- &\triangleq \frac{P^0 - P^3}{\sqrt{2}}, & B^2 &\triangleq \frac{K^2 - J^1}{\sqrt{2}}, & S^2 &\triangleq \frac{K^2 + J^1}{\sqrt{2}}. \end{aligned} \quad (\text{A.3})$$

In order to deduce how the Poincaré generators transform under the change of coordinates $x^\alpha = (x^0, x^1, x^2, x^3) \mapsto \tilde{x}^\mu = (\tilde{x}^+, x^1, x^2, x^-)$, we first compute the matrix associated to the transformation $\tilde{x}^\mu = C_\alpha^\mu x^\alpha$ as

$$C_\alpha^\mu = \frac{1}{\sqrt{2}} \begin{pmatrix} 1 & 0 & 0 & 1 \\ 0 & \sqrt{2} & 0 & 0 \\ 0 & 0 & \sqrt{2} & 0 \\ 1 & 0 & 0 & -1 \end{pmatrix}.$$

Hence, the four momentum, which is a four-vector, transforms as

$$\tilde{P}^\mu = C_\alpha^\mu P^\alpha = \begin{pmatrix} \frac{1}{\sqrt{2}} & 0 & 0 & \frac{1}{\sqrt{2}} \\ 0 & 1 & 0 & 0 \\ 0 & 0 & 0 & 1 \\ \frac{1}{\sqrt{2}} & 0 & 0 & -\frac{1}{\sqrt{2}} \end{pmatrix} (P^0, P^1, P^2, P^3) = \left(\frac{P^0 + P^3}{\sqrt{2}}, P^1, P^2, \frac{P^0 - P^3}{\sqrt{2}} \right)$$

Similarly, a four-tensor of second rank will transform according to

$$\begin{aligned} \tilde{M}^{\mu\nu} &= C_\alpha^\mu M^{\alpha\beta} (C_\beta^\nu)^T \\ &= \begin{pmatrix} \frac{1}{\sqrt{2}} & 0 & 0 & \frac{1}{\sqrt{2}} \\ 0 & 1 & 0 & 0 \\ 0 & 0 & 0 & 1 \\ \frac{1}{\sqrt{2}} & 0 & 0 & -\frac{1}{\sqrt{2}} \end{pmatrix} \begin{pmatrix} 0 & -K^1 & -K^2 & -K^3 \\ K^1 & 0 & J^3 & -J^2 \\ K^2 & -J^3 & 0 & J^1 \\ K^3 & J^2 & -J^1 & 0 \end{pmatrix} \begin{pmatrix} \frac{1}{\sqrt{2}} & 0 & 0 & \frac{1}{\sqrt{2}} \\ 0 & 1 & 0 & 0 \\ 0 & 0 & 0 & 1 \\ \frac{1}{\sqrt{2}} & 0 & 0 & -\frac{1}{\sqrt{2}} \end{pmatrix} \\ &= \begin{pmatrix} 0 & -\frac{K^1 - J^2}{\sqrt{2}} & -\frac{K^2 + J^1}{\sqrt{2}} & K^3 \\ \frac{K^1 - J^2}{\sqrt{2}} & 0 & J^3 & \frac{K^1 + J^2}{\sqrt{2}} \\ \frac{K^2 + J^1}{\sqrt{2}} & -J^3 & 0 & \frac{K^2 - J^1}{\sqrt{2}} \\ -K^3 & -\frac{K^1 + J^2}{\sqrt{2}} & -\frac{K^2 - J^1}{\sqrt{2}} & 0 \end{pmatrix}. \end{aligned}$$

All the above results, after making use of the notations from Equation (A.3), lead exactly to the expected results given in Equation (A.2).

Hence, the generators of the Poincaré group in the light-front framework may schematically be written as

$$\left\{ \tilde{P}^\mu \triangleq (P^+, \vec{P}_\perp, P^-), \vec{B}_\perp \triangleq (B^1, B^2), \vec{S}_\perp \triangleq (S^1, S^2), J^3, K^3 \right\} \quad (\text{A.4})$$

Two-dimensional Galilean sub-group structure

One important feature of the light-front parametrization is that the Poincaré group possesses a sub-group isomorphic to the two-dimensional Galilean group. In order to explicitly see this structure, we begin by writing the commutation relations for all the light-front Poincaré generators

$$\begin{aligned} [P^+, P^-] &= 0, & [P^+, \vec{P}_\perp^i] &= 0, \\ [P^+, \vec{B}_\perp^i] &= 0, & [P^+, J^3] &= 0, \\ [P^-, \vec{P}_\perp^i] &= 0, & [P^-, \vec{B}_\perp^i] &= i\vec{P}_\perp^i, \\ [P^-, J^3] &= 0, & [\vec{P}_\perp^i, \vec{B}_\perp^j] &= i\delta^{ij}P^+, \\ [J^3, \vec{P}_\perp^i] &= i\epsilon^{ij}\vec{P}_\perp^j, & [J^3, \vec{B}_\perp^i] &= i\epsilon^{ij}\vec{B}_\perp^j. \end{aligned} \tag{A.5}$$

Let us now write down the defining commutators for the two-dimensional Galilei group, whose associated algebra is generated by the rotation \mathcal{J} , the boost along two directions \mathcal{B}^i , the two spatial translations \mathcal{P}^i , the Hamiltonian \mathcal{H} and the mass \mathcal{M} as

$$\begin{aligned} [\mathcal{M}, \mathcal{H}] &= 0, & [\mathcal{M}, \mathcal{P}^i] &= 0, \\ [\mathcal{M}, \mathcal{B}^i] &= 0, & [\mathcal{M}, \mathcal{J}] &= 0, \\ [\mathcal{H}, \mathcal{P}^i] &= 0, & [\mathcal{H}, \mathcal{B}^i] &= i\mathcal{P}^i, \\ [\mathcal{H}, \mathcal{J}] &= 0, & [\mathcal{P}^i, \mathcal{B}^j] &= i\delta^{ij}\mathcal{M}, \\ [\mathcal{J}, \mathcal{P}^i] &= i\epsilon^{ij}\mathcal{P}^j, & [\mathcal{J}, \mathcal{B}^i] &= i\epsilon^{ij}\mathcal{B}^j. \end{aligned} \tag{A.6}$$

After a direct comparison between Equations (A.5) and (A.6), one may immediately establish the correspondences: $P^+ \leftrightarrow \mathcal{M}$, $P^i \leftrightarrow \mathcal{H}$, $\vec{P}_\perp^i \leftrightarrow \mathcal{P}^i$, $\vec{B}_\perp^i \leftrightarrow \mathcal{B}^i$ and $J^3 \leftrightarrow \mathcal{J}$. Hence, we may conclude that indeed the Poincaré group consisting of $\{\tilde{P}^\mu, \vec{B}_\perp \vec{S}_\perp, J^3, K^3\}$ has a sub-group $\{P^+, P^-, \vec{P}_\perp^i, \vec{B}_\perp^i, J^3\}$ who is isomorphic with the two-dimensional Galilean group. Consequently, we may assign physical interpretations of some light-cone Poincaré generators as

$$\begin{aligned} P^+ &\longleftrightarrow \text{mass}, \\ P^- &\longleftrightarrow \text{time translation}, \\ \vec{P}_\perp^i &\longleftrightarrow \text{spatial translations}, \\ \vec{B}_\perp^i &\longleftrightarrow \text{boosts}, \\ J^3 &\longleftrightarrow \text{rotation}. \end{aligned}$$

The generator P^- represents the Hamiltonian of the system, and since the Hamiltonian is the generator of translations in time, we may now interpret x^+ as the light-cone time. The existence of this particular isomorphism assures that the Hamiltonian expressed in these coordinates has an intrinsic non-relativistic structure [87]. This may explicitly be

seen from the dispersion relation $M^2 = P_\mu P^\mu = 2P^+P^- - \vec{P}_\perp^2$, which then gives

$$P^- = \frac{1}{2P^+} \underbrace{\vec{P}_\perp^2 + M^2}_{\triangleq M_\perp^2}. \quad (\text{A.7})$$

Let us also notice that, as a consequence of this expression, the light-cone momentum P^+ always has only positive values, in comparison with the momenta on the instant form which may also take negative values. This implies that the vacuum state, defined for a free theory as $a_{\vec{P}}|0\rangle = 0$ in normal coordinates or $a_{P^+, \vec{P}_\perp}|0\rangle = 0$ on the light-cone, becomes much simpler for an interacting theory in the light-front form. In light-cone coordinates, the vacuum may consist only excitations of the state given by $P^+ = 0$, whereas in general many other excited states also contribute, hence complicating its underlying structure. From this, the light-cone vacuum is said to be trivial [88]. This turns out to be extremely useful since one may compute, using light-cone coordinates, any interacting state by simply applying creation operators upon this trivial vacuum.

Comparison between generators in the instant and light-front forms

free Hamiltonian	$H = \sqrt{\vec{P}^2 + M^2}$	$P^- = \frac{\vec{P}_\perp^2 + M^2}{2P^+}$
conserved quantities	E, \vec{P}	P^-, P^+, \vec{P}_\perp
momenta	$P_z \in (-\infty, +\infty)$	$P^+ \in (0, +\infty)$
quantized Hamiltonian	$P^0 = \sum_{\vec{k}} a_{\vec{k}}^\dagger a_{\vec{k}} \sqrt{m^2 + \vec{k}^2}$	$P_+ = \sum_{k_-, \vec{k}_\perp} a_{k_-, \vec{k}_\perp}^\dagger a_{k_-, \vec{k}_\perp} \frac{m^2 + \vec{k}_\perp^2}{2k_-}$
vacuum of free theory	$a_{\vec{k}} 0\rangle = 0$	$a_{k_-, \vec{k}_\perp} 0\rangle = 0$
vacuum of interacting theory	many states with $\vec{P} = 0$	only zero-mode states $P^+ = 0$

A.3 Light-cone QCD

Conventions

Let us proceed by stating our conventions and notations. The gamma matrices in the usual instant form are given by

$$\{\gamma^\mu, \gamma^\nu\} = 2g^{\mu\nu}\mathbb{1}, \quad (\text{A.8a})$$

$$\gamma^{\mu\dagger} = \gamma^0 \gamma^\mu \gamma^0. \quad (\text{A.8b})$$

In light-cone coordinates, they are defined as

$$\gamma^\pm \triangleq \frac{\gamma^0 \pm \gamma^3}{\sqrt{2}}. \quad (\text{A.9})$$

It follows that the conjugates are given by

$$(\gamma^\pm)^\dagger = \gamma^\mp. \quad (\text{A.10})$$

The last relation is straight-forward to prove

$$(\gamma^\pm)^\dagger \xrightarrow{\text{(A.9)}} \left(\frac{\gamma^0 \pm \gamma^3}{\sqrt{2}} \right)^\dagger = \frac{(\gamma^0)^\dagger \pm (\gamma^3)^\dagger}{\sqrt{2}} \xrightarrow{\text{(A.8b)}} \frac{\gamma^0 \pm (-\gamma^3)}{\sqrt{2}} \xrightarrow{\text{(A.9)}} \gamma^\mp.$$

An useful relation involving these matrices is

$$\gamma^\pm \gamma^\mp \gamma^\pm = 2\gamma^\pm. \quad (\text{A.11})$$

This relation may directly be obtained from their definition and anti-commutation relations

$$\begin{aligned} \gamma^\pm \gamma^\mp \gamma^\pm &\xrightarrow{\text{(A.9)}} \left(\frac{\gamma^0 \pm \gamma^3}{\sqrt{2}} \right) \left(\frac{\gamma^0 \mp \gamma^3}{\sqrt{2}} \right) \left(\frac{\gamma^0 \pm \gamma^3}{\sqrt{2}} \right) \\ &\xrightarrow{\text{(A.8a)}} \frac{1}{2\sqrt{2}} \left(\underbrace{\gamma^0 \gamma^0}_{\mathbb{1}} \mp \underbrace{\gamma^0 \gamma^3}_{-\gamma^3 \gamma^0} \pm \underbrace{\gamma^3 \gamma^0}_{-\mathbb{1}} - \underbrace{\gamma^3 \gamma^3}_{\mathbb{1}} \right) (\gamma^0 \pm \gamma^3) \\ &= \frac{1}{2\sqrt{2}} 2(1 \pm \gamma^3 \gamma^0) (\gamma^0 \pm \gamma^3) \xrightarrow{\text{(A.8a)}} \frac{1}{\sqrt{2}} (\gamma^0 \pm \gamma^3 \pm \gamma^3 \underbrace{\gamma^0 \gamma^0}_{\mathbb{1}} + \gamma^3 \underbrace{\gamma^0 \gamma^3}_{-\gamma^3 \gamma^0}) \\ &\xrightarrow{\text{(A.8a)}} \frac{1}{\sqrt{2}} (\gamma^0 \pm 2\gamma^3 - \underbrace{\gamma^3 \gamma^3 \gamma^0}_{\mathbb{1}}) \xrightarrow{\text{(A.9)}} 2 \underbrace{\frac{1}{\sqrt{2}} (\gamma^0 \pm \gamma^3)}_{\gamma^\pm}. \end{aligned}$$

Let us now introduce the projection operators

$$\Lambda_\pm \triangleq \frac{1}{2} \gamma^\mp \gamma^\pm = \frac{1}{\sqrt{2}} \gamma^0 \gamma^\pm. \quad (\text{A.12})$$

We are going to evaluate the square of such a projector and obtain

$$\begin{aligned} \left(\frac{1}{2}\gamma^\mp\gamma^\pm\right)^2 &\stackrel{\text{(A.11)}}{=} \underbrace{\frac{\gamma^\mp\gamma^\mp\gamma^\mp}{2}}_{\gamma^\mp} \frac{\gamma^\pm}{2} \stackrel{\text{(A.9)}}{=} \left(\frac{\gamma^0 \mp \gamma^3}{\sqrt{2}}\right) \frac{\gamma^\pm}{2} \stackrel{\text{(A.8a)}}{=} (\gamma^0 \mp \gamma^3 \underbrace{\gamma^0\gamma^0}_{\mathbb{1}}) \frac{\gamma^\pm}{2\sqrt{2}} \\ &\stackrel{\text{(A.8a)}}{=} (\gamma^0 \pm \underbrace{\gamma^0\gamma^3}_{-\gamma^3\gamma^0} \gamma^0) \frac{\gamma^\pm}{2\sqrt{2}} \stackrel{\text{(A.9)}}{=} \frac{1}{2}\gamma^0 \underbrace{\frac{\gamma^0 \pm \gamma^3}{\sqrt{2}}}_{\gamma^\pm} \gamma^0 \gamma^\pm = \left(\frac{1}{\sqrt{2}}\gamma^0\gamma^\pm\right)^2 \end{aligned}$$

These operators satisfy the usual properties of projector operators, namely

$$\Lambda_\pm\Lambda_\mp = 0, \quad (\text{A.13a})$$

$$\Lambda_+ + \Lambda_- = \mathbb{1}. \quad (\text{A.13b})$$

These relations may immediately be obtained from the properties of the gamma matrices

$$\begin{aligned} \Lambda_\pm\Lambda_\mp &\stackrel{\text{(A.12)}}{=} \frac{1}{2}\gamma^0\gamma^\pm\gamma^0\gamma^\mp \stackrel{\text{(A.8a)}}{=} \frac{1}{4}\underbrace{\gamma^0(\gamma^0 \pm \gamma^3)}_{\mathbb{1} \pm \gamma^0\gamma^3} \underbrace{\gamma^0(\gamma^0 \mp \gamma^3)}_{\mathbb{1} \mp \gamma^0\gamma^3} \\ &\stackrel{\text{(A.9)}}{=} \frac{1}{4}(\mathbb{1} \pm \gamma^0\gamma^3 \mp \gamma^0\gamma^3 - \gamma^0 \underbrace{\gamma^3\gamma^0}_{-\gamma^0\gamma^3} \gamma^3) \stackrel{\text{(A.9)}}{=} \frac{1}{4}(\mathbb{1} + \gamma^0 \underbrace{\gamma^3\gamma^3}_{-\mathbb{1}} \gamma^0) = 0, \end{aligned}$$

and similarly

$$\Lambda_+ + \Lambda_- \stackrel{\text{(A.12)}}{=} \frac{1}{\sqrt{2}}\gamma^0(\gamma^+ + \gamma^-) \stackrel{\text{(A.9)}}{=} \frac{1}{\sqrt{2}}\gamma^0 \frac{2\gamma^0}{\sqrt{2}} = \mathbb{1}.$$

Their adjoint is given by

$$(\Lambda_\pm)^\dagger = \Lambda_\pm. \quad (\text{A.14})$$

This statement immediately follows from

$$(\Lambda_\pm)^\dagger \stackrel{\text{(A.12)}}{=} \left(\frac{1}{2}\gamma^\mp\gamma^\pm\right)^\dagger = \frac{1}{2}(\gamma^\pm)^\dagger(\gamma^\mp)^\dagger \stackrel{\text{(A.10)}}{=} \frac{1}{2}\gamma^\mp\gamma^\pm \stackrel{\text{(A.12)}}{=} \Lambda_\pm.$$

They are idempotent

$$(\Lambda_\pm)^2 = \Lambda_\pm. \quad (\text{A.15})$$

The above expression is equivalent to

$$(\Lambda_{\pm})^2 \xrightarrow{\text{(A.12)}} \left(\frac{1}{2} \gamma^{\mp} \gamma^{\pm} \right)^2 \xrightarrow{\text{(A.11)}} \frac{1}{4} \gamma^{\mp} \underbrace{\gamma^{\pm} \gamma^{\mp} \gamma^{\pm}}_{2\gamma^{\pm}} \xrightarrow{\text{(A.12)}} \underbrace{\frac{1}{2} \gamma^{\mp} \gamma^{\pm}}_{\Lambda_{\pm}}.$$

When applied to the quark or anti-quark fields, they give two two-component fields, which we will denote by ψ_{\pm}

$$\Lambda_{\pm} \psi = \psi_{\pm}, \quad (\text{A.16a})$$

and similarly for the conjugate relation

$$\psi_{\pm}^{\dagger} = \psi^{\dagger} \Lambda_{\pm}. \quad (\text{A.16b})$$

Let us perform our calculations in the chiral representation, in which the instant form gamma matrices take the explicit expressions

$$\gamma^0 = \begin{pmatrix} 0 & \mathbb{1} \\ \mathbb{1} & 0 \end{pmatrix}, \quad \gamma^i = \begin{pmatrix} 0 & \sigma^i \\ -\sigma^i & 0 \end{pmatrix}, \quad \gamma^5 \triangleq i \gamma^0 \gamma^1 \gamma^2 \gamma^3 = \begin{pmatrix} \mathbb{1} & 0 \\ 0 & -\mathbb{1} \end{pmatrix},$$

where σ^i with $i = 1, 2, 3$ are the Pauli matrices. Therefore, the projector operators become

$$\Lambda_+ = \begin{pmatrix} 1 & 0 & 0 & 0 \\ 0 & 0 & 0 & 0 \\ 0 & 0 & 0 & 0 \\ 0 & 0 & 0 & 1 \end{pmatrix}, \quad \Lambda_- = \begin{pmatrix} 0 & 0 & 0 & 0 \\ 0 & 1 & 0 & 0 \\ 0 & 0 & 1 & 0 \\ 0 & 0 & 0 & 0 \end{pmatrix}.$$

When applied on the quark field ψ , they yield

$$\Lambda_+ \psi = \begin{pmatrix} \Psi_1 \\ 0 \\ 0 \\ \Psi_4 \end{pmatrix} \triangleq \psi_+, \quad \Lambda_- \psi = \begin{pmatrix} 0 \\ \Psi_2 \\ \Psi_3 \\ 0 \end{pmatrix} \triangleq \psi_-.$$

The conjugate of the above expressions, written more compressed as $\Lambda_{\pm} \psi = \psi_{\pm}$ give

$$\psi_{\pm}^{\dagger} = (\Lambda_{\pm} \psi)^{\dagger} = \psi^{\dagger} \Lambda_{\pm}^{\dagger} \xrightarrow{\text{(A.14)}} \psi^{\dagger} \Lambda_{\pm}.$$

Light-cone $\tilde{\mathcal{L}}_{\text{gluons}}$

In the light-cone gauge $A^+ = 0$, Equation (2.4) gives the light-cone components of the field strength tensor

$$\begin{aligned} F^{+-} &= \partial^+ A^-, \\ F^{+i} &= \partial^+ A^i, \\ F^{-i} &= \partial^- A^i - \partial^i A^- - ig[A^-, A^i], \\ F^{ij} &= \partial^i A^j - \partial^j A^i - ig[A^i, A^j], \end{aligned} \tag{A.17}$$

where $i, j = 1, 2$. From these, one may derive the light-cone gluonic content of the Lagrangian from Equation (2.7)

$$\tilde{\mathcal{L}}_{\text{gluons}} = -\frac{1}{4}F_a^{ij}F_{a,ij} - \frac{1}{2}F_a^{+-}F_a^{-+} + F_a^{+i}F_a^{-i}. \tag{A.18}$$

We begin by expanding in terms of the indices $\alpha, \beta = -, +$ and $i, j = 1, 2$

$$\tilde{\mathcal{L}}_{\text{gluons}} = \underbrace{\left(-\frac{1}{4}F_a^{ij}F_{a,ij} \right)}_{\triangleq \mathcal{L}_{\text{gluons}}^{ij}} + \underbrace{\left(-\frac{1}{4}F_a^{\alpha\beta}F_{a,\alpha\beta} \right)}_{\triangleq \mathcal{L}_{\text{gluons}}^{\alpha\beta}} + \underbrace{\left(-\frac{1}{2}F_a^{\alpha i}F_{a,\alpha i} \right)}_{\triangleq \mathcal{L}_{\text{gluons}}^{\alpha i}}, \tag{A.19}$$

where the last term has an extra factor of 2, in order to also take into account the term $F^{i\alpha}F_{i\alpha} = (-F^{\alpha i})(-F_{\alpha i}) = F^{\alpha i}F_{\alpha i}$. Afterwards, we may further express

$$\mathcal{L}_{\text{gluons}}^{\alpha\beta} = -\frac{1}{4}F_a^{\alpha\beta}F_{a,\alpha\beta} = -\frac{1}{4}(2F_a^{+-}F_{a,+-}) = -\frac{1}{2}\left(\underbrace{\tilde{g}_{+\mu}}_{\delta_{-\mu}} \underbrace{\tilde{g}_{-\nu}}_{\delta_{+\nu}} F_a^{+-}F_a^{\mu\nu}\right) = -\frac{1}{2}F_a^{+-}F_a^{-+}.$$

Similarly, we obtain

$$\begin{aligned} \mathcal{L}_{\text{gluons}}^{\alpha i} &= -\frac{1}{2}F_a^{\alpha i}F_{a,\alpha i} = -\frac{1}{2}(F_a^{+i}F_{a,+i} + F_a^{-i}F_{a,-i}) = -\frac{1}{2}\left(\underbrace{\tilde{g}_{+\mu}}_{\delta_{-\mu}} \underbrace{\tilde{g}_{i\nu}}_{-\delta_{i\nu}} F_a^{+i}F_a^{\mu\nu} + \underbrace{\tilde{g}_{-\mu}}_{\delta_{+\mu}} \underbrace{\tilde{g}_{i\nu}}_{-\delta_{i\nu}} F_a^{-i}F_a^{\mu\nu}\right) \\ &= \frac{1}{2}(F_a^{+i}F_a^{-i} + F_a^{-i}F_a^{+i}) = F_a^{+i}F_a^{-i}. \end{aligned}$$

After plugging all of these terms back in Equation (A.19), we finally obtain

$$\tilde{\mathcal{L}}_{\text{gluons}} = -\frac{1}{4}F_a^{ij}F_{a,ij} - \frac{1}{2}F_a^{+-}F_a^{-+} + F_a^{+i}F_a^{-i}.$$

Light-cone $\tilde{\mathcal{L}}_{\text{quarks}}$

The fermionic Lagrangian takes the form

$$\begin{aligned}\tilde{\mathcal{L}}_{\text{quarks}} = & -\frac{1}{\sqrt{2}} \left[\psi_+^\dagger \gamma^- \left(\mathsf{M} + i\vec{\gamma}_\perp \vec{\mathsf{D}}_\perp \right) \psi_- + \psi_-^\dagger \gamma^+ \left(\mathsf{M} + i\vec{\gamma}_\perp \vec{\mathsf{D}}_\perp \right) \psi_+ \right] + \\ & + i\sqrt{2} \left(\psi_+^\dagger \mathsf{D}^- \psi_+ + \psi_-^\dagger \partial^+ \psi_- \right)\end{aligned}\tag{A.20}$$

We will begin by expressing the quark content of the Lagrangian, given in Equation (2.5), in light-cone coordinates

$$\tilde{\mathcal{L}}_{\text{quarks}} = \bar{\psi} (i\tilde{g}^{\mu\nu} \gamma^\nu \mathsf{D}^\mu - \mathsf{M}) \psi = \bar{\psi} \left[i \left(\gamma^+ \mathsf{D}^- + \gamma^- \mathsf{D}^+ - \vec{\gamma}_\perp \vec{\mathsf{D}}_\perp \right) - \mathsf{M} \right] \psi,$$

in which $(\gamma^1, \gamma^2) \stackrel{\Delta}{=} \vec{\gamma}_\perp$ and $(\mathsf{D}^1, \mathsf{D}^2) \stackrel{\Delta}{=} \vec{\mathsf{D}}_\perp$. Further, we are going to decompose this result in four terms as

$$\tilde{\mathcal{L}}_{\text{quarks}} = \underbrace{i\bar{\psi} \gamma^+ \mathsf{D}^- \psi}_{\stackrel{\Delta}{=} \mathcal{L}_{\text{quarks}}^{+-}} + \underbrace{i\bar{\psi} \gamma^- \mathsf{D}^+ \psi}_{\stackrel{\Delta}{=} \mathcal{L}_{\text{quarks}}^{-+}} - \underbrace{i\bar{\psi} \vec{\gamma}_\perp \vec{\mathsf{D}}_\perp \psi}_{\stackrel{\Delta}{=} \mathcal{L}_{\text{quarks}}^\perp} - \underbrace{\mathsf{M} \bar{\psi} \psi}_{\stackrel{\Delta}{=} \mathcal{L}_{\text{quarks}}^M},$$

and afterwards express each of them in terms of the projected bispinorial fields ψ_\pm and their conjugates ψ_\pm^\dagger . Some simple manipulations provide

$$\begin{aligned}\mathcal{L}_{\text{quarks}}^{+-} &= i\bar{\psi} \gamma^+ \mathsf{D}^- \psi = i\psi^\dagger (\gamma^0 \gamma^+) \mathsf{D}^- \psi \stackrel{(A.12)}{=} i\psi^\dagger \sqrt{2} \Lambda_+ \mathsf{D}^- \psi \\ &\stackrel{(A.15)}{=} i\sqrt{2} \psi^\dagger (\Lambda_+)^2 \mathsf{D}^- \psi \stackrel{(A.16a)}{=} i\sqrt{2} \underbrace{\psi^\dagger \Lambda_+}_{\psi_+^\dagger} \mathsf{D}^- \underbrace{\Lambda_+ \psi}_{\psi_+} = i\sqrt{2} \psi_+^\dagger \mathsf{D}^- \psi_+, \end{aligned}$$

and analogously, after replacing $\mathsf{D}^+ = \partial^+ - igA^+ = \partial^+$, valid in the light-cone gauge:

$$\begin{aligned}\mathcal{L}_{\text{quarks}}^{-+} &= i\bar{\psi} \gamma^- \mathsf{D}^+ \psi = i\psi^\dagger (\gamma^0 \gamma^-) \mathsf{D}^+ \psi \stackrel{(A.12)}{=} i\psi^\dagger \sqrt{2} \Lambda_- \mathsf{D}^+ \psi \\ &\stackrel{(A.15)}{=} i\sqrt{2} \psi^\dagger (\Lambda_-)^2 \mathsf{D}^+ \psi \stackrel{(A.16a)}{=} i\sqrt{2} \underbrace{\psi^\dagger \Lambda_-}_{\psi_-^\dagger} \mathsf{D}^+ \underbrace{\Lambda_- \psi}_{\psi_-} = \psi_-^\dagger \mathsf{D}^+ \psi_-. \end{aligned}$$

Further, applying a similar treatment, we may compute:

$$\begin{aligned}
\mathcal{L}_{\text{quarks}}^{\perp} &= i\bar{\psi}(\vec{\gamma}_{\perp}\vec{D}_{\perp})\psi = i\psi^{\dagger}\gamma^0(\vec{\gamma}_{\perp}\vec{D}_{\perp})\psi \xrightarrow{\text{(A.8a)}} \frac{i}{2}\psi^{\dagger}\gamma^0(\vec{\gamma}_{\perp}\vec{D}_{\perp})\underbrace{(\gamma^{+}\gamma^{-} + \gamma^{-}\gamma^{+})}_{2\mathbb{1}}\psi \\
&\xrightarrow{\text{(A.11)}} \frac{i}{2}\psi^{\dagger}\gamma^0(\vec{\gamma}_{\perp}\vec{D}_{\perp})\left(\underbrace{\frac{\gamma^{+}\gamma^{-}\gamma^{+}}{2}}_{\gamma^{+}}\gamma^{-} + \underbrace{\frac{\gamma^{-}\gamma^{+}\gamma^{-}}{2}}_{\gamma^{-}}\gamma^{+}\right)\psi \\
&= \frac{i}{4}\psi^{\dagger}\gamma^0\left[\underbrace{(\vec{\gamma}_{\perp}\vec{D}_{\perp})\gamma^{+}\gamma^{-}\gamma^{+}\gamma^{-}}_{\gamma^{+}\gamma^{-}(\vec{\gamma}_{\perp}\vec{D}_{\perp})} + \underbrace{(\vec{\gamma}_{\perp}\vec{D}_{\perp})\gamma^{-}\gamma^{+}\gamma^{-}\gamma^{+}}_{\gamma^{-}\gamma^{+}(\vec{\gamma}_{\perp}\vec{D}_{\perp})}\right]\psi \\
&\xrightarrow{\text{(A.12)}} \frac{i}{4}\psi^{\dagger}\left[\underbrace{\gamma^0\gamma^{+}\gamma^{-}(\vec{\gamma}_{\perp}\vec{D}_{\perp})\gamma^{+}\gamma^{-}}_{\sqrt{2}\Lambda_{+}} + \underbrace{\gamma^0\gamma^{-}\gamma^{+}(\vec{\gamma}_{\perp}\vec{D}_{\perp})\gamma^{-}\gamma^{+}}_{\sqrt{2}\Lambda_{-}}\right]\psi \\
&\xrightarrow{\text{(A.16a)}} \frac{i}{\sqrt{2}}\left[\underbrace{\psi^{\dagger}\Lambda_{+}\gamma^{-}(\vec{\gamma}_{\perp}\vec{D}_{\perp})\Lambda_{-}\psi}_{\psi_{+}^{\dagger}} + \underbrace{\psi^{\dagger}\Lambda_{-}\gamma^{+}(\vec{\gamma}_{\perp}\vec{D}_{\perp})\Lambda_{+}\psi}_{\psi_{-}^{\dagger}}\right] \\
&\xrightarrow{\text{(A.16b)}} \frac{i}{\sqrt{2}}\left[\psi_{+}^{\dagger}\gamma^{-}(\vec{\gamma}_{\perp}\vec{D}_{\perp})\psi_{-} + \psi_{-}^{\dagger}\gamma^{+}(\vec{\gamma}_{\perp}\vec{D}_{\perp})\psi_{+}\right],
\end{aligned}$$

and also

$$\begin{aligned}
\mathcal{L}_{\text{quarks}}^{\text{M}} &= \text{M}\bar{\psi}\psi = m\psi^{\dagger}\gamma^0\psi \xrightarrow{\text{(A.8a)}} \frac{\text{M}}{2}\psi^{\dagger}\gamma^0\underbrace{(\gamma^{+}\gamma^{-} + \gamma^{-}\gamma^{+})}_{2\mathbb{1}}\psi \xrightarrow{\text{(A.11)}} \frac{\text{M}}{2}\psi^{\dagger}\gamma^0\left(\underbrace{\frac{\gamma^{+}\gamma^{-}\gamma^{+}}{2}}_{\gamma^{+}}\gamma^{-} + \right. \\
&\quad \left. + \underbrace{\frac{\gamma^{-}\gamma^{+}\gamma^{-}}{2}}_{\gamma^{-}}\gamma^{+}\right)\psi \xrightarrow{\text{(A.12)}} \frac{\text{M}}{4}\psi^{\dagger}\left(\underbrace{\gamma^0\gamma^{+}\gamma^{-}\gamma^{+}\gamma^{-}}_{\sqrt{2}\Lambda_{+}} + \underbrace{\gamma^0\gamma^{-}\gamma^{+}\gamma^{-}\gamma^{+}}_{\sqrt{2}\Lambda_{-}}\right)\psi \\
&\xrightarrow{\text{(A.16a)}} \frac{\text{M}}{\sqrt{2}}\left(\underbrace{\psi^{\dagger}\Lambda_{+}\gamma^{-}\Lambda_{-}\psi}_{\psi_{+}^{\dagger}} + \underbrace{\psi^{\dagger}\Lambda_{-}\gamma^{+}\Lambda_{+}\psi}_{\psi_{-}^{\dagger}}\right) = \frac{\text{M}}{\sqrt{2}}\left(\psi_{+}^{\dagger}\gamma^{-}\psi_{-} + \psi_{-}^{\dagger}\gamma^{+}\psi_{+}\right).
\end{aligned}$$

Light-cone field equations

The colored Dirac equations from Equation (2.9) written in light-cone gauge, such that $D^{+} = \partial^{+}$, become

$$\left[i\left(\gamma^{+}D^{-} + \gamma^{-}\partial^{+} - \vec{\gamma}_{\perp}\vec{D}_{\perp}\right) - m\right]\psi = 0, \quad (\text{A.21})$$

and afterwards may be decoupled to

$$\partial^+ \psi_- = -\frac{i}{2} \left(-i\vec{\gamma}_\perp \vec{D}_\perp + m \right) \gamma^+ \psi_+, \quad (\text{A.22a})$$

$$D^- \psi_+ = -\frac{i}{2} \left(-i\vec{\gamma}_\perp \vec{D}_\perp + m \right) \gamma^- \psi_-. \quad (\text{A.22b})$$

After multiplying Equation (A.21) to the left by γ^+ , it becomes, according to the definition of the fermionic projection operators from Equation (A.12):

$$\left[i \left(\underbrace{(\gamma^+)^2}_{0} D^- + \underbrace{\gamma^+ \gamma^-}_{2\Lambda_-} \partial^+ - \underbrace{\gamma^+ \vec{\gamma}_\perp \vec{D}_\perp}_{-\vec{\gamma}_\perp \gamma^+} \right) - \gamma^+ m \right] \psi = 0.$$

Afterwards, we plug in the expression $\gamma^+ = \frac{1}{2}\gamma^+\gamma^-\gamma^+$ from Equation (A.11), such that we get

$$\left(2i\partial^+ \Lambda_- - \frac{1}{2}(-i\vec{\gamma}_\perp \vec{D}_\perp + m)\gamma^+ \underbrace{\gamma^- \gamma^+}_{2\Lambda_+} \right) \psi = 0.$$

This yields

$$2i \left[\underbrace{\partial^+ \Lambda_- \psi}_{\psi_-} + (-i\vec{\gamma}_\perp \vec{D}_\perp + m)\gamma^+ \underbrace{\Lambda_+ \psi}_{\psi_+} \right] = 0,$$

which after a simple manipulation results in Equation (A.22a). In the same way, after multiplying Equation (A.21) to the right by γ^- , one obtains Equation (A.22b).

On the other hand, the Yang-Mills equations from Equation (2.10) give

$$D_a^- (\partial^+ A_a^i) + \partial^+ F_a^{-i} + (D_j F^{ji})_a = g J_a^i, \quad (\text{A.23a})$$

$$(\partial^+)^2 A_a^- + (D_i \partial^+ A^i)_a = g J_a^+. \quad (\text{A.23b})$$

If we explicitly write Equation (2.10) for the $\nu = i$ with $i = 1, 2$ and $\nu = +$ components, we obtain

$$\begin{aligned} D_+ F^{+i} + D_- F^{-i} + D_j F^{ji} &= g J^i, \\ D_- F^{-+} + D_i F^{i+} &= g J^+. \end{aligned}$$

which after using Equation (A.17) and $D_+ = D^-$ along with $D_- = \partial^+$, lead to

$$\begin{aligned} D^- (\partial^+ A^i) + \partial^+ F^{-i} + D_j F^{ji} &= g J^i, \\ (\partial^+)^2 A^- + D_i \partial^+ A^i &= g J^+. \end{aligned}$$

Light-cone Lagrangian $\tilde{\mathcal{L}}$ and Hamiltonian $\tilde{\mathcal{H}}$

Let us merge the previously obtained results and write the QCD Lagrangian in light-cone coordinates and light-cone gauge as

$$\begin{aligned}\tilde{\mathcal{L}} = & -\frac{1}{4}F_a^{ij}F_{a,ij} + \frac{1}{2}(F_a^{+-})^2 + F_a^{+i}F_a^{-i} + i\sqrt{2}\left(\psi_+^\dagger D^- \psi_+ + \psi_-^\dagger \partial^+ \psi_-\right) - \\ & - \frac{1}{\sqrt{2}}\left[\psi_+^\dagger \gamma^- \left(m + i\vec{\gamma}_\perp \vec{D}_\perp\right) \psi_- + \psi_-^\dagger \gamma^+ \left(m + i\vec{\gamma}_\perp \vec{D}_\perp\right) \psi_+\right]\end{aligned}$$

The conjugate momenta corresponding to the fields A_a^i and ψ_+ are

$$\Pi_{A_a^i} = \frac{\delta \tilde{\mathcal{L}}}{\delta (\partial^- A_a^i)} = \frac{\partial}{\partial (\partial^- A_a^i)} (\dots + F_a^{+i}F_a^{-i} + \dots) \quad (\text{A.24a})$$

$$= \frac{\delta}{\delta (\partial^- A_a^i)} \left\{ \dots + \partial^+ A_a^i (\partial^- A_a^i - \partial^i A_a^i - ig [A_a^-, A_a^i]) + \dots \right\} = \partial^+ A_a^i, \quad (\text{A.24b})$$

$$\Pi_{\psi_+} = \frac{\delta \tilde{\mathcal{L}}}{\delta (\partial^- \psi_+)} = \frac{\delta}{\delta (\partial^- \psi_+)} \left[\dots + i\sqrt{2} \psi_+^\dagger (\partial^- \psi_+ - ig A^- \psi_+) + \dots \right] = i\sqrt{2} \psi_+^\dagger, \quad (\text{A.24c})$$

whereas those associated to A_a^- and ψ_- are

$$\begin{aligned}\Pi_{A_a^-} &= \frac{\delta \tilde{\mathcal{L}}}{\delta (\partial^- A_a^-)} = 0, \\ \Pi_{\psi_-} &= \frac{\delta \tilde{\mathcal{L}}}{\delta (\partial^- \psi_-)} = 0.\end{aligned}$$

The fact that these conjugate momenta are null has as consequence a slight modification in the usual quantization technique. Following Dirac's [25] quantization procedure, let us begin by explicitly identifying the constraints. We may notice that Equation (A.22b) gives the time evolution of the fermionic field ψ_+ , whereas Equation (A.22a) represents a constraint for ψ_- . Similarly, Equation (A.23b) contains the time derivative of the gluonic field A_a^+ , while Equation (A.23a) relates it to A_a^i and thus provides another constraint. They may formally be solved by writing

$$\psi_- = -\frac{i}{2\partial^+} \left(m - i\vec{\gamma}_\perp \vec{D}_\perp \right) \gamma^+ \psi_+, \quad (\text{A.25a})$$

$$A_a^- = \frac{1}{(\partial^+)^2} \left\{ g J_a^+ - [D_i (\partial^+ A_a^i)]_a \right\}. \quad (\text{A.25b})$$

It is now relevant to notice the importance of choosing the light-cone gauge $A^+ = 0$. If this choice wouldn't be employed, one would obtain terms containing A^+ in the denominator, which will then be inherited by the Hamiltonian and thus complicate its structure.

Afterwards, the formal solutions from Equations (A.25a) and (A.25b) must be plugged in the Lagrangian and express it only in terms of the dynamical fields. Let us do the necessary replacements in steps:

Step 1

First, after replacing the expression from Equation (A.25a) back in all the terms of the Lagrangian containing ψ_- , we will get

$$\tilde{\mathcal{L}}_{\psi_-} = \frac{i}{\sqrt{2}} \psi_+^\dagger \left(m - i \vec{\gamma}_\perp \vec{D}_\perp \right) \frac{1}{\partial^+} \left(m + i \vec{\gamma}_\perp \vec{D}_\perp \right) \psi_+. \quad (\text{A.26})$$

Let us introduce the notations $\tilde{\mathcal{L}}_{\psi_-} = \tilde{\mathcal{L}}_{\psi_-}^{--} + \tilde{\mathcal{L}}_{\psi_-}^{+-} + \tilde{\mathcal{L}}_{\psi_-}^{-+}$, where

$$\begin{aligned} \tilde{\mathcal{L}}_{\psi_-}^{--} &\triangleq i\sqrt{2} \psi_-^\dagger \partial^+ \psi_-, \\ \tilde{\mathcal{L}}_{\psi_-}^{+-} &\triangleq -\frac{1}{\sqrt{2}} \psi_+^\dagger \gamma^- \left(m + i \vec{\gamma}_\perp \vec{D}_\perp \right) \psi_-, \\ \tilde{\mathcal{L}}_{\psi_-}^{-+} &\triangleq -\frac{1}{\sqrt{2}} \psi_-^\dagger \gamma^+ \left(m + i \vec{\gamma}_\perp \vec{D}_\perp \right) \psi_+. \end{aligned}$$

These will give

$$\begin{aligned} \tilde{\mathcal{L}}_{\psi_-}^{--} &\stackrel{(\text{A.25a})}{=} i\sqrt{2} \left[-\frac{i}{2\partial^+} \left(m - i \vec{\gamma}_\perp \vec{D}_\perp \right) \gamma^+ \psi_+ \right]^\dagger \left[-\frac{i}{2} \left(m - i \vec{\gamma}_\perp \vec{D}_\perp \right) \gamma^+ \psi_+ \right] \\ &\stackrel{(\text{A.8a})}{=} \frac{i}{2\sqrt{2}} \psi_+^\dagger \underbrace{(\gamma^+)^\dagger}_{\gamma^-} \left(m + i \underbrace{\vec{\gamma}_\perp^\dagger}_{-\vec{\gamma}_\perp} \vec{D}_\perp \right) \frac{1}{\partial^+} \left(m - i \vec{\gamma}_\perp \vec{D}_\perp \right) \gamma^+ \psi_+ \\ &\stackrel{(\text{A.8a})}{=} \frac{i}{2\sqrt{2}} \psi_+^\dagger \left(m + i \vec{\gamma}_\perp \vec{D}_\perp \right) \frac{1}{\partial^+} \left(m + i \vec{\gamma}_\perp \vec{D}_\perp \right) \underbrace{\gamma^- \gamma^+}_{2\Lambda_+} \psi_+ \\ &= \frac{i}{\sqrt{2}} \psi_+^\dagger \left(m + i \vec{\gamma}_\perp \vec{D}_\perp \right) \frac{1}{\partial^+} \left(m + i \vec{\gamma}_\perp \vec{D}_\perp \right) \underbrace{\Lambda_+ \psi_+}_{\psi_+}. \end{aligned}$$

Similarly, we obtain

$$\begin{aligned} \tilde{\mathcal{L}}_{\psi_-}^{+-} &\stackrel{(\text{A.25a})}{=} -\frac{1}{\sqrt{2}} \psi_+^\dagger \gamma^- \left(m + i \vec{\gamma}_\perp \vec{D}_\perp \right) \left[-\frac{i}{2\partial^+} \left(m - i \vec{\gamma}_\perp \vec{D}_\perp \right) \gamma^+ \psi_+ \right] \\ &\stackrel{(\text{A.8a})}{=} \frac{i}{2\sqrt{2}} \psi_+^\dagger \left(m - i \vec{\gamma}_\perp \vec{D}_\perp \right) \frac{1}{\partial^+} \left(m + i \vec{\gamma}_\perp \vec{D}_\perp \right) \underbrace{\gamma^- \gamma^+}_{2\Lambda_+} \psi_+ \\ &= \frac{i}{\sqrt{2}} \psi_+^\dagger \left(m - i \vec{\gamma}_\perp \vec{D}_\perp \right) \frac{1}{\partial^+} \left(m + i \vec{\gamma}_\perp \vec{D}_\perp \right) \underbrace{\Lambda_+ \psi_+}_{\psi_+}, \end{aligned}$$

and also

$$\begin{aligned}
\tilde{\mathcal{L}}_{\psi_-}^{-+} &\stackrel{\text{(A.25a)}}{=} -\frac{1}{\sqrt{2}}\psi_+^\dagger \gamma^- \left(m - i\vec{\gamma}_\perp \vec{\mathsf{D}}_\perp \right) \frac{i}{2\partial^+} \gamma^+ \left(m + i\vec{\gamma}_\perp \vec{\mathsf{D}}_\perp \right) \psi_+ \\
&\stackrel{\text{(A.8a)}}{=} -\frac{i}{2\sqrt{2}}\psi_+^\dagger \left(m + i\vec{\gamma}_\perp \vec{\mathsf{D}}_\perp \right) \frac{1}{\partial^+} \left(m + i\vec{\gamma}_\perp \vec{\mathsf{D}}_\perp \right) \underbrace{\gamma^- \gamma^+}_{2\Lambda_+} \psi_+ \\
&= -\frac{i}{\sqrt{2}}\psi_+^\dagger \left(m + i\vec{\gamma}_\perp \vec{\mathsf{D}}_\perp \right) \frac{1}{\partial^+} \left(m + i\vec{\gamma}_\perp \vec{\mathsf{D}}_\perp \right) \underbrace{\Lambda_+ \psi_+}_{\psi_+}.
\end{aligned}$$

Step 2

Further, we will introduce the terms involving A_a^- with the constraint from Equation (A.25b) in the Lagrangian. Before attempting to perform this replacement, let us remark that the color current along x^+ may be written as

$$\begin{aligned}
J_a^+ &= \bar{\psi} \gamma^+ \psi t^a \stackrel{\text{(A.12)}}{=} \psi^\dagger \underbrace{\gamma^0 \gamma^+}_{\sqrt{2}\Lambda_+} \psi t^a \stackrel{\text{(A.15)}}{=} \sqrt{2} \psi^\dagger \underbrace{(\Lambda_+)^2}_{\Lambda_+} \psi t^a \\
&\stackrel{\text{(A.16a)}}{=} \sqrt{2} \underbrace{\psi^\dagger \Lambda_+}_{\psi_+^\dagger} \underbrace{\Lambda \psi}_{\psi_+} t^a = \sqrt{2} \psi_+^\dagger t^a \psi_+. \tag{A.27}
\end{aligned}$$

We will begin by writing Equation (A.25b) as

$$\begin{aligned}
(\partial^+)^2 A^- &= g J^+ + \underbrace{(-\mathsf{D}_i)}_{\mathsf{D}^i} (\partial^+ A^i) = g J^+ + \partial^i (\partial^+ A^i) - ig [A^i, \partial^+ A^i] \\
&= g J_a^+ t^a + \partial^i (\partial^+ A_a^i) t^a - ig A_b^i (\partial^+ A_c^i) \underbrace{[t^b, t^c]}_{if^{abc} t^a},
\end{aligned}$$

which, since $A^- = A_a^- t^a$, yields

$$\partial^i (\partial^+ A_a^i) + g f^{abc} A_b^i (\partial^+ A_c^i) = (\partial^+)^2 A_a^- - g J_a^+ \tag{A.28}$$

Further, we are going to rewrite the Lagrangian parts containing A_a^- , which are

$$\tilde{\mathcal{L}}_{A_a^-} = \underbrace{\frac{1}{2} (F_a^{+-})^2}_{\triangleq \tilde{\mathcal{L}}_{A_a^-}^{+-}} + \underbrace{F_a^{+i} F_a^{-i}}_{\triangleq \tilde{\mathcal{L}}_{A_a^-}^i} + \underbrace{i\sqrt{2} \psi_+^\dagger \mathsf{D}^- \psi_+}_{\triangleq \tilde{\mathcal{L}}_{A_a^-}^{\psi+}}.$$

We have

$$\tilde{\mathcal{L}}_{A_a^-}^{+-} \stackrel{\text{(A.20)}}{=} \frac{1}{2} (\partial^+ A_a^-)^2 = \frac{1}{2} \left\{ \underbrace{\partial^+ [A_a^- (\partial^+ A_a^-)]}_0 - \left[(\partial^+)^2 A_a^- \right] A_a^- \right\} = -\frac{1}{2} \left[(\partial^+)^2 A_a^- \right] A_a^-,$$

in which we discarded the surface term. Following a similar procedure, we obtain

$$\begin{aligned}
\tilde{\mathcal{L}}_{A_a^-}^i &\stackrel{(A.20)}{=} (\partial^+ A_a^i) (\partial^- A_a^i - \partial^i A_a^- + g f^{abc} A_b^- A_c^i) = (\partial^+ A_a^i) (\partial^- A_a^i) - \\
&- \left\{ \underbrace{\partial^i [A_a^- (\partial^+ A_a^i)]}_0 - [\partial^i (\partial^+ A_a^i)] A_a^- \right\} + g \underbrace{f^{abc} (\partial^+ A_a^i) A_b^- A_c^i}_{f^{abc} (\partial^+ A_c^i) A_a^- A_b^i} \\
&\stackrel{(A.28)}{=} (\partial^+ A_a^i) (\partial^- A_a^i) + \underbrace{[\partial^i (\partial^+ A_a^i) + g f^{abc} A_b^i (\partial^+ A_c^i)] A_a^-}_{(\partial^+)^2 A_a^- - g J_a^+} \\
&= (\partial^+ A_a^i) (\partial^- A_a^i) + [(\partial^+)^2 A_a^- - g J_a^+] A_a^-.
\end{aligned}$$

The last term immediately reduces to

$$\tilde{\mathcal{L}}_{A_a^-}^{\psi_+} = i\sqrt{2}\psi_+^\dagger (\partial^- - ig A^-) \psi_+ \stackrel{(A.27)}{=} i\sqrt{2}\psi_+^\dagger \partial^- \psi_+ + g A_a^- \underbrace{\sqrt{2}\psi_+^\dagger t^a \psi_+}_{J_a^+}.$$

Collecting all the results obtained above, the Lagrangian part containing A_a^- becomes

$$\begin{aligned}
\tilde{\mathcal{L}}_{A_a^-} &= (\partial^+ A_a^i) (\partial^- A_a^i) + i\sqrt{2}\psi_+^\dagger \partial^- \psi_+ + \frac{1}{2} [(\partial^+)^2 A_a^-] A_a^- \\
&\stackrel{(A.25b)}{=} (\partial^+ A_a^i) (\partial^- A_a^i) + i\sqrt{2}\psi_+^\dagger \partial^- \psi_+ + \\
&+ \frac{1}{2} \{g J_a^+ - [D_i (\partial^+ A^i)]_a\} \frac{1}{(\partial^+)^2} \{g J_a^+ - [D_i (\partial^+ A^i)]_a\}
\end{aligned} \tag{A.29}$$

Step 3

After collecting the results from Equations (A.26) and (A.29), the light-cone Lagrangian becomes

$$\begin{aligned}
\tilde{\mathcal{L}} &= -\frac{1}{4} F_a^{ij} F_{ij}^a + (\partial^+ A_a^i) (\partial^- A_a^i) + i\sqrt{2}\psi_+^\dagger \partial^- \psi_+ + \\
&+ \frac{1}{2} \{g J_a^+ - [D_i (\partial^+ A^i)]_a\} \frac{1}{(\partial^+)^2} \{g J_a^+ - [D_i (\partial^+ A^i)]_a\} + \\
&+ \frac{i}{\sqrt{2}} \psi_+^\dagger (m - i\vec{\gamma}_\perp \vec{D}_\perp) \frac{1}{\partial^+} (m + i\vec{\gamma}_\perp \vec{D}_\perp) \psi_+.
\end{aligned}$$

The Hamiltonian may now be obtained via a Legendre transformation

$$\begin{aligned}
\tilde{\mathcal{H}} &= \tilde{\mathcal{L}} - \Pi_{\psi_+} (\partial^- \psi_+) - \Pi_{A_a^i} (\partial^- A_a^i) \\
&= \frac{1}{2} \{g J_a^+ - [D_i (\partial^+ A^i)]_a\} \frac{1}{(\partial^+)^2} \{g J_a^+ - [D_i (\partial^+ A^i)]_a\} + \\
&+ \frac{i}{\sqrt{2}} \psi_+^\dagger (m - i\vec{\gamma}_\perp \vec{D}_\perp) \frac{1}{\partial^+} (m + i\vec{\gamma}_\perp \vec{D}_\perp) \psi_+ - \frac{1}{4} F_a^{ij} F_{ij}^a.
\end{aligned} \tag{A.30}$$

Light-cone quantization

Finally, we may perform the usual quantization for the gluon fields

$$A_a^\mu(x^+, \vec{x}) = \int_{k^+ > 0} \frac{dk^+ d^2 k_\perp}{\sqrt{(2\pi)^3 2k^+}} \sum_\lambda \left[a_a^\lambda(x^+, \vec{k}) \epsilon_\lambda^\mu(\vec{k}) e^{i\vec{k}\cdot\vec{x}} + a_a^{\lambda\dagger}(x^+, \vec{k}) \epsilon_\lambda^{\mu\dagger}(\vec{k}) e^{-i\vec{k}\cdot\vec{x}} \right], \quad (\text{A.31})$$

where we introduced the notation $\vec{x} \stackrel{\Delta}{=} (x^-, \vec{x}_\perp)$, which further gives $\vec{k} \cdot \vec{x} = k^+ x^- - \vec{k}_\perp \cdot \vec{x}_\perp$. The index $\lambda = \pm 1$ labels the polarization vectors

$$\epsilon_\lambda^\mu = \left(0, \frac{\vec{\epsilon}_\perp \cdot \vec{k}_\perp}{k^+}, \vec{\epsilon}_\perp \right),$$

which obey the usual $k_\mu \epsilon_\lambda^\mu = 0$. The creation and annihilation operators satisfy

$$\begin{aligned} \left[a_a^\lambda(x^+, \vec{k}), a_b^{\lambda'}(x^+, \vec{k}') \right] &= 0, & \left[a_a^{\lambda\dagger}(x^+, \vec{k}), a_b^{\lambda'\dagger}(x^+, \vec{k}') \right] &= 0 \\ \left[a_a^\lambda(x^+, \vec{k}), a_b^{\lambda'\dagger}(x^+, \vec{k}') \right] &= \delta_{ab} \delta^{\lambda\lambda'} \delta(k^+ - k'^+) \delta(\vec{k}_\perp - \vec{k}'_\perp), \end{aligned} \quad (\text{A.32})$$

which then imply equal light-cone time canonical commutation relations for the fields and their conjugate

$$\begin{aligned} \left[A_a^i(x), A_b^j(y) \right]_{x^+ = y^+} &= 0, & \left[\Pi_{A_a^i}(x), \Pi_{A_b^j}(y) \right]_{x^+ = y^+} &= 0, \\ \left[A_a^i(x), \Pi_{A_b^j}(y) \right]_{x^+ = y^+} &= i \delta_{ab} \delta^{ij} \delta(x^- - y^-) \delta(\vec{x}_\perp - \vec{y}_\perp). \end{aligned}$$

In the case of the fermionic field $\psi_+ = \Lambda_+ \psi$, let us remark that it spans a two-dimensional space, therefore we need only two fundamental spinors, which will be the conventional

$$\chi_{\frac{1}{2}} = \begin{pmatrix} 1 \\ 0 \end{pmatrix}, \quad \chi_{-\frac{1}{2}} = \begin{pmatrix} 0 \\ 1 \end{pmatrix}.$$

Hence, the quantized fermionic field ψ_+ is given by

$$\psi_+(x) = \int_{k^+ > 0} \frac{dk^+ d^2 k_\perp}{\sqrt{(2\pi)^3 2k^+}} \sum_s \left[\chi_s b_s(x^+, \vec{k}) e^{i\vec{k}\cdot\vec{x}} + \chi_{-s} d_s^\dagger(x^+, \vec{k}) e^{-i\vec{k}\cdot\vec{x}} \right] \quad (\text{A.33})$$

in which the fermionic creation and annihilation operators obey the anti-commutation relations

$$\begin{aligned} \left\{ b_s(x^+, \vec{k}), b_{s'}(x^+, \vec{k}') \right\} &= 0, & \left\{ b_s^\dagger(x^+, \vec{k}), b_{s'}^\dagger(x^+, \vec{k}') \right\} &= 0 \\ \left\{ b_s(x^+, \vec{k}), b_{s'}^\dagger(x^+, \vec{k}') \right\} &= \delta_{ss'} \delta(k^+ - k'^+) \delta(\vec{k}_\perp - \vec{k}'_\perp), \\ \left\{ d_s(x^+, \vec{k}), d_{s'}(x^+, \vec{k}') \right\} &= 0, & \left\{ d_s^\dagger(x^+, \vec{k}), d_{s'}^\dagger(x^+, \vec{k}') \right\} &= 0 \\ \left\{ d_s(x^+, \vec{k}), d_{s'}^\dagger(x^+, \vec{k}') \right\} &= \delta_{ss'} \delta(k^+ - k'^+) \delta(\vec{k}_\perp - \vec{k}'_\perp). \end{aligned} \quad (\text{A.34})$$

From these, we obtain

$$\begin{aligned}\{\psi_+(x), \psi_+(y)\}_{x^+=y^+} &= 0, & \{\Pi_{\psi_+}(x), \Pi_{\psi_+}(y)\}_{x^+=y^+} &= 0, \\ \{\psi_+(x), \Pi_{\psi_+}(y)\}_{x^+=y^+} &= i\Lambda_+\delta(x^- - y^-)\delta(\vec{x}_\perp - \vec{y}_\perp),\end{aligned}$$

and similarly for the corresponding anti-quark fields.

Let us remark that Equation (A.30), due to the inversion of the constraints from Equations (A.25a) and (A.25b), exhibits a singularity at $P^+ = 0$. In the literature there exist various prescriptions for dealing with this pole, which are sensitive to the boundary conditions. Since these fields will further be involved in some computations which are not dependent on any prescription, we are simply going to eliminate this pole by performing the integrations starting from $P^+ > 0$ in Equations (A.31) and (A.33).

BIBLIOGRAPHY

Here are the references in citation order.

- [1] Edward V. Shuryak. ‘What RHIC experiments and theory tell us about properties of quark-gluon plasma?’ In: *Nucl. Phys. A* 750 (2005). Ed. by D. Rischke and G. Levin, pp. 64–83. DOI: [10.1016/j.nuclphysa.2004.10.022](https://doi.org/10.1016/j.nuclphysa.2004.10.022) (cited on page 1).
- [2] Xin-Nian Wang and Miklos Gyulassy. ‘Gluon shadowing and jet quenching in A + A collisions at $\sqrt{s_{NN}} = 200$ GeV’. In: *Phys. Rev. Lett.* 68 (1992), pp. 1480–1483. DOI: [10.1103/PhysRevLett.68.1480](https://doi.org/10.1103/PhysRevLett.68.1480) (cited on page 1).
- [3] Dmytro Oliynychenko. ‘Interfaces between relativistic hydrodynamics and transport for the dynamical description of heavy ion collisions’. PhD thesis. Frankfurt U., July 2017 (cited on page 1).
- [4] J. Bernhard et al. ‘Applying Bayesian parameter estimation to relativistic heavy-ion collisions: simultaneous characterization of the initial state and quark-gluon plasma medium’. In: *Phys. Rev. C* 94.2 (2016), p. 024907. DOI: [10.1103/PhysRevC.94.024907](https://doi.org/10.1103/PhysRevC.94.024907) (cited on page 1).
- [5] S. Ryu et al. ‘Importance of the Bulk Viscosity of QCD in Ultrarelativistic Heavy-Ion Collisions’. In: *Phys. Rev. Lett.* 115.13 (2015), p. 132301. DOI: [10.1103/PhysRevLett.115.132301](https://doi.org/10.1103/PhysRevLett.115.132301) (cited on pages 1, 69).
- [6] D. Devetak et al. ‘Global fluid fits to identified particle transverse momentum spectra from heavy-ion collisions at the Large Hadron Collider’. In: *JHEP* 06 (2020), p. 044. DOI: [10.1007/JHEP06\(2020\)044](https://doi.org/10.1007/JHEP06(2020)044) (cited on page 1).
- [7] F. Gelis. ‘Color Glass Condensate and Glasma’. In: *Int. J. Mod. Phys. A* 28 (2013), p. 1330001. DOI: [10.1142/S0217751X13300019](https://doi.org/10.1142/S0217751X13300019) (cited on page 2).
- [8] ‘The history of QCD’. In: *CERN Courier* 52.8 (Oct 2012), pp. 21–25 (cited on page 5).
- [9] Murray Gell-Mann. ‘The Eightfold Way: A Theory of strong interaction symmetry’. In: (Mar. 1961). DOI: [10.2172/4008239](https://doi.org/10.2172/4008239) (cited on page 5).
- [10] Richard P. Feynman. ‘Very High-Energy Collisions of Hadrons’. In: *Phys. Rev. Lett.* 23 (24 Dec 1969), pp. 1415–1417. DOI: [10.1103/PhysRevLett.23.1415](https://doi.org/10.1103/PhysRevLett.23.1415) (cited on page 5).
- [11] J. D. Bjorken. ‘Asymptotic Sum Rules at Infinite Momentum’. In: *Phys. Rev.* 179 (5 Mar 1969), pp. 1547–1553. DOI: [10.1103/PhysRev.179.1547](https://doi.org/10.1103/PhysRev.179.1547) (cited on page 5).
- [12] C. N. Yang and R. L. Mills. ‘Conservation of Isotopic Spin and Isotopic Gauge Invariance’. In: *Phys. Rev.* 96 (1 Oct 1954), pp. 191–195. DOI: [10.1103/PhysRev.96.191](https://doi.org/10.1103/PhysRev.96.191) (cited on page 5).

- [13] M. Maggiore. *A Modern introduction to quantum field theory*. Sept. 2005 (cited on page 5).
- [14] M E. Peskin and D. V. Schroeder. *An Introduction to quantum field theory*. Reading, USA: Addison-Wesley, 1995 (cited on pages 5, 11, 44).
- [15] W. Greiner, S. Schramm, and E. Stein. *Quantum chromodynamics*. Nov. 2002 (cited on page 5).
- [16] F. Gelis. *Quantum Field Theory II*. 2017-2018. URL: <https://www.ipht.fr/Pisp/francois.gelis/Teaching/index.php> (cited on page 6).
- [17] G. Eichmann. *Introduction to hadron physics*. 2014-2015. URL: <http://cftp.ist.utl.pt/~gernot.eichmann/ws2014> (cited on page 6).
- [18] C. Torre. *Introduction to Classical Field Theory*. 2016. URL: https://digitalcommons.usu.edu/lib_mono/3/ (cited on pages 6, 7).
- [19] M. Tanabashi et al. ‘Review of Particle Physics’. In: *Phys. Rev. D* 98 (3 Aug. 2018), p. 030001. DOI: [10.1103/PhysRevD.98.030001](https://doi.org/10.1103/PhysRevD.98.030001) (cited on page 7).
- [20] D. Tong. *Lectures on Gauge Theory*. URL: <http://www.damtp.cam.ac.uk/user/tong/gaugetheory.html> (cited on page 8).
- [21] M. D. Schwartz. *Quantum Field Theory and the Standard Model*. Cambridge University Press, Mar. 2014 (cited on pages 8, 44).
- [22] S. J. Brodsky, H. C Pauli, and S. S. Pinsky. ‘Quantum chromodynamics and other field theories on the light cone’. In: *Phys. Rept.* 301 (1998), pp. 299–486. DOI: [10.1016/S0370-1573\(97\)00089-6](https://doi.org/10.1016/S0370-1573(97)00089-6) (cited on page 8).
- [23] P. A. M. Dirac. ‘Forms of Relativistic Dynamics’. In: *Reviews of Modern Physics* 21 (3 July 1949), pp. 392–399. DOI: [10.1103/RevModPhys.21.392](https://doi.org/10.1103/RevModPhys.21.392) (cited on pages 8, 79).
- [24] R. Venugopalan. ‘Introduction to light cone field theory and high-energy scattering’. In: *Lect. Notes Phys.* 516 (1999). Ed. by J. Cleymans, H.B. Geyer, and F.G. Scholtz, p. 89. DOI: [10.1007/BFb0107312](https://doi.org/10.1007/BFb0107312) (cited on page 8).
- [25] P. A. M. Dirac. ‘Generalized Hamiltonian dynamics’. In: *Canadian Journal of Mathematics* 2 (Jan. 1950), pp. 129–148. DOI: [10.4153/CJM-1950-012-1](https://doi.org/10.4153/CJM-1950-012-1) (cited on pages 10, 93).
- [26] E. Iancu. ‘Physics of the Color Glass Condensate’. PhD thesis. Institut de Physique Theorique, Centre CEA de Saclay, 2005 (cited on pages 11, 15).
- [27] URL: <https://www.ellipsix.net/blog/2014/02/what-s-in-a-proton.html> (cited on pages 12, 13).
- [28] H. Abramowicz et al. ‘Combination of measurements of inclusive deep inelastic $e^\pm p$ scattering cross sections and QCD analysis of HERA data’. In: *Eur. Phys. J. C* 75.12 (2015), p. 580. DOI: [10.1140/epjc/s10052-015-3710-4](https://doi.org/10.1140/epjc/s10052-015-3710-4) (cited on page 12).
- [29] L. McLerran and R. Venugopalan. ‘Computing quark and gluon distribution functions for very large nuclei’. In: *Phys. Rev. D* 49 (5 Mar. 1994), pp. 2233–2241. DOI: [10.1103/PhysRevD.49.2233](https://doi.org/10.1103/PhysRevD.49.2233) (cited on pages 13, 15).

- [30] L. McLerran and R. Venugopalan. ‘Gluon distribution functions for very large nuclei at small transverse momentum’. In: *Phys. Rev. D* 49 (7 Apr. 1994), pp. 3352–3355. DOI: [10.1103/PhysRevD.49.3352](https://doi.org/10.1103/PhysRevD.49.3352) (cited on pages 13, 15).
- [31] L. McLerran and R. Venugopalan. ‘Green’s function in the color field of a large nucleus’. In: *Phys. Rev. D* 50 (3 Aug. 1994), pp. 2225–2233. DOI: [10.1103/PhysRevD.50.2225](https://doi.org/10.1103/PhysRevD.50.2225) (cited on pages 13, 15).
- [32] J. Jalilian-Marian, A. Kovner, and H. Weigert. ‘The Wilson renormalization group for low x physics: Gluon evolution at finite parton density’. In: *Phys. Rev. D* 59 (1998), p. 014015. DOI: [10.1103/PhysRevD.59.014015](https://doi.org/10.1103/PhysRevD.59.014015) (cited on page 13).
- [33] E. Iancu, A. Leonidov, and L. McLerran. ‘Nonlinear gluon evolution in the color glass condensate: I’. In: *Nucl. Phys. A* 692 (2001), pp. 583–645. DOI: [10.1016/S0375-9474\(01\)00642-X](https://doi.org/10.1016/S0375-9474(01)00642-X) (cited on pages 13, 15).
- [34] E. Ferreiro et al. ‘Nonlinear gluon evolution in the color glass condensate II’. In: *Nucl. Phys. A* 703 (2002), pp. 489–538. DOI: [10.1016/S0375-9474\(01\)01329-X](https://doi.org/10.1016/S0375-9474(01)01329-X) (cited on page 13).
- [35] E. Iancu, A. Leonidov, and L. McLerran. ‘The Color glass condensate: An Introduction’. In: *Cargese Summer School on QCD Perspectives on Hot and Dense Matter*. Feb. 2002, pp. 73–145 (cited on page 15).
- [36] A. H. Mueller. ‘Small x physics, high parton densities and parton saturation in QCD’. In: *NATO Sci. Ser. C* 554 (2000). Ed. by L.S. Ferreira, Paulo Nogueira, and J.I. Silva-Marcos, pp. 71–99. DOI: [10.1007/978-94-011-4126-0__2](https://doi.org/10.1007/978-94-011-4126-0__2) (cited on page 15).
- [37] P. Taels. ‘Quantum Chromodynamics at small Bjorken- x ’. PhD thesis. Antwerp U., 2017 (cited on page 15).
- [38] Y. V. Kovchegov. ‘Non-Abelian Weizsäcker-Williams field and a two-dimensional effective color charge density for a very large nucleus’. In: *Phys. Rev. D* 54 (9 Nov. 1996), pp. 5463–5469. DOI: [10.1103/PhysRevD.54.5463](https://doi.org/10.1103/PhysRevD.54.5463) (cited on page 22).
- [39] J. Jalilian-Marian et al. ‘The Intrinsic glue distribution at very small- x ’. In: *Phys. Rev. D* 55 (1997), pp. 5414–5428. DOI: [10.1103/PhysRevD.55.5414](https://doi.org/10.1103/PhysRevD.55.5414) (cited on page 34).
- [40] K. Fukushima. ‘Randomness in infinitesimal extent in the McLerran-Venugopalan model’. In: *Phys. Rev. D* 77 (2008), p. 074005. DOI: [10.1103/PhysRevD.77.074005](https://doi.org/10.1103/PhysRevD.77.074005) (cited on page 34).
- [41] A. Kovner, L. McLerran, and H. Weigert. ‘Gluon production from non-Abelian Weizsäcker-Williams fields in nucleus-nucleus collisions’. In: *Phys. Rev. D* 52 (1995), pp. 6231–6237. DOI: [10.1103/PhysRevD.52.6231](https://doi.org/10.1103/PhysRevD.52.6231) (cited on page 43).
- [42] A. Kovner, L. McLerran, and H. Weigert. ‘Gluon production at high transverse momentum in the McLerran-Venugopalan model of nuclear structure functions’. In: *Phys. Rev. D* 52 (1995), pp. 3809–3814. DOI: [10.1103/PhysRevD.52.3809](https://doi.org/10.1103/PhysRevD.52.3809) (cited on page 43).

- [43] S. McDonald. ‘The initial State of heavy ion collisions in the IP-Glasma framework’. PhD thesis. McGill University, Department of Physics, 2017 (cited on pages 43, 48, 63).
- [44] Lappi, T. *Initial stages of heavy ion collisions*. 2018. URL: https://indico.ectstar.eu/event/14/sessions/58/attachments/259/330/Lappi_dtp_notes.pdf (cited on page 43).
- [45] D. Müller. ‘Simulations of the Glasma in 3+1D’. PhD thesis. TU Vienna, 2019 (cited on pages 47, 48, 54).
- [46] A. Krasnitz and R. Venugopalan. ‘Non-perturbative computation of gluon mini-jet production in nuclear collisions at very high-energies’. In: *Nucl. Phys. B* 557 (1999), p. 237. DOI: [10.1016/S0550-3213\(99\)00366-1](https://doi.org/10.1016/S0550-3213(99)00366-1) (cited on page 47).
- [47] E. Iancu and R. Venugopalan. ‘The Color glass condensate and high-energy scattering in QCD’. In: *Quark-gluon plasma 4*. Ed. by Rudolph C. Hwa and Xin-Nian Wang. Mar. 2003, pp. 249–3363. DOI: [10.1142/9789812795533_0005](https://doi.org/10.1142/9789812795533_0005) (cited on page 52).
- [48] T. Lappi. ‘Energy density of the glasma’. In: *Phys. Lett. B* 643 (2006), pp. 11–16. DOI: [10.1016/j.physletb.2006.10.017](https://doi.org/10.1016/j.physletb.2006.10.017) (cited on page 54).
- [49] T. Epelbaum and F. Gelis. ‘Isotropization of the Quark Gluon Plasma’. In: *Nucl. Phys. A* 926 (2014). Ed. by Nestor Armesto et al., pp. 122–127. DOI: [10.1016/j.nuclphysa.2014.02.014](https://doi.org/10.1016/j.nuclphysa.2014.02.014).
- [50] A. Kurkela et al. ‘Effective kinetic description of event-by-event pre-equilibrium dynamics in high-energy heavy-ion collisions’. In: *Phys. Rev. C* 99.3 (2019), p. 034910. DOI: [10.1103/PhysRevC.99.034910](https://doi.org/10.1103/PhysRevC.99.034910) (cited on page 56).
- [51] A. Kurkela et al. ‘Matching the Nonequilibrium Initial Stage of Heavy Ion Collisions to Hydrodynamics with QCD Kinetic Theory’. In: *Phys. Rev. Lett.* 122.12 (2019), p. 122302. DOI: [10.1103/PhysRevLett.122.122302](https://doi.org/10.1103/PhysRevLett.122.122302) (cited on page 56).
- [52] M. Alqahtani, M. Nopoush, and M. Strickland. ‘Relativistic anisotropic hydrodynamics’. In: *Prog. Part. Nucl. Phys.* 101 (2018), pp. 204–248. DOI: [10.1016/j.ppnp.2018.05.004](https://doi.org/10.1016/j.ppnp.2018.05.004) (cited on page 56).
- [53] M. Strickland. ‘Anisotropic Hydrodynamics: Three lectures’. In: *Acta Phys. Polon. B* 45.12 (2014). Ed. by Michal Praszalowicz, pp. 2355–2394. DOI: [10.5506/APhysPolB.45.2355](https://doi.org/10.5506/APhysPolB.45.2355) (cited on page 56).
- [54] K. Golec-Biernat and M. Wusthoff. ‘Saturation effects in deep inelastic scattering at low $Q^{\ast\ast 2}$ and its implications on diffraction’. In: *Phys. Rev. D* 59 (1998), p. 014017. DOI: [10.1103/PhysRevD.59.014017](https://doi.org/10.1103/PhysRevD.59.014017) (cited on page 59).
- [55] J. Albacete and C. Marquet. ‘Gluon saturation and initial conditions for relativistic heavy ion collisions’. In: *Prog. Part. Nucl. Phys.* 76 (2014), pp. 1–42. DOI: [10.1016/j.ppnp.2014.01.004](https://doi.org/10.1016/j.ppnp.2014.01.004) (cited on page 59).
- [56] T. Lappi. ‘Wilson line correlator in the MV model: Relating the glasma to deep inelastic scattering’. In: *Eur. Phys. J. C* 55 (2008), pp. 285–292. DOI: [10.1140/epjc/s10052-008-0588-4](https://doi.org/10.1140/epjc/s10052-008-0588-4) (cited on pages 59, 60).

- [57] P. Romatschke and U. Romatschke. *Relativistic Fluid Dynamics In and Out of Equilibrium*. Cambridge Monographs on Mathematical Physics. Cambridge University Press, May 2019 (cited on page 60).
- [58] P. Kolb and U. Heinz. ‘Hydrodynamic description of ultrarelativistic heavy ion collisions’. In: (May 2003). Ed. by R. Hwa and X. Wang, pp. 634–714 (cited on page 61).
- [59] P. Huovinen. ‘Hydrodynamical description of collective flow. Chapter 1.’ In: (May 2003). Ed. by R. Hwa and X. Wang, pp. 600–633. DOI: [10.1142/9789812795533_0009](https://doi.org/10.1142/9789812795533_0009) (cited on page 61).
- [60] S. McDonald et al. ‘Pre-equilibrium Longitudinal Flow in the IP-Glasma Framework for Pb+Pb Collisions at the LHC’. In: *Nucl. Part. Phys. Proc.* 289-290 (2017). Ed. by Guang-You Qin et al., pp. 461–464. DOI: [10.1016/j.nuclphysbps.2017.05.108](https://doi.org/10.1016/j.nuclphysbps.2017.05.108) (cited on page 63).
- [61] J.D. Bjorken. ‘Highly Relativistic Nucleus-Nucleus Collisions: The Central Rapidity Region’. In: *Phys. Rev. D* 27 (1983), pp. 140–151. DOI: [10.1103/PhysRevD.27.140](https://doi.org/10.1103/PhysRevD.27.140) (cited on page 64).
- [62] S. McDonald et al. ‘Hydrodynamic predictions for Pb+Pb collisions at 5.02 TeV’. In: *Phys. Rev. C* 95.6 (2017), p. 064913. DOI: [10.1103/PhysRevC.95.064913](https://doi.org/10.1103/PhysRevC.95.064913) (cited on page 66).
- [63] A. Jaiswal. ‘Formulation of relativistic dissipative fluid dynamics and its applications in heavy-ion collisions’. Other thesis. Aug. 2014 (cited on page 66).
- [64] H. Song. ‘Causal Viscous Hydrodynamics for Relativistic Heavy Ion Collisions’. Other thesis. Aug. 2009 (cited on page 66).
- [65] S. Ryu. ‘Integrated description of heavy ion collisions at RHIC and the LHC’. PhD thesis. McGill University, 2016 (cited on pages 67, 69).
- [66] G. S. Denicol et al. ‘Derivation of transient relativistic fluid dynamics from the Boltzmann equation’. In: *Phys. Rev. D* 85 (11 June 2012), p. 114047. DOI: [10.1103/PhysRevD.85.114047](https://doi.org/10.1103/PhysRevD.85.114047) (cited on page 67).
- [67] E. Molnár et al. ‘Relative importance of second-order terms in relativistic dissipative fluid dynamics’. In: *Phys. Rev. D* 89 (7 Apr. 2014), p. 074010. DOI: [10.1103/PhysRevD.89.074010](https://doi.org/10.1103/PhysRevD.89.074010) (cited on page 67).
- [68] G. S. Denicol, S. Jeon, and C. Gale. ‘Transport coefficients of bulk viscous pressure in the 14-moment approximation’. In: *Phys. Rev. C* 90 (2 Aug. 2014), p. 024912. DOI: [10.1103/PhysRevC.90.024912](https://doi.org/10.1103/PhysRevC.90.024912) (cited on page 67).
- [69] F. Cooper and G. Frye. ‘Single-particle distribution in the hydrodynamic and statistical thermodynamic models of multiparticle production’. In: *Phys. Rev. D* 10 (1 July 1974), pp. 186–189. DOI: [10.1103/PhysRevD.10.186](https://doi.org/10.1103/PhysRevD.10.186) (cited on page 68).
- [70] K. Dusling, G. Moore, and D. Teaney. ‘Radiative energy loss and v(2) spectra for viscous hydrodynamics’. In: *Phys. Rev. C* 81 (2010), p. 034907. DOI: [10.1103/PhysRevC.81.034907](https://doi.org/10.1103/PhysRevC.81.034907) (cited on page 68).

- [71] J. Paquet et al. ‘Production of photons in relativistic heavy-ion collisions’. In: *Phys. Rev. C* 93.4 (2016), p. 044906. DOI: [10.1103/PhysRevC.93.044906](https://doi.org/10.1103/PhysRevC.93.044906) (cited on pages 68, 69).
- [72] P. Bozek. ‘Bulk and shear viscosities of matter created in relativistic heavy-ion collisions’. In: *Phys. Rev. C* 81 (2010), p. 034909. DOI: [10.1103/PhysRevC.81.034909](https://doi.org/10.1103/PhysRevC.81.034909) (cited on page 68).
- [73] B. Schenke, S. Jeon, and C. Gale. ‘(3+1)D hydrodynamic simulation of relativistic heavy-ion collisions’. In: *Phys. Rev. C* 82 (2010), p. 014903. DOI: [10.1103/PhysRevC.82.014903](https://doi.org/10.1103/PhysRevC.82.014903) (cited on page 69).
- [74] B. Schenke, S. Jeon, and C. Gale. ‘Elliptic and triangular flow in event-by-event (3+1)D viscous hydrodynamics’. In: *Phys. Rev. Lett.* 106 (2011), p. 042301. DOI: [10.1103/PhysRevLett.106.042301](https://doi.org/10.1103/PhysRevLett.106.042301) (cited on page 69).
- [75] S. Ryu et al. ‘Effects of bulk viscosity and hadronic rescattering in heavy ion collisions at energies available at the BNL Relativistic Heavy Ion Collider and at the CERN Large Hadron Collider’. In: *Phys. Rev. C* 97.3 (2018), p. 034910. DOI: [10.1103/PhysRevC.97.034910](https://doi.org/10.1103/PhysRevC.97.034910) (cited on pages 69, 72).
- [76] P. Kolb, J. Sollfrank, and U. Heinz. ‘Anisotropic transverse flow and the quark hadron phase transition’. In: *Phys. Rev. C* 62 (2000), p. 054909. DOI: [10.1103/PhysRevC.62.054909](https://doi.org/10.1103/PhysRevC.62.054909) (cited on page 69).
- [77] P. Huovinen and P. Petreczky. ‘QCD Equation of State and Hadron Resonance Gas’. In: *Nucl. Phys. A* 837 (2010), pp. 26–53. DOI: [10.1016/j.nuclphysa.2010.02.015](https://doi.org/10.1016/j.nuclphysa.2010.02.015) (cited on page 69).
- [78] B. Schenke, S. Jeon, and C. Gale. ‘Higher flow harmonics from (3+1)D event-by-event viscous hydrodynamics’. In: *Phys. Rev. C* 85 (2012), p. 024901. DOI: [10.1103/PhysRevC.85.024901](https://doi.org/10.1103/PhysRevC.85.024901) (cited on page 70).
- [79] S. Adler et al. ‘Identified charged particle spectra and yields in Au+Au collisions at $S(NN)^{1/2} = 200\text{-GeV}$ ’. In: *Phys. Rev. C* 69 (2004), p. 034909. DOI: [10.1103/PhysRevC.69.034909](https://doi.org/10.1103/PhysRevC.69.034909) (cited on pages 71, 73, 74).
- [80] B. Abelev et al. ‘Systematic Measurements of Identified Particle Spectra in pp , d+Au and Au+Au Collisions from STAR’. In: *Phys. Rev. C* 79 (2009), p. 034909. DOI: [10.1103/PhysRevC.79.034909](https://doi.org/10.1103/PhysRevC.79.034909) (cited on pages 72, 73).
- [81] B. Abelev et al. ‘Centrality dependence of charged hadron and strange hadron elliptic flow from $\sqrt{s_{NN}} = 200\text{ GeV}$ Au + Au collisions’. In: *Phys. Rev. C* 77 (2008), p. 054901. DOI: [10.1103/PhysRevC.77.054901](https://doi.org/10.1103/PhysRevC.77.054901) (cited on pages 72, 74).
- [82] A. Adare et al. ‘Measurements of Higher-Order Flow Harmonics in Au+Au Collisions at $\sqrt{s_{NN}} = 200\text{ GeV}$ ’. In: *Phys. Rev. Lett.* 107 (2011), p. 252301. DOI: [10.1103/PhysRevLett.107.252301](https://doi.org/10.1103/PhysRevLett.107.252301) (cited on pages 72, 74).
- [83] J. Adams et al. ‘Azimuthal anisotropy in Au+Au collisions at $\sqrt{s_{NN}} = 200\text{ GeV}$ ’. In: *Phys. Rev. C* 72 (2005), p. 014904. DOI: [10.1103/PhysRevC.72.014904](https://doi.org/10.1103/PhysRevC.72.014904) (cited on pages 72, 74).

- [84] L. Mantovani. ‘Applications of Light-Front Quantization in QED and QCD’. PhD thesis. Universita’ Di Pavia, 2018 (cited on page 80).
- [85] T. Heinzl. ‘Light cone quantization: Foundations and applications’. In: *Lect. Notes Phys.* 572 (2001). Ed. by H. Latal and W. Schweiger, pp. 55–142. DOI: [10.1007/3-540-45114-5_2](https://doi.org/10.1007/3-540-45114-5_2) (cited on page 81).
- [86] J. B. Kogut and D. E. Soper. ‘Quantum Electrodynamics in the Infinite Momentum Frame’. In: *Phys. Rev. D* 1 (1970), pp. 2901–2913. DOI: [10.1103/PhysRevD.1.2901](https://doi.org/10.1103/PhysRevD.1.2901) (cited on page 82).
- [87] L. Susskind. ‘Model of Self-Induced Strong Interactions’. In: *Physical Review* 165 (5 Jan. 1968), pp. 1535–1546. DOI: [10.1103/PhysRev.165.1535](https://doi.org/10.1103/PhysRev.165.1535) (cited on page 84).
- [88] M. Burkardt. ‘Light Front Quantization’. In: *Advances in Nuclear Physics*. Ed. by J. W. Negele, E. Vogt. Boston, MA: Springer US, 2002, pp. 1–74. DOI: [10.1007/0-306-47067-5_1](https://doi.org/10.1007/0-306-47067-5_1) (cited on page 85).